

Electronic Thesis and Dissertation Repository

10-1-2020 2:30 PM

Synthesis of Stable Organic Radical Homo- and Co-Polymers and Their Applications in Solid-State Devices

Michael Anghel, *The University of Western Ontario*

Supervisor: Gilroy, Joe B., *The University of Western Ontario*

A thesis submitted in partial fulfillment of the requirements for the Master of Science degree in Chemistry

© Michael Anghel 2020

Follow this and additional works at: <https://ir.lib.uwo.ca/etd>

 Part of the [Polymer Chemistry Commons](#)

Recommended Citation

Anghel, Michael, "Synthesis of Stable Organic Radical Homo- and Co-Polymers and Their Applications in Solid-State Devices" (2020). *Electronic Thesis and Dissertation Repository*. 7411.
<https://ir.lib.uwo.ca/etd/7411>

This Dissertation/Thesis is brought to you for free and open access by Scholarship@Western. It has been accepted for inclusion in Electronic Thesis and Dissertation Repository by an authorized administrator of Scholarship@Western. For more information, please contact wlsadmin@uwo.ca.

Abstract

This thesis outlines the synthesis and characterization of a stable organic radical homopolymer incorporating nitronyl nitroxide radicals, as well as the synthesis and characterization of random and block co-polymers incorporating nitronyl nitroxide and 6-oxoverdazyl radicals.

The nitronyl nitroxide homopolymer was synthesized using ring-opening metathesis polymerization (ROMP), yielding polymers with controlled molecular weights and narrow molecular weight distributions. Studies of polymer growth as a function of time and monomer:catalyst ratio revealed the ROMP to be well-behaved. Spectroscopic analysis of the polymer showed that the radicals possessed high radical content, indicating that they are tolerated by ROMP. Conductivity studies of thin-films made of the nitronyl nitroxide polymer were performed, exhibiting memory effects.

The nitronyl nitroxide and 6-oxoverdazyl random and block co-polymers were also synthesized using ROMP. It was found that the order of polymerization was key towards generating the block co-polymers. The co-polymers were fully characterized using spectroscopic, thermal, and electrochemical methods. Both radicals were incorporated into the co-polymers, and it was found that there was slightly more nitronyl nitroxide incorporation into the polymers than expected, which was attributed to its faster reaction rate.

Overall, this work examines the implementation of stable radicals into polymers, while also probing their behaviour as the functional component of solid-state electronics.

Keywords

Stable Radical Polymers, Ring-Opening Metathesis Polymerization, Organic Electronics, Electrochemistry, Cyclic Voltammetry, Thin-Films, Non-conjugated Polymers.

Lay Summary for Audience

Polymers are large molecules, called macromolecules, which themselves are composed of smaller molecular building blocks, deemed monomers. Polymers are found everywhere in day-to-day life ranging from the proteins in your body, to the plastic on your laptop. Scientists are actively searching for polymers with new applications to provide uses to our society. They do this by changing the chemical compositions that polymers have. By altering the composition, the physical (flexibility, toughness) and chemical (reactivity, toxicity) properties change. Some of this work has led to the production of functional polymers, polymers which change according to their surrounding environment. One such example is stable radical polymers. Radicals are molecules which are inherently very reactive species, however, fine-tuning of the structures of the molecules has led some examples to become stable enough to be used in polymers. One unique ability that stable radicals possess is their ease in gaining or losing electrons, which led them to be of interest for their application in electronics. For example, they have seen great potential in the use in organic batteries and solid-state devices such as flash memory (*i.e.*, USB flash drives). The work in this thesis focuses on expanding on the field of stable radical polymers. New examples were made in this work and are presented. The performance of a flash memory produced from a stable organic radical polymer as the functional component is also described.

Co-Authorship Statement

The work described in this thesis contains contributions from the author as well as co-workers Dr. François Magnan, Sara D. Catingan, Matthew A. McCready, Elaheh Aawani, Victor Wong, Dr. Paul Bazylewski, Dr. Deepa Singh, Prof. Giovanni Fanchini, and my supervisor Prof. Joe B. Gilroy. The contributions of each is listed below.

Chapter 1 was written by the author and edited by Prof. Joe Gilroy.

Chapter 2 describes the synthesis and characterization of a nitronyl nitroxide monomer and polymer performed by the author. EPR measurements were done with the assistance of Dr. François Magnan, Dr. Paul Bazylewski, and Dr. Deepa Singh. The processing of the thin-films as well as all solid-state device manufacturing and conductivity measurements were executed by Sara Catingan, Matthew McCready, Elaheh Aawani, Victor Wong, Dr. Deepa Singh with the assistance of Prof. Giovanni Fanchini. The chapter was written by the author and edited by Prof. Joe Gilroy.

Chapter 3 describes a project where all synthesis and characterization was performed by the author. The chapter was written by the author and edited by Prof. Joe Gilroy.

Chapter 4 was written by the author and edited by Prof. Joe Gilroy.

Acknowledgements

To begin, none of this work would have been possible without the tutelage and support that Professor Joe Gilroy has offered me. Thank you for accepting me into the group, and helping me accommodate to a new chapter in my life. The experience I've gained under your mentorship is invaluable, and you helped push me to be the best researcher possible.

I would like to extend a thank you to all the staff in the Department of Chemistry. Matt Wilans always helped me with the NMR, especially for the troublesome undergrad late-night samples. Thank you to Doug Harsine for always running my mass spectrometry experiments. The office staff was always phenomenal, so thank you to Darlene for all the graduate help and thank you Clara for your assistance. Also, thank you to the Chem BioStores staff, especially Monica, who has helped me settle in to this new chapter as well, your help was greatly appreciated.

Thank you to all my lab mates, past and present, who have helped me become the chemist and person I am today. Special thanks to Ryan and Frank, who were of tremendous help when I first started out, helping me figure out how to be a grad student. Jasveer, Daniela, Francis and Ben, you guys were the best lab mates that anyone could ask for. Thank you for your consistent moral support and all the fun trips and memories we had together. I could not have done any of this without you. You all are fantastic chemists and people.

Thank you to the various collaborators at the university. I was grateful to have the opportunity to work in collaboration with Professor Giovanni Fanchini and his research group. You were instrumental to this project with your help in thin-film and device fabrication, so many thanks.

Finally, I would like to thank my family and friends. My parents, Catalin and Daniela, thank you for all the sacrifices you have made for me to be where I am today. You both have always given 110% at everything, and I aspire to be like you some day. Thank you to my grandparents: Nana, Didi, Tataia, si Mamaia. You guys raised me to be the best person I can be, and taught me how to work hard. Thank you to my brother Eddie for always pushing me to be the best. Thank you to my roommates who were along for the ride, you guys helped me keep on track the whole time. And thank you to all my friends back home, for the support and love you've always shown me no matter how far I was. I love you all.

Table of Contents

Abstract.....	ii
Lay Summary for Audience.....	iii
Co-Authorship Statement.....	iv
Acknowledgements.....	v
Table of Contents.....	vi
List of Tables.....	ix
List of Figures.....	x
List of Schemes.....	xiv
List of Appendices.....	xvi
List of Abbreviations.....	xvii
Chapter 1.....	1
1 Introduction.....	1
1.1 Stable Organic Radicals.....	1
1.2 Polymers Incorporating Radicals.....	4
1.2.1 Nitroxide Polymers.....	4
1.2.2 Nitronyl Nitroxide Polymers.....	11
1.2.3 Verdazyl and Galvinoxyl Polymers.....	13
1.2.4 Radical Polymers for Use in Memristors.....	17
1.3 Scope of Thesis.....	18
1.4 References.....	19

Chapter 2.....	24
2 Synthesis and Characterization of Nitronyl Nitroxide Polymers <i>via</i> ROMP	24
2.1 Introduction.....	24
2.2 Results and Discussion	26
2.2.1 Synthesis of Nitronyl Nitroxide Monomer and Polymer.....	26
2.2.2 ROMP Studies for NN.....	32
2.2.3 Electrochemical Properties of NN and PNN	34
2.2.4 Thermal Properties of NN and PNN.....	37
2.2.5 Thin Films of PNN	39
2.3 Conclusion	41
2.4 Experimental.....	42
2.4.1 General Considerations.....	42
2.4.2 Gel Permeation Chromatography (GPC).....	42
2.4.3 Electron Paramagnetic Resonance (EPR) Spectroscopy	43
2.4.4 Cyclic Voltammetry.....	44
2.4.5 Thermal Analysis.....	44
2.4.6 Synthetic Procedures.....	44
2.5 References.....	47
Chapter 3.....	49
3 6-Oxoverdazyl and Nitronyl Nitroxide Radical Co-Polymers.....	49
3.1 Introduction.....	49
3.2 Results and Discussion	52
3.2.1 Synthesis of Random Co-Polymers Containing 6OV and NN	52
3.2.2 Synthesis of Block Co-Polymers Containing 6OV and NN	57

3.2.3 Thermal Properties of Co-Polymers	62
3.2.4 Electrochemical Properties of Co-Polymers	65
3.3 Conclusion	67
3.4 Experimental	67
3.4.1 General Considerations	67
3.4.2 Gel Permeation Chromatography (GPC)	68
3.4.3 Cyclic Voltammetry	68
3.4.4 Thermal Analysis	68
3.4.5 Synthetic Procedures	69
3.5 References	71
Chapter 4	73
4 Conclusions and Future Work	73
4.1 References	77
Appendices	78
Appendix 1 - Permission to Reuse Copyrighted Material	78
Curriculum Vitae	81

List of Tables

Table 2.1. Electrochemical properties of NN and PNN.....	35
Table 3.1. M_n , M_w and D values for P6OV_{m-r}-PNN_n random co-polymers.	54
Table 3.2. Calculated ratios for random co-polymers P6OV_{m-r}-PNN_n with their respective R-factor.	57
Table 3.3. M_n , M_w , and D values for aliquots of the first P6OV block and P6OV_{m-b}-PNN_n block co-polymers.....	60
Table 3.4. Calculated block ratios for block co-polymers P6OV_{m-b}-PNN_n with R-factor... ..	61
Table 3.5. Onset of decomposition temperatures for P6OV_{m-r}-PNN_n random co-polymers.....	62
Table 3.6. Onset of Decomposition temperatures for P6OV_{m-b}-PNN_n block co-polymers.	63

List of Figures

Figure 1.1. Redox reactions for a neutral stable radical.....	2
Figure 1.2. Reversible oxidation and reduction by a nitroxide radical as well as structure of PTMA	6
Figure 1.3. Depiction of electron transport mechanism within a radical polymer electrode. Image adapted from Ref. 32.....	6
Figure 1.4. A fully organic radical battery composed of an n-type radical polymer and a p-type radical polymer as the cathode. Image reproduced with permission from Ref. 45.	6
Figure 1.5. Comparison of conductivity between PTMA , P3HT , and polymer 1.25 . Figure adapted with permission from Ref 50 (Published by the Royal Society of Chemistry), which is licensed under a Creative Commons Attribution-Non Commercial 3.0 Unported Licence.	9
Figure 1.6. (a) Schematic of a redox-flow battery. (b) The electrochemistry present at the respective electrodes. Figure reproduced with permission from Ref. 51.	10
Figure 1.7. Oxidation and reduction of a nitronyl nitroxide radical.	11
Figure 1.8. (a) AFM images of P6OV thin film and Al contact. (b) Memristor device architecture. The structure of P6OV is shown on the right. Images reproduced with permission from Ref 54.	18
Figure 2.1. FT-IR spectra of NN (blue) and PNN (black).	29
Figure 2.2. UV-vis absorption spectrum of NN (blue) vs. PNN (black) (a). Zoomed inset for absorption region between 450-800 nm (b) shows that the two absorption regions are in very close agreement with 97% radical loading in the polymer as per extinction coefficient ratios.	30

Figure 2.3. Simulated EPR spectrum of NN (top), experimental spectrum of NN (middle), and experimental spectrum of PNN (bottom). Simulation of the spectrum of NN yielded these parameters: linewidth = 0.120 mT, $a_{N1} = 0.754$ mT, $g = 2.0060$	31
Figure 2.4. GPC trace for a representative sample of PNN ($M_n = 51,400$ g mol ⁻¹ , $M_w = 60,600$ g mol ⁻¹ , $D = 1.18$).	32
Figure 2.5 (a) Molecular weight (M_n) and dispersity as a function of reaction time. (b) The relationship between feed molar ratio and the DP_n of polymers as determined by GPC. Linear line represents the theoretical relationship between feed molar ratio and DP_n . (c) Representative GPC traces for the catalyst loading study with colour coding for each ratio as presented in (b).	34
Figure 2.6. Cyclic voltammograms collected for monomer NN (top) and PNN (bottom) recorded at a scan rate of 250 mV s ⁻¹ in degassed 50:50 v/v CH ₂ Cl ₂ /MeCN solutions containing 1 mM analyte and 0.1 M [<i>n</i> Bu ₄ N][PF ₆] as supporting electrolyte.....	35
Figure 2.7. Cyclic voltammograms collected for PNN recorded in both directions at a scan rate of 250 mV s ⁻¹ in degassed 50:50 v/v CH ₂ Cl ₂ /MeCN solutions containing 1 mM analyte and 0.1 M [<i>n</i> Bu ₄ N][PF ₆] as supporting electrolyte.....	36
Figure 2.8. Cyclic voltammograms collected for PNN recorded at a scan rates ranging from 50 to 1000 mV s ⁻¹ in degassed 50:50 v/v of CH ₂ Cl ₂ /MeCN solutions containing 1 mM analyte and 0.1 M [<i>n</i> Bu ₄ N][PF ₆] as supporting electrolyte.....	36
Figure 2.9. Cyclic voltammograms collected for PNN recorded at a scan rate of 50 mV s ⁻¹ over the span of 25 cycles. Experiments were conducted in degassed 50:50 v/v CH ₂ Cl ₂ /MeCN solutions containing 1 mM analyte and 0.1 M [<i>n</i> Bu ₄ N][PF ₆] as supporting electrolyte. The 1 st scan as well as every 5 th are depicted for clarity.....	37
Figure 2.10. (a) TGA trace of PNN from 0 to 1000 °C. (b) DSC data for the second heating/cooling cycle for PNN . The sample was heated to 150 °C followed by cooling to 20 °C with a heating range of 10 °C min ⁻¹	38

Figure 2.11. IR spectra of fresh PNN (top) and charred PNN (bottom). Red rectangle indicates the region of importance, where the N-O• stretching frequency is significantly diminished when comparing top spectrum to bottom.....	39
Figure 2.12. AFM image for PNN at 30 nm ± 10% thickness. A small fragment of the film was scraped off to reveal the glass substrate underneath (right side of image). Thin films were spun at 2000 RPM.....	40
Figure 2.13. Sandwich-type device architecture fabricated for conductivity measurements.	40
Figure 2.14. Current response as a function of applied voltage for PNN device represented by a Poole-Frenkel fit (dashed line, low conductivity) and an Ohmic behaviour fit (linear line, high conductivity).	41
Figure 3.1 GPC traces (in THF) for polymers (a) P6OV , (b) P6OV_{75-r}-PNN₂₅ , (c) P6OV_{50-r}-PNN₅₀ , (d) P6OV_{25-r}-PNN₇₅ , and (e) PNN	54
Figure 3.2. FT-IR spectra for 6OV , P6OV , P6OV_{75-r}-PNN₂₅ , P6OV_{50-r}-PNN₅₀ , P6OV_{25-r}-PNN₇₅ , PNN and NN with red boxes highlighting regions between 1400–1300 cm ⁻¹ and 1800–1600 cm ⁻¹	55
Figure 3.3. UV-Vis absorption spectra for homopolymers PNN and P6OV (a), as well as absorption spectra and model fits for random co-polymers (b) P6OV_{75-r}-PNN₂₅ , (c) P6OV_{50-r}-PNN₅₀ , and (d) P6OV_{25-r}-PNN₇₅	56
Figure 3.4. GPC traces for PNN aliquot (blue) and block co-polymer PNN_{50-b}-P6OV₅₀ (black) where NN was used as the starting block.	57
Figure 3.5. GPC traces of (in THF) for polymers (a) P6OV , (b) P6OV_{75-b}-PNN₂₅ , (c) P6OV_{50-b}-PNN₅₀ , (d) P6OV_{25-b}-PNN₇₅ , and (e) PNN . The orange GPC traces present in (b), (c) and (d) belong to the aliquot of the first P6OV block prior to secondary block addition.	59

Figure 3.6. FT-IR spectra for 6OV , P6OV , P6OV_{75-b-PNN₂₅} , P6OV_{50-b-PNN₅₀} , P6OV_{25-b-PNN₇₅} , PNN and NN with red boxes highlighting regions between 1400–1350 cm ⁻¹ and 1600–1800 cm ⁻¹	60
Figure 3.7. UV-Vis absorption spectra for homopolymers PNN and P6OV (a), as well as absorption spectra and model fits for block co-polymers (b) P6OV_{75-b-PNN₂₅} , (c) P6OV_{50-b-PNN₅₀} , and (d) P6OV_{25-b-PNN₇₅}	61
Figure 3.8. TGA graphs for P6OV_{m-r-PNN_n} random co-polymers.....	62
Figure 3.9. TGA graphs for P6OV_{m-b-PNN_n} block co-polymers.....	63
Figure 3.10. DSC traces for P6OV_{m-r-PNN_n} random co-polymers.....	64
Figure 3.11. DSC traces for P6OV_{m-b-PNN_n} block co-polymers.....	64
Figure 3.12. Cyclic voltammograms collected for P6OV_{m-r-PNN_n} random co-polymers. Experiments were conducted in degassed mixtures of 50:50 v/v CH ₂ Cl ₂ /CH ₃ CN containing approximately 1 mM of analyte and 0.1 M [nBu ₄][NPF ₆] at scan rates of 250 mV s ⁻¹ . Blue vertical line indicates PNN oxidation potential, while the two orange vertical lines indicate P6OV oxidation and reduction potentials.....	66
Figure 3.13. Cyclic voltammograms collected for P6OV_{m-b-PNN_n} block co-polymers. Scan is in the negative direction at 250 mV s ⁻¹ scan rate. Experiments were conducted in degassed mixtures of 50:50 v/v CH ₂ Cl ₂ /CH ₃ CN containing approximately 1 mM of analyte and 0.1 M [nBu ₄][NPF ₆] at scan rates of 250 mV s ⁻¹ . Blue vertical line indicates PNN oxidation potential, while the two orange vertical lines indicate P6OV oxidation and reduction potentials.....	66
Figure 4.1 Graphical summary of Chapter 2.....	74
Figure 4.2 Graphical summary of Chapter 3.....	76

List of Schemes

Scheme 1.1. Nitronyl nitroxide reacting with nitric oxide forming an imino-nitroxide radical. Imino-nitroxide resonance structures are shown.	3
Scheme 1.2. Oxidation of primary and secondary alcohols using a nitroxide radical as a catalyst.	4
Scheme 1.3. Synthesis of PTMA via free radical polymerization. ⁴⁵	7
Scheme 1.4. Synthesis of PTMA via anionic polymerization. ⁴⁵	8
Scheme 1.5. Synthesis of acrylamide-based nitroxide polymer 1.22 via free radical polymerization. ⁴⁷	8
Scheme 1.6. Synthesis of 1.25 via anionic polymerization. ⁴⁸	9
Scheme 1.7. Synthesis of nitronyl nitroxide polymer 1.28 . ⁵²	12
Scheme 1.8. Synthesis of nitronyl nitroxide polymer 1.30 . ⁵⁵	12
Scheme 1.9. (a) Synthesis of nitronyl nitroxide polymer 1.32 . (b) Synthesis of nitroxide polymer 1.34 . (c) Synthesis of nitronyl nitroxide block co-polymer 1.37	13
Scheme 1.10. Synthesis of vinyl-based verdazyl polymer 1.39 . ⁵⁷	14
Scheme 1.11. Synthesis of 6-oxoverdazyl methacrylate-based polymer 1.44 . ⁵⁹	15
Scheme 1.12. Synthesis of 6-oxoverdazyl norbornene-based polymer P6OV . ⁵⁹	15
Scheme 1.13. Synthesis of styrene-based galvinoxyl polymer 1.49 . ⁶¹	16
Scheme 1.14. (a) Synthesis of acetylene-based galvinoxyl polymer 1.50 . (b) Synthesis of acetylene-based galvinoxyl polymer 1.51	16

Scheme 2.1. Synthetic route for nitronyl nitroxide radical 2.14	27
Scheme 2.2. Synthesis of monomer NN and polymer PNN	28
Scheme 3.1. Synthesis of random co-polymers P6OV_{m-r}-PNN_n	53
Scheme 3.2. Synthesis of block co-polymers P6OV_{m-b}-PNN_n	58
Scheme 4.1. Proposed synthesis of a Kuhn verdazyl polymer using ROMP.....	75

List of Appendices

Appendix 1 - Permission to Reuse Copyrighted Material	78
---	----

List of Abbreviations

°	degree
°C	degree Celsius
6OV	6-oxoverdazyl monomer
abs	absorbance
a.u.	arbitrary units
AIBN	2,2'-azo-bis(2-methylproprionitrile)
AFM	atomic force microscopy
ATR	attenuated total reflectance
BASi	Bioanalytical Systems Inc.
br	broad
Bu	butyl
<i>ca.</i>	circa – signifies approximately
cm	centimeter
cm ⁻¹	wavenumber
cod	1,5-cyclooctadiene
CV	cyclic voltammetry
<i>D</i>	dispersity
DCC	dicyclohexylcarbodiimide
d	doublet
dd	doublet of doublets
DFS	double focusing sensor
DMAP	dimethylaminopyridine
DMSO	dimethylsulfoxide
DP _n	degree of polymerization
DPE	diphenyl ether
DSC	differential scanning calorimetry
<i>E</i>	potential
<i>E</i> _{1/2}	half-wave potential
EA	elemental analysis
EPR	electron paramagnetic resonance

eq.	equivalent(s)
ESI-MS	electrospray ionization mass spectrometry
Et	ethyl
Et ₂ O	diethyl ether
Et ₃ N	triethylamine
EtOAc	ethyl acetate
EtOH	ethanol
eV	electron volts
EVE	ethyl vinyl ether
EtOAc	ethyl acetate
Fc	ferrocene
Fc ⁺	ferrocenium
FLG	few-layer graphene
FT-IR	Fourier transform infra-red spectroscopy
FW	formula weight
g	grams
<i>g</i>	electron spin g-factor
GIII	Grubbs' third generation catalyst
GPC	gel permeation chromatography
h	hours
hex	hexyl
HOMO	highest occupied molecular orbital
Hz	hertz
ITO	indium tin oxide
I	current
I-V	current-voltage
<i>J</i>	NMR coupling constant
K	degrees Kelvin
kg	kilograms
LUMO	lowest-unoccupied molecular orbital
<i>m</i>	meta
<i>m</i> CPBA	meta-chloroperoxybenzoic acid

M	molar
m	multiplet
mA	milliamps
max	maximum
Me	methyl
MeCN	acetonitrile
MeOH	methanol
mg	milligram
MHz	megahertz
min	minute/minutes
mL	millilitres
mM	millimolar
mmol	millimoles
M_n	number average molecular weight
mol	moles
mV	millivolts
MW	molecular weight
M_w	weighted average molecular weight
nbd	norbornadiene
nm	nanometers
NMR	nuclear magnetic resonance
NN	nitronyl nitroxide monomer
n-type	negative (-'ve) doping
OAc	acetate
ORB	organic radical battery
<i>p</i>	para
P3HT	poly(3-hexylthiophene)
P6OV	6-oxoverdazyl polymer
Ph	phenyl
PNN	nitronyl nitroxide polymer
ppm	parts per million
PS	poly(styrene)

PTMA	poly(2,2,6,6-tetramethylpiperidinyloxy methacrylate)
p-type	positive (+ve) doping
q	quartet
r.t.	room temperature
R•	stable radical group
RI	refractive index
ROMP	ring-opening metathesis polymerization
S	siemens
<i>S</i>	low-field, low-voltage conductance
SOMO	singly occupied molecular orbital
t	triplet
TBAHS	tetrabutylammonium hydrogensulfate
TEMPO	(2,2,6,6)-tetramethylpiperidinyloxy
T _g	glass transition temperature
TEA	triethylamine
TGA	thermal gravimetric analysis
THF	tetrahydrofuran
TMS	tetramethylsilane
UV	ultraviolet
UV-vis	ultraviolet-visible
V	volts
v/v	volume to volume ratio
viol	viologen
WORM	write-once-read-many
w	weak
<i>x</i>	Cartesian axis
<i>y</i>	Cartesian axis
<i>z</i>	Cartesian axis
δ	chemical shift
ε	molar absorptivity
λ	wavelength
λ _{max}	wavelength of maximum absorption

μA	microamps
ν	wavenumber

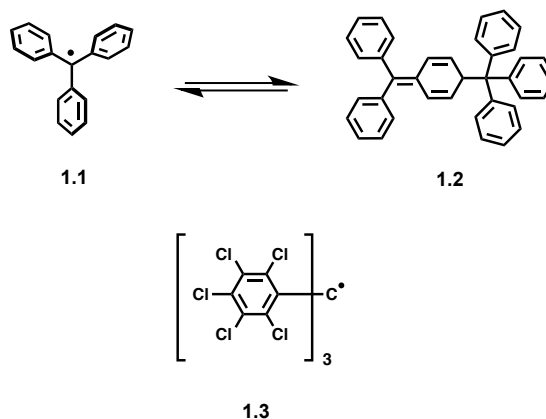
Chapter 1

1 Introduction

Polymers are one of the most versatile functional materials used today.¹⁻³ From plastic bags (polyethylene) to rubber tires (polystyrene-*co*-butadiene), polymers have always found specific niche uses for humans. Within the last few decades polymers have found their way into electronics. The majority of these polymers depend on π -conjugation to conduct electricity, or the addition of inorganic dopants. A newer class of polymers, known as stable organic radical polymers, has emerged as a promising alternative candidate for use in electronics. These polymers benefit from the redox chemistry of stable radicals embedded within their structure. The text below is a brief review on organic stable radicals, as well as their incorporation into various polymer architectures.

1.1 Stable Organic Radicals

Organic compounds that possess paramagnetic character, often referred to as organic radicals, are a family of compounds that have orbitals containing one or more unpaired electrons. The subvalent nature of the singly occupied molecular orbital (SOMO), where the electron resides, is often implicated in reactions such as disproportionation, hydrogen abstraction or dimerization. However, some organic radicals do not, and can be classified into two distinct categories: persistent or stable. Persistent radicals are long-lived enough to be observable by spectroscopic methods while stable radicals are isolable as pure compounds.^{4, 5} In 1900, Gomberg reported the first persistent radical, the triphenylmethyl radical **1.1**. Its classification as a persistent radical was due to the rapid dimerization which occurred in solution, forming the dimer **1.2**.⁶ Fine-tuning of the structure of **1.1** by replacing all aryl hydrogen atoms with chlorine atoms lead to the formation of the exceptionally stable radical **1.3**, which only underwent reactions under harsh conditions. The steric effects provided by the chlorines were attributed to this increased stability by shielding the carbon-centred radical from dimerization.⁷



The stability of radicals can also be enhanced if the lone electron is delocalized by being near π -systems or heteroatoms, leading to the investigation and discovery of a variety of heteroatom based stable radicals.^{4,8} Currently there are multiple families of stable organic radicals known, such as the nitroxide **1.4**,⁹ nitronyl nitroxide **1.5**,¹⁰⁻¹³ proxyl **1.6**,¹⁴ verdazyl **1.7**,¹⁵⁻¹⁷ galvinoxyl **1.8**,¹⁸ and phenoxyl **1.9**^{19, 20} radicals. These radicals can be stabilized by both electron delocalization and steric effects and they often exhibit reversible redox reactions to their corresponding anionic and cationic forms as presented in Figure 1.1.⁵

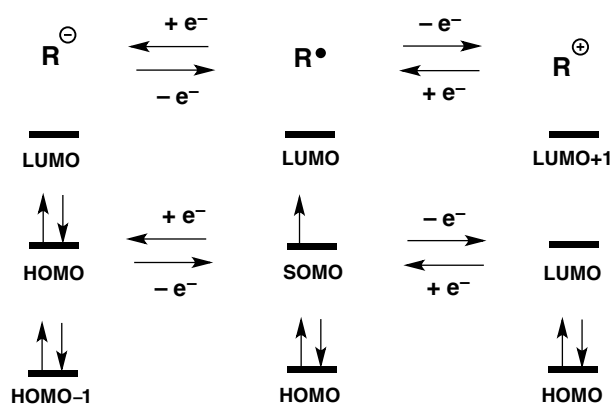
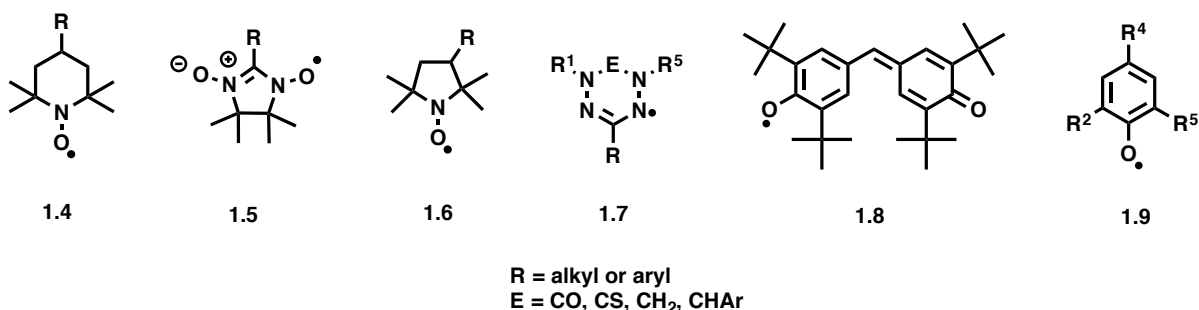
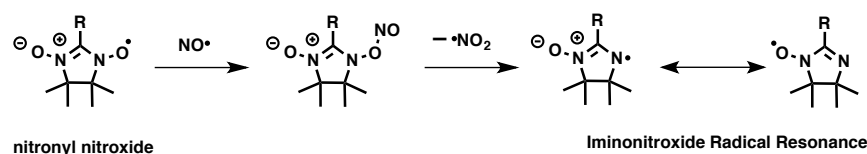


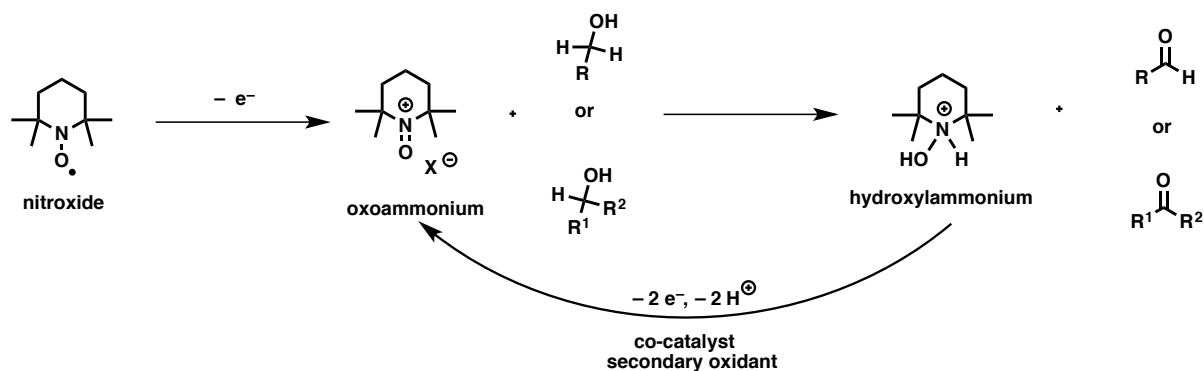
Figure 1.1. Redox reactions for a neutral stable radical.

The stability of radicals has led researchers to explore their potential uses. One prominent use for stable radicals is as spin traps; molecules used for the detection of paramagnetic species through covalent bonding to short-lived radical species, forming a stable radical adduct which is observable by electron paramagnetic resonance (EPR) spectroscopy. Stable radicals can facilitate this process as they provide a standard to compare to, as they are themselves inherently paramagnetic. An example of this is with nitric oxide, a radical compound that's commonly found as an intermediate in multiple biological processes. However, the quantities observed in physiological systems are minute ($< \mu\text{M}$ concentrations) and possess a very short half-life, making them difficult to monitor *in situ*. Nitronyl nitroxides have been implemented as spin traps where the radical specifically reacts with nitric oxide forming an imino nitroxide (Scheme 1.1). In this experiment, the EPR spectrum of the nitronyl nitroxide would feature a characteristic five line pattern. Upon reaction with nitric oxide, the newly formed imino nitroxide adduct would feature a seven line pattern (1:1:2:1:2:1:1), indicating the formation of a new species *in situ*, and with analysis of the EPR spectrum, one can reveal information about the species trapped such as concentration and structure.²¹



Scheme 1.1. Nitronyl nitroxide reacting with nitric oxide forming an imino-nitroxide radical. Imino-nitroxide resonance structures are shown.²¹

Furthermore, the redox reactions radicals have undertaken have led them be of use as catalysts in the oxidation of alcohols. Nitroxide radicals have been widely used for this application due to the strong oxidizing capabilities of the oxidized oxoammonium species, as well as their tolerability to side reactions in the presence of various functional groups such as alkenes, alkynes and azides.^{5, 22} In the process for oxidation of alcohols, the nitroxide radical first gets oxidized to the oxoammonium cation. Primary or secondary alcohols then react with the oxoammonium cation, oxidizing them to aldehydes or ketones, respectively, while the oxoammonium cation gets reduced to a hydroxylammonium salt. Using a secondary oxidant, the hydroxylammonium cation undergoes a two-electron oxidation back to its oxoammonium cation form, repeating the cycle (Scheme 1.2).²²



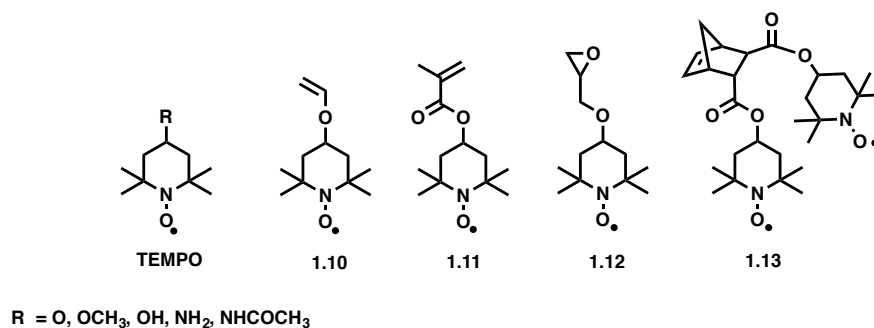
Scheme 1.2. Oxidation of primary and secondary alcohols using a nitroxide radical as a catalyst.²²

1.2 Polymers Incorporating Radicals

Because of the reversible redox reactions that stable radicals can undergo, they have been implemented into polymeric structures as pendent units or in the main chain. The polymer backbone can be varied to be conducting through π -conjugation, or insulating. For relevance and brevity, polymers based on organic insulating backbones with pendent radical units will be discussed solely. The insulating (*i.e.*, nonconjugated) backbone allows for limited interference with the electrochemistry of the radicals, as redox events will happen solely between radical species interchangeably. The combination of the processability of polymers with the unique redox properties of radicals has seen them applied in diagnostic imaging,²³⁻²⁵ biomedical applications,^{26, 27} catalysis,^{28, 29} organic batteries³⁰⁻³⁵ and memristors.^{11, 36} In contrast to metallic or inorganic counterparts, organic devices are often sought after due to the abundant nature of their precursors as well as the lower cost of production.

1.2.1 Nitroxide Polymers

Polymers based on the nitroxide radical family are the most prevalent in the literature due to the commercial availability of monomer precursors. The most common nitroxides found in polymers are dialkyl nitroxides such as 2,2,6,6-tetramethylpiperidinyloxy (**TEMPO**). The polymerizable group of nitroxide radical monomers has been widely varied across the literature spanning from vinyl ether **1.10**,³⁷ methacrylate **1.11**,³⁸ epoxide **1.12**,³⁹ and norbornene-based **1.13**.⁴⁰ The relatively low molecular weight of the nitroxide radical unit allows for high radical density when synthesizing polymers.



The organic radical polymer poly(2,2,6,6-tetramethylpiperidinyloxy methacrylate) (**PTMA**),^{35, 38, 41} is the most well-known radical polymer and was first synthesized in 1972 by Okawara *et al.*⁹ Further studies on this system by Nishide *et al.* revealed that **PTMA** is an ideal candidate in energy storage materials such as organic radical batteries (ORBs).^{38, 42, 43} Nitroxide radicals possess rapid and reversible redox kinetics at the radical site, with exceptional stability shown for the oxidized oxoammonium cation (Figure 1.2). However, its reduced aminoxyl anion form has been observed to be irreversible prompting researchers to use **PTMA** as a cathodic material rather than anodic. Nishide and coworkers used **PTMA** as the active material in a cathode for construction of an organic battery device, with Li metal being used as the anode.^{30, 38, 42} Cyclic voltammetry studies on the cathodes composed of **PTMA** have shown oxidation potentials of 0.76 V versus Ag/AgCl.³⁸ A visual illustration of the electrochemistry that happens in a nitroxide radical polymer electrode can be seen in Figure 1.3, where electrons hop from current collector to polymer, and in-between the radical groups. **PTMA** has shown exceptional charge-discharge capacity and a long cycle life being able to be fully charged and discharged over 1000 times.³⁰⁻³⁵ The polymer also withstood high temperatures up to 240 °C prior to radical degradation, while also maintaining a constant radical content after 5 months of storage under ambient lab conditions.^{38, 41} It is also stable to moisture and light, with no negative effects on the electrochemistry of the polymer and no degradation observed.⁴⁴ This work prompts the search for a commercial fully organic battery, as it would provide a more environmentally friendly and cheaper substitute to the current metal-based batteries. A schematic of a fully organic radical battery can be seen in Figure 1.4 where an n-type polymer is used as the anode and a p-type polymer as the cathode.⁴⁵

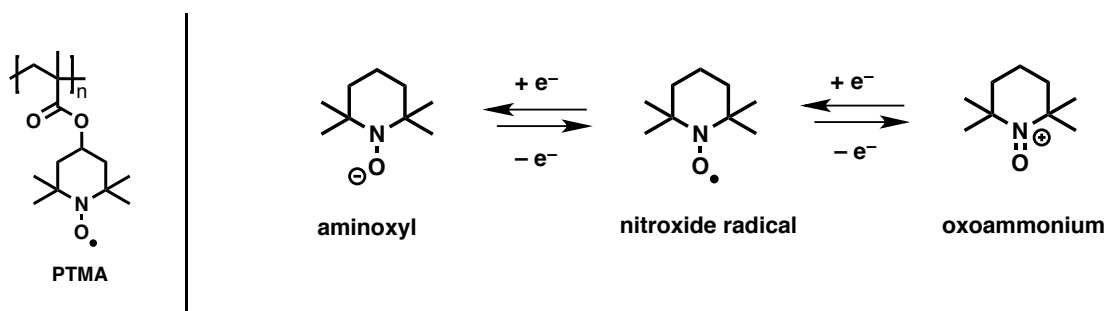


Figure 1.2. Reversible oxidation and reduction by a nitroxide radical as well as structure of PTMA.

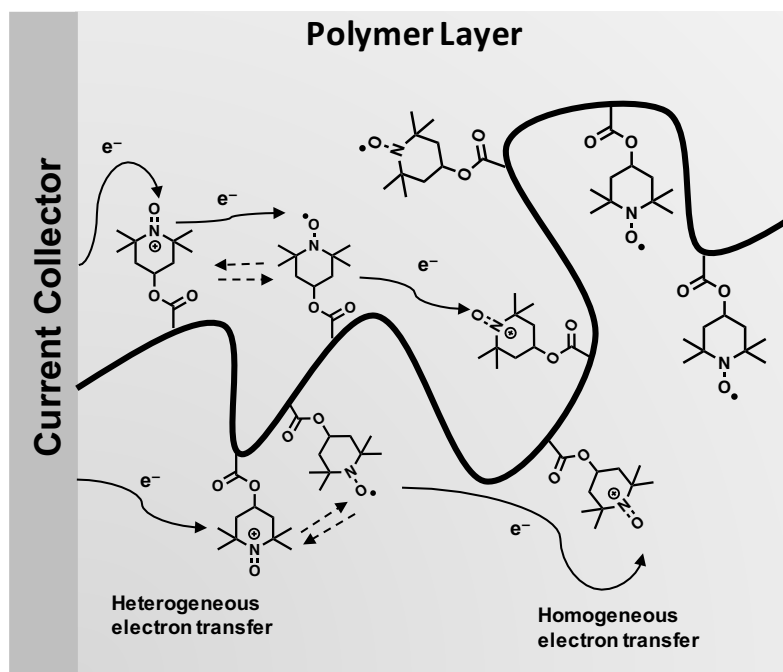


Figure 1.3. Depiction of electron transport mechanism within a radical polymer electrode. Image adapted from Ref. 32.

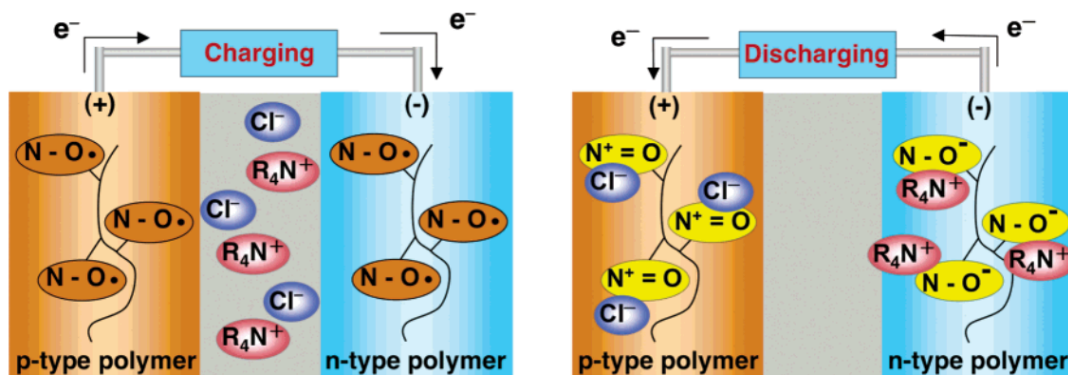
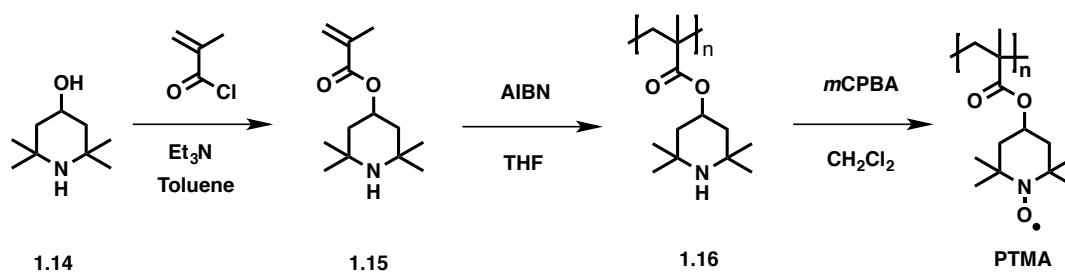
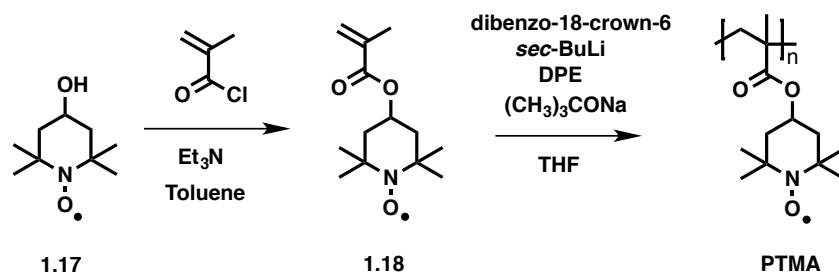


Figure 1.4. A fully organic radical battery composed of an n-type radical polymer and a p-type radical polymer as the cathode. Image reproduced with permission from Ref. 45.

Synthesis of **PTMA** begins by the reaction between 4-methacryloyloxy-2,2,6,6-tetramethylpiperidine **1.14** and methacryloyl chloride in toluene with triethylamine employed as a base. The yielding monomer, 2,2,6,6-tetramethylpiperidyl-4-methacrylate (**1.15**), is then polymerized using free radical polymerization with azobisisobutyronitrile (AIBN) as an initiator yielding its polymer counterpart **1.16**. Oxidation of the polymer precursor **1.16** is typically done using 3-chloroperbenzoic acid (*m*CPBA) in CH_2Cl_2 , yielding **PTMA** (Scheme 1.3).⁴⁶ This specific synthetic route depends on subsequent oxidation of a precursor polymer to yield the radical polymer due to the interference of the radicals generated during the polymerization process. These side reactions end up quenching the radical yielding low radical density within the polymers. However, this is not always the case, as other polymerization methodologies have been employed such as ring-opening metathesis polymerization (ROMP) and anionic/cationic polymerization, where the radicals can survive the polymerization conditions.^{46,47} An example of this can be seen in Scheme 1.4 where the anionic polymerization of **PTMA** was executed using the TEMPO radical **1.17** as the starting material. A methacrylate functional group was appended to the radical, and direct polymerization of the methacrylate radical monomer **1.18** yielded **PTMA**. Both methodologies offered moderate incorporation of radicals ranging between 70–80% with low conductivities in the range of $1.1 \times 10^{-11} \text{ S cm}^{-1}$ to $5.6 \times 10^{-11} \text{ S cm}^{-1}$, inferring that these are insulating materials.⁴⁶

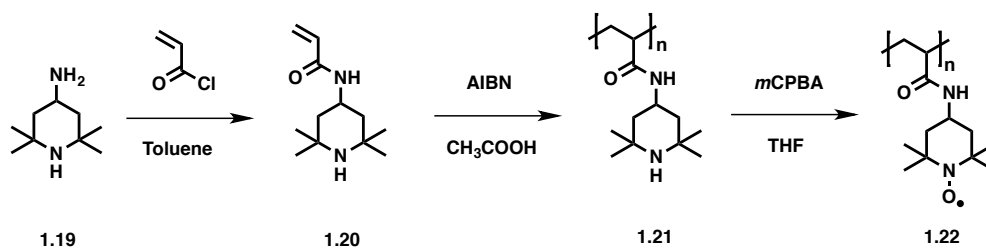


Scheme 1.3. Synthesis of **PTMA** via free radical polymerization.⁴⁶



Scheme 1.4. Synthesis of **PTMA** via anionic polymerization.⁴⁶

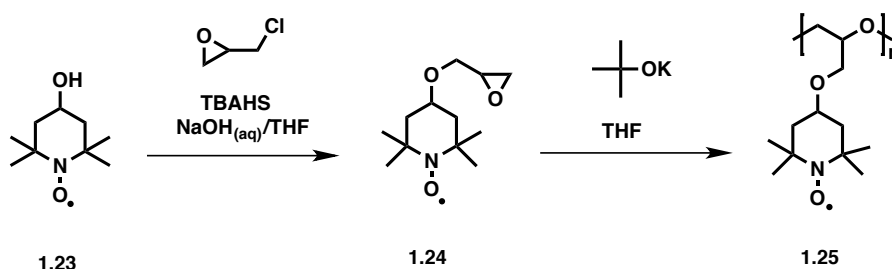
Variations in the backbone architecture can provide distinguishable properties for radical polymers. Nishide *et al.* synthesized the polymer **1.22**, an acrylamide-based polymer, which when compared to **PTMA** has an amide group instead of an ester in the backbone.⁴⁸ This leads to an increase in hydrophilicity, allowing for its potential application in electrolyte-based batteries. Synthesis began by the reaction between amine-substituted piperidine **1.19** and acryloyl chloride, yielding the acrylate monomer **1.20**. Free radical polymerization to synthesize the reduced precursor polymer **1.21** was done using AIBN, and then subsequent oxidation using *m*CPBA yielded the radical polymer **1.22** (Scheme 1.5). An aqueous electrolyte-based organic battery using **1.22** as the cathodic active material and a polyviologen as the anodic. This battery exceeded 2000 charging-discharging cycles without significant degradation.



Scheme 1.5. Synthesis of acrylamide-based nitroxide polymer **1.22** via free radical polymerization.⁴⁸

Boudouris *et al.* synthesized poly(4-glycidyloxy-2,2,6,6-tetramethylpiperidine-1-oxyl) (**1.25**),⁴⁹ a nitroxide polymer with an epoxide backbone (Scheme 1.6). The precursor monomer **1.24** was prepared using the TEMPO radical **1.23** as the starting material. Anionic polymerization of **1.24** using potassium *tert*-butoxide as the initiator yielded **1.25**. Polymer **1.25** exhibited very high conductivity upon thermal annealing at 80 °C, with a value of

0.2 S cm^{-1} . When compared to **PTMA** and un-doped π -conjugated polymers such as poly(3-hexylthiophene) (P3HT), this value is 2–4 orders of magnitude higher, extending almost to the metallic conductor regime (Figure 1.5).⁵⁰ This is a remarkable finding as radical polymers are often perceived as insulating materials with poor conductivity. Thin films of **1.25** (1 μm thickness) were highly transparent with an optical transparency of 98%, making these suitable candidates for flexible, transparent fully-organic semiconducting solid-state devices.



Scheme 1.6. Synthesis of **1.25** via anionic polymerization.⁴⁹

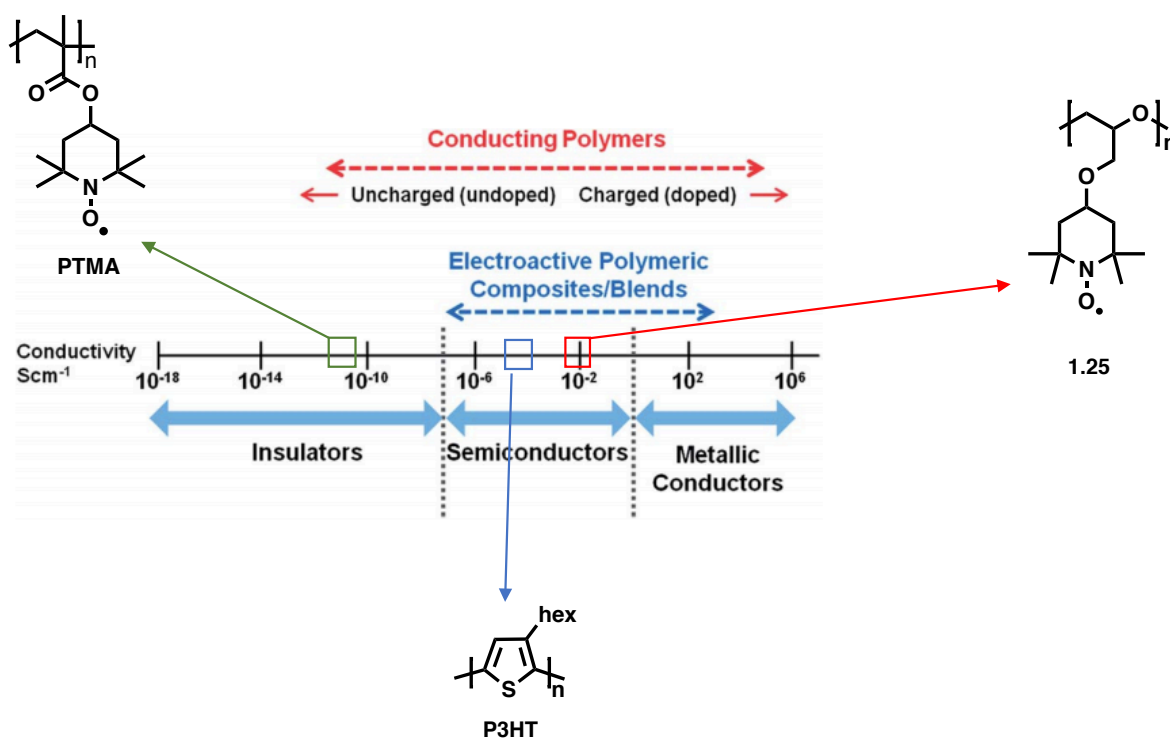


Figure 1.5 Comparison of conductivity between **PTMA**, **P3HT**, and polymer **1.25**. Figure adapted from Ref 50 (Published by the Royal Society of Chemistry), which is licensed under a Creative Commons Attribution-Non Commercial 3.0 Unported Licence.

Radical polymers have also been widely incorporated into redox-flow batteries, a type of battery which is based on liquid rather than solid components. Schubert *et al.* have designed an aqueous redox-flow battery using a radical-ionic co-polymer based on **PTMA** as the cathode material and a viologen-based co-polymer as the anode active material (Figure 1.6).^{51, 52} During the charging process of the battery, solutions of the redox-active polymers travel between their respective reservoirs and the electrochemical cell. Using a permeable size-exclusion membrane, the polymers cannot diffuse between the two separate electrolyte solutions, allowing only small salt ions to permeate and thus preventing self-discharging processes. The advantages of this type of battery include cheaper materials (organic-based), inexpensive filter membranes (dialysis membranes), and non-toxic electrolytes (aqueous sodium chloride).

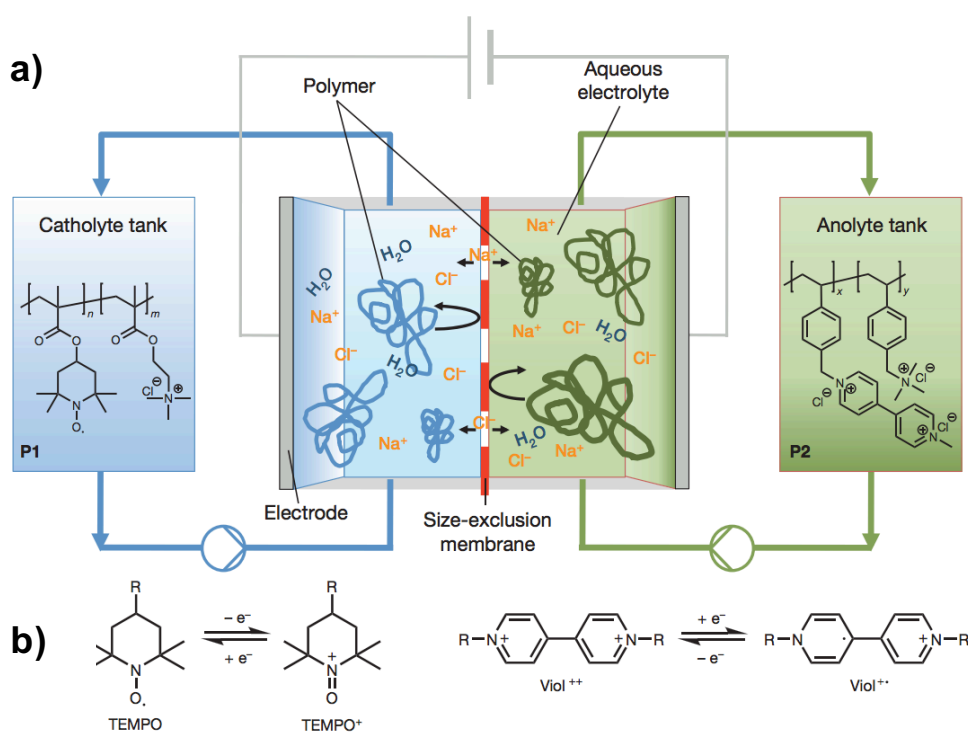


Figure 1.6. (a) Schematic of a redox-flow battery. (b) The electrochemistry present at the respective electrodes. Figure reproduced with permission from Ref. 51.

1.2.2 Nitronyl Nitroxide Polymers

Nitronyl nitroxides are another family of radicals that have been incorporated in radical polymers. Just like the nitroxide radicals, nitronyl nitroxides can be reversibly oxidized and reduced (Figure 1.7). In contrast to the nitroxides, nitronyl nitroxides also possess π -conjugation within their structures, increasing their stability *via* resonance.

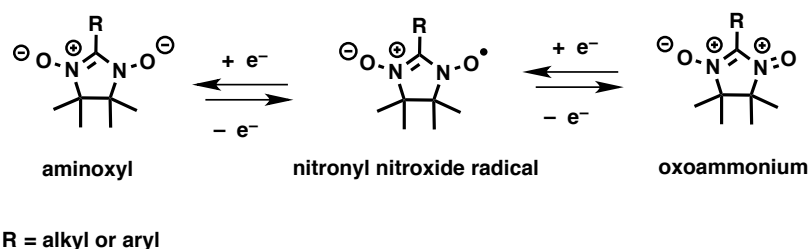
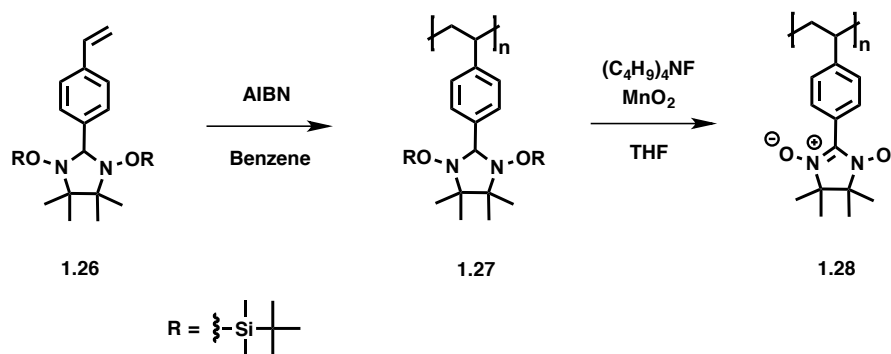
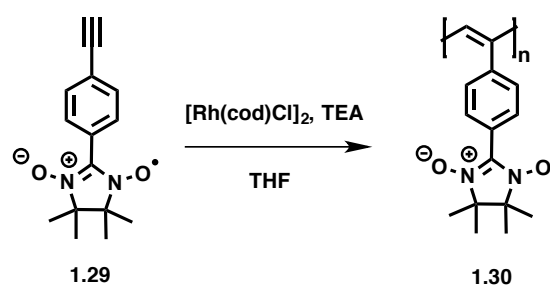


Figure 1.7 Oxidation and reduction of a nitronyl nitroxide radical.

Nishide and co-workers synthesized nitronyl nitroxide polymer **1.28** by radical polymerization of its silyl protected precursor monomer **1.26**, and subsequent oxidation of the precursor polymer **1.27** using MnO_2 as the oxidizing agent (Scheme 1.7).⁵³ Electrochemical studies by cyclic voltammetry of a polymer electrode composed of **1.28** revealed that the polymer possessed ambipolar redox properties with two reversible reduction and oxidation waves observed at -0.61 and 0.72 V versus Ag/AgCl reference electrode respectively. This finding demonstrated that radical polymers can be used as ambipolar redox materials in batteries as well as other solid-state devices such as memristors,^{11, 54, 55} as opposed to nitroxide polymers which are often limited to cathodic materials. Nishide *et al.* expanded upon this finding by polymerizing the alkyne nitronyl nitroxide monomer **1.29** using Rh-catalyzed polymerization yielding polymer **1.30** (Scheme 1.8).⁵⁶ Cyclic voltammetry studies of a carbon nanocomposite electrode composed of **1.30** as the active material highlighted two reversible reduction and oxidation waves at -0.86 V and 0.80 V versus Ag/AgCl reference electrode respectively, yet again highlighting the ambipolar redox properties of nitronyl nitroxide polymers.

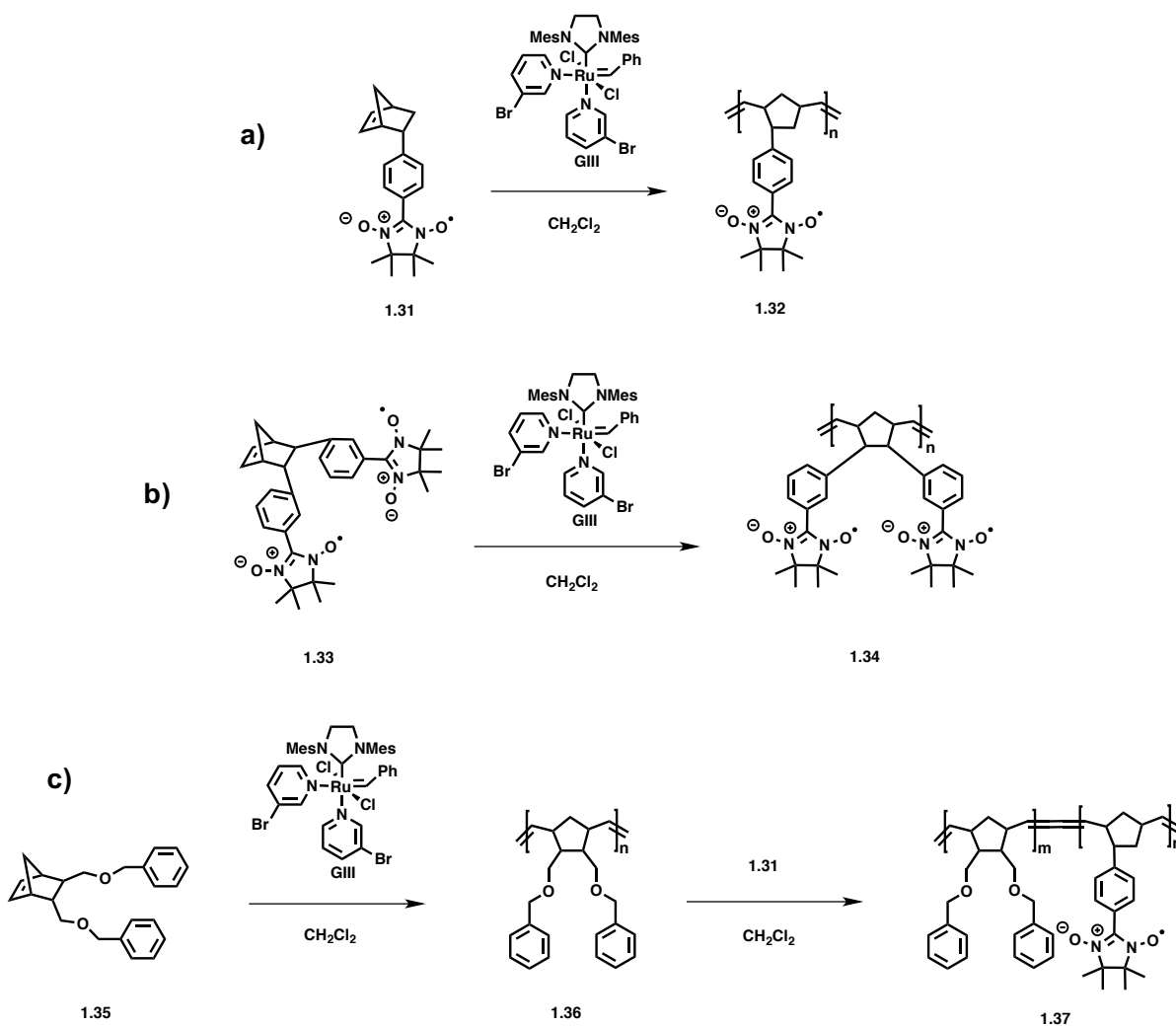


Scheme 1.7 Synthesis of nitronyl nitroxide polymer **1.28**.⁵³



Scheme 1.8 Synthesis of nitronyl nitroxide polymer **1.30**.⁵⁶

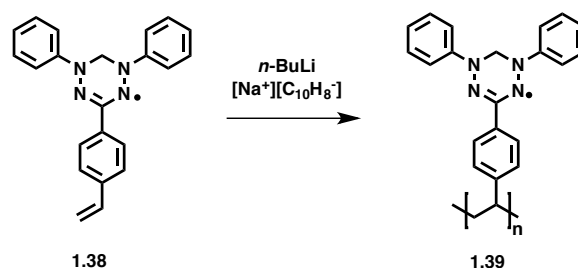
Nitronyl nitroxide polymers have also been synthesized using ROMP by the Nishide group. As opposed to free radical polymerizations, there is no protection required for the radical precursors as the 3-bromopyridine derivative of Grubbs 3rd generation catalyst (**GIII**) causes no observed side reactions with the monomers. The polymers were synthesized using both mono- and disubstituted norbornenes as the backbone allowing for the implantation of one or two radical moieties per monomer unit. ROMP of nitronyl nitroxide monomer **1.31** yielding polymer **1.32** was executed using **GIII** (Scheme 1.9a), while polymer **1.34** was synthesized in a similar manner starting from monomer **1.33** (Scheme 1.9b). The polymers possessed a narrow dispersity (D) of *ca.* 1.2, well-controlled molecular weights, and a high radical content (approx. 100%). The living polymerization character provided by ROMP also allowed for the polymerization of nitronyl nitroxide block co-polymers. The researchers first polymerized a dibenzylether norbornene **1.35** *via* ROMP using **GIII** yielding the norbornene polymer **1.36**, whereby *insitu* the researchers added nitronyl nitroxide monomer **1.31** in turn creating the block co-polymer **1.37** in high yields (>95%) (Scheme 1.9c). The ability to synthesise block co-polymers unlocks versatile methods for synthesizing well-defined nanostructured radical polymers for the use in various organic electronics.⁵⁷



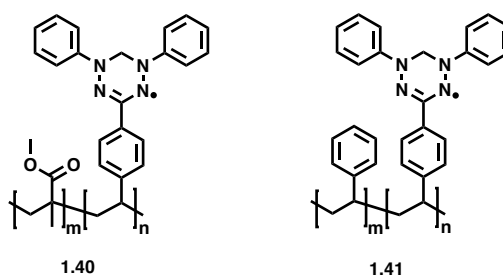
Scheme 1.9 (a) Synthesis of nitronyl nitroxide polymer **1.32**.³³ (b) Synthesis of nitroxide polymer **1.34**.³³ (c) Synthesis of nitronyl nitroxide block co-polymer **1.37**.⁵⁷

1.2.3 Verdazyl and Galvinoxyl Polymers

Verdazyl and galvinoxyl radicals have also been implemented in polymers, expanding the field past the more commonly found nitroxides and nitronyl nitroxides. Early verdazyl polymer examples include a polyvinyl verdazyl polymer and various co-polymers synthesized by Imoto *et al.*⁵⁸ Vinyl verdazyl monomer **1.38** was polymerized *via* anionic polymerization using *n*-butyllithium (*n*-BuLi) and sodium naphthalide as initiators yielding the verdazyl polymer **1.39**. Co-polymerizations with styrene and methyl methacrylate yielded verdazyl polymers **1.40** and **1.41**, respectively. Both homopolymers and copolymers were low-yielding with low radical content (30–60%).⁵⁸

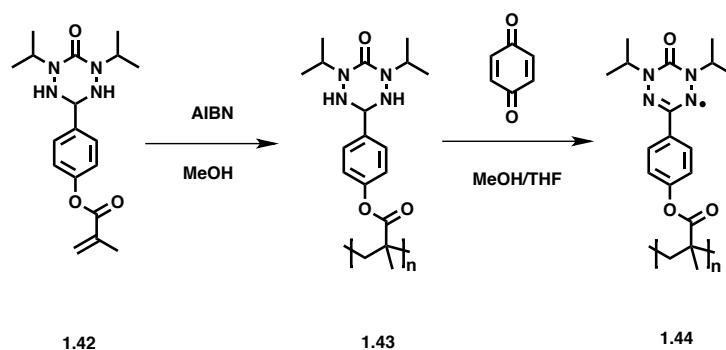


Scheme 1.10 Synthesis of vinyl-based verdazyl polymer **1.39**.⁵⁸

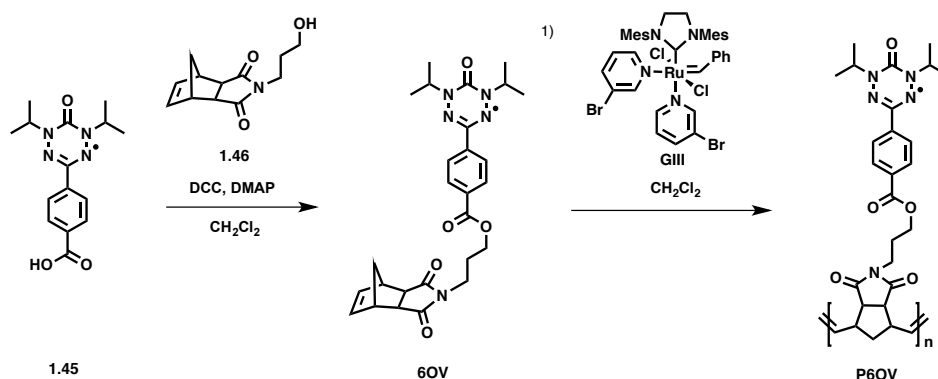


The Gilroy group has shown the first examples of 6-oxoverdazyl radicals being implemented into two different polymers and studied their spectrochemical, electrochemical, and thin-film properties.^{59, 60} The first 6-oxoverdazyl polymer was synthesized starting by the free radical polymerization of the phenyl methacrylate-substituted tetrazane **1.42** using AIBN to yield the corresponding tetrazane polymer **1.43**. Subsequent oxidation of polymer **1.43** with benzoquinone yielded the 6-oxoverdazyl polymer **1.44** (Scheme 1.11).⁵⁹ Cyclic voltammetry studies of polymer **1.44** showed that the polymer exhibited two reversible oxidation and reduction waves at half-wave potentials of 0.17 and -1.50 V with reference to the Fc/Fc^+ redox couple, respectively, rendering it as an ambipolar material. Polymer **1.44** formed uniform thin films with few defects, and inferred a high radical content present. The Gilroy group also synthesized norbornene derivative polymers of 6-oxoverdazyl polymers using ROMP (Scheme 1.12).⁶⁰ The 6-oxoverdazyl radical **1.45** was coupled to N-(3-hydroxypropyl)-*cis*-5-norbornene-*exo*-2,3-dicarboximide **1.46** through Steglich esterification yielding the monomer **6OV**. Polymerization of the norbornene-based 6-oxoverdazyl monomer **6OV** was done using **GIII** yielding **P6OV**. **P6OV** possessed D values of 1.13 indicating narrow dispersity. Studies of the ROMP behaviour was done using GPC to analyze the molecular weight growth as a function of time or amount of catalyst loading. The studies revealed a well-behaved but not

formally living polymerization indicating limited side reactions occurring during the process. Cyclic voltammetry studies of **P6OV** revealed oxidation and reduction potentials of 0.25 and -1.35 V with reference to the Fc/Fc^+ redox couple, respectively, yet again showing that these materials are ambipolar.



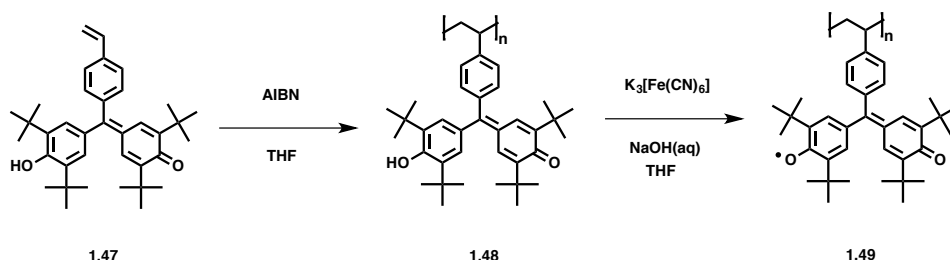
Scheme 1.11. Synthesis of 6-oxoverdazyl methacrylate-based polymer **1.44**.⁵⁹



Scheme 1.12. Synthesis of 6-oxoverdazyl norbornene-based polymer **P6OV**.⁶⁰

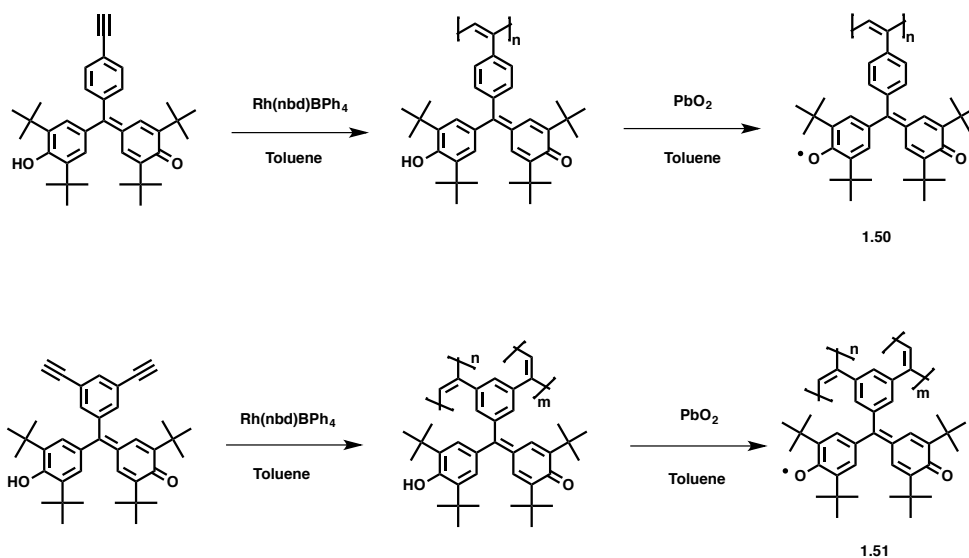
Galvinoxyl radicals have shown good stability towards their reduced phenolate anion form, leading them to be of interest towards n-type materials.⁶¹ Nishide and co-workers have shown the potential of galvinoxyl polymers as functional components of memristors⁵⁵ as well as anodic components of batteries.⁶² In both cases, the same styrene-based galvinoxyl polymer **1.49** was used (Scheme 1.13). Synthesis of **1.49** began by free radical polymerization of hydrogalvinoxyl styrene **1.47**, yielding the polymer precursor **1.48**. Subsequent oxidation using NaOH and potassium ferricyanide in CH_2Cl_2 yielded the galvinoxyl styrene polymer

1.49. An organic battery using **1.45** as the anodic material was fully charged in 10 seconds, exhibiting the fast redox processes of the radicals, however, the battery did have a low specific capacity when compared to conventional Li-ion batteries.⁶²



Scheme 1.13. Synthesis of styrene-based galvinoxyl polymer **1.49**.⁶²

Schubert and co-workers expanded upon the previous work by synthesizing the acetylene-based galvinoxyl polymers **1.50** and **1.51** using Rh-catalyzed polymerization and subsequent oxidation with PbO_2 (Scheme 1.14a,b).⁶³ Both polymers were used as anodic components of a fully organic battery with an aqueous electrolyte, with **PTMA** as the cathodic component. Once again, the relative specific capacity of the battery was low, however, the study showed the possibility of making cheap and non-hazardous organic batteries using an aqueous electrolyte with potential applications in biological environments.^{51, 63}



Scheme 1.14. (a) Synthesis of acetylene-based galvinoxyl polymer **1.50**. (b) Synthesis of acetylene-based galvinoxyl polymer **1.51**.

1.2.4 Radical Polymers for Use in Memristors

As highlighted in the previous subchapters, radical polymers are versatile materials used for the development of novel solid-state devices. Memristors are a new class of solid-state computing devices which possess high-performance memory effects, making them important for the advancement of new computer technologies. Memristors belong to the same class of passive circuit elements (electrical components which do not generate power but instead dissipate, store and/or release it) such as resistors, capacitors and inductors. Through different chemical processing, memristors can be constructed to possess non-volatile or volatile memory effects.⁶⁴ Non-volatile memory effects indicate that the upon the application of an external voltage, memristors retain their resistance states after the removal of said voltage. These stable resistance states indicate that these devices can be used as long-term data storage units. The most common non-volatile memory devices are writable once readable multiple times (WORM). In comparison, flash memories which can be writable, readable, and erasable multiple times are more appealing, however their production cost is high.⁶⁴ Memristors with volatile memory do not maintain their resistance state and relax down to a thermodynamically stable thermal state, and thus do not store data after the voltage is removed. These types of memory devices have been of use in the simulation of biological synapses.⁶⁵

Memristor devices are built using electrodes and an active switching layer. The active switching layer is typically composed of dielectrics, which are insulating materials which can be polarized upon placement in an electric field. The majority of memristors use binary oxide materials (*i.e.*, SiO₂, TiO₂, ZnO) as the dielectrics. More recently, organic radical polymers have been highlighted as good potential candidates as dielectrics due to the ease of production through wet-process fabrication, as well as the ability of the polymers to form smooth, thin films, which are required to minimize the size of the devices.^{36, 55} However, most current organic memristor devices require additional layers to achieve high cycling numbers and durability, increasing their thickness as a result.⁵⁵

In a recent study, ultrathin (10 nm) memristor devices using **P6OV** as the active material were constructed by Gilroy, Fanchini and co-workers (Figure 1.7).⁵⁴ The memristor devices were composed of four aluminum/calcium (Al/Ca) anodes and four cathodes which were

individually tested (indium tin oxide (ITO), few-layer graphene (FLG), aluminum (Al), and Al/Ca), and **P6OV** as the functional component (Figure 1.8). The memristor fabricated with the Al cathode highlighted write-once-read-many (WORM) memory effects, while the memristor devices containing the ITO cathode exhibited flash memory effects, where the device could be writable, readable, and erasable up to 10^3 times without significant degradation.⁵⁴ This is an important finding as current organic memristors are most commonly limited to WORM memory effects while still also requiring additional layers to access multiple write-read-erase cycles.

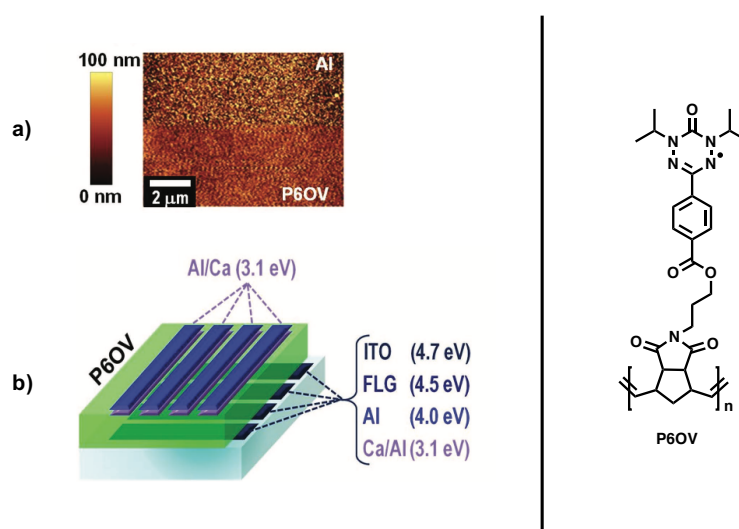


Figure 1.8. (a) AFM image of **P6OV** thin film and Al contact. (b) Memristor device architecture. The structure of **P6OV** is shown on the right. Images reproduced with permission from Ref 54.

1.3 Scope of Thesis

This thesis will focus on the synthesis and characterization of a novel nitronyl nitroxide-based monomer as well as its incorporation into homo, block and random copolymers using ROMP. The spectrochemical, electrochemical and thermal properties of the polymers will be investigated, alongside with their behavior in simple solid-state devices.

A recent study in the Gilroy and Fanchini groups presented a norbornene-substituted 6-oxoverdazyl radical polymer with remarkable memristive effects, making the polymer a good candidate for bistable electronics.⁶⁰ Previous studies of ROMP process of the norbornene

backbone of the polymer using Grubbs' 3rd generation catalyst exhibited well-behaved and controllable polymerizations.^{66, 67} The control and versatility that the norbornene backbone offers allows for an enhanced tunability for organic radical polymers. Nitronyl nitroxides are a family of stable radicals with interesting ambipolar redox properties, which have been not as widely studied when compared to their nitroxide counterparts. Henceforth, there is a need for further studies on nitronyl nitroxide polymer systems to better understand their physical and electrochemical properties.

Chapter 2 will focus on the synthesis and characterization of a nitronyl nitroxide radical monomer and its corresponding polymer. This chapter entails details about the behaviour of the ROMP reaction, exploring the tolerability of the radical to side reactions. ATR FT-IR and UV-Vis spectroscopy studies of the monomer and polymer also reveal that the radical survived the polymerization process. Electron paramagnetic resonance (EPR) spectroscopy studies revealed that there was a high radical content incorporation in the polymer. Thus, the development of bistable memory devices was executed.

Chapter 3 will focus on the copolymerization of nitronyl nitroxide and 6-oxoverdayzl radical monomers making block and random copolymers *via* ROMP. The copolymers were fully characterized and their redox properties were studied. During the studies, it was found that the order of polymerization was crucial for successful copolymerizations. Cyclic voltammetry studies revealed that, upon copolymerization, the oxidation and reduction events were still observed, corresponding to the potentials of their homopolymer counterparts. These findings set the stage for performance benchmarking in memristors.

1.4 References

- (1) Stuart, M. A. C.; Huck, W. T. S.; Genzer, J.; Müller, M.; Ober, C.; Stamm, M.; Sukhorukov, G. B.; Szleifer, I.; Tsukruk, V. V.; Urban, M.; Winnik, F.; Zauscher, S.; Luzinov, I.; Minko, S. *Nat. Mater.* **2010**, *9*, 101–113.
- (2) Sekine, C.; Tsubata, Y.; Yamada, T.; Kitano, M.; Doi, S. *Sci. Technol. Adv. Mater.* **2014**, *15*, 1–15.

- (3) Aminabhavi, T. M.; Balundgi, R. H.; Cassidy, P. E. *Polym. Plast. Technol. Eng.* **1990**, *29*, 235–262.
- (4) Hicks, R. G. *Org. Biomol. Chem.* **2007**, *5*, 1321–1338.
- (5) Hicks, R. G. *Stable radicals : fundamentals and applied aspects of odd-electron compounds*. Chichester, UK, 2010.
- (6) Gomberg, M. *J. Am. Chem. Soc.* **1900**, *22*, 757–771.
- (7) Ballester, M.; Riera, J.; Castaner, J.; Badia, C.; Monso, J. M. *J. Am. Chem. Soc.* **1971**, *93*, 2215–2225.
- (8) Power, P. P. *Chem. Rev.* **2003**, *103*, 789–810.
- (9) Kurosaki, T.; Lee, K. W.; Okawara, M. *J. Polym. Sci., Part A: Polym. Chem.* **1972**, *10*, 3295–3310.
- (10) Kurata, T.; Koshika, K.; Kato, F.; Kido, J.; Nishide, H. *Polyhedron* **2007**, *26*, 1776–1780.
- (11) Lee, J.; Lee, E.; Kim, S.; Bang, G. S.; Shultz, D. A.; Schmidt, R. D.; Forbes, M. D.; Lee, H. *Angew. Chem. Int. Ed.* **2011**, *50*, 4414–4418.
- (12) Gilroy, J.; Workentin, M.; Barbon, S.; Gobbo, P.; Luo, W.; Price, J.; Biesinger, M. *Synlett.* **2015**, *27*, 304–308.
- (13) Suzuki, S.; Nakamura, F.; Naota, T. *Mater. Chem. Front.* **2018**, *2*, 591–596.
- (14) Qu, J.; Katsumata, T.; Satoh, M.; Wada, J.; Masuda, T. *Macromolecules* **2007**, *40*, 3136–3144.
- (15) Petunin, P. V.; Martynko, E. A.; Trusova, M. E.; Kazantsev, M. S.; Rybalova, T. V.; Valiev, R. R.; Uvarov, M. N.; Mostovich, E. A.; Postnikov, P. S. *Eur. J. Org. Chem.* **2018**, *2018*, 4802–4811.
- (16) Gilroy, J. B.; McKinnon, S. D. J.; Koivisto, B. D.; Hicks, R. G. *Org. Lett.* **2007**, *9*, 4837–4840.
- (17) Berry, D. E.; Hicks, R. G.; Gilroy, J. B. *J. Chem. Educ.* **2009**, *86*, 76–79.
- (18) Coppinger, G. M. *Tetrahedron* **1962**, *18*, 61–62.
- (19) Jähnert, T.; Häupler, B.; Janoschka, T.; Hager, M. D.; Schubert, U. S. *Macromol. Rapid Commun.* **2014**, *35*, 882–887.
- (20) Foti, M.; Ingold, K. U.; Luszytk, J. *J. Am. Chem. Soc.* **1994**, *116*, 9440–9447.
- (21) Samuni, U.; Samuni, Y.; Goldstein, S. *J. Am. Chem. Soc.* **2010**, *132*, 8428–8432.
- (22) Merbouh, N.; Bobbitt, J. M.; Bruckner, C. *Org. Prep. Proced. Int.* **2004**, *36*, 1–26.

- (23) Pei, D. J.; Hong, J. Q.; Lin, F.; Shi, Z.; Chen, Z. X.; Nie, H. Y.; Guo, X. Q. *Chem. Commun.* **2011**, *47*, 9492–9494.
- (24) Rajca, A.; Wang, Y.; Boska, M.; Paletta, J. T.; Olankitwanit, A.; Swanson, M. A.; Mitchell, D. G.; Eaton, S. S.; Eaton, G. R.; Rajca, S. *J. Am. Chem. Soc.* **2012**, *134*, 15724–15727.
- (25) Sowers, M. A.; McCombs, J. R.; Wang, Y.; Paletta, J. T.; Morton, S. W.; Dreaden, E. C.; Boska, M. D.; Ottaviani, M. F.; Hammond, P. T.; Rajca, A.; Johnson, J. A. *Nat. Commun.* **2014**, *5*, 1–9.
- (26) Yoshitomi, T.; Miyamoto, D.; Nagasaki, Y. *Biomacromolecules* **2009**, *10*, 596–601.
- (27) Yoshitomi, T.; Suzuki, R.; Mamiya, T.; Matsui, H.; Hirayama, A.; Nagasaki, Y. *Bioconjugate Chem* **2009**, *20*, 1792–1798.
- (28) Shi, Y.; Nabae, Y.; Hayakawa, T.; Kakimoto, M. A. *RSC Adv.* **2015**, *5*, 1923–1928.
- (29) Liu, Y. J.; Wang, X. P.; Song, W. G.; Wang, G. W. *Polym. Chem.* **2015**, *6*, 7514–7523.
- (30) Nishide, H.; Oyaizu, K. *Science* **2008**, *319*, 737–738.
- (31) Oyaizu, K.; Nishide, H. *Adv. Mater.* **2009**, *21*, 2339–2344.
- (32) Nakahara, K.; Oyaizu, K.; Nishide, H. *Chem. Lett.* **2011**, *40*, 222–227.
- (33) Sukegawa, T.; Kai, A.; Oyaizu, K.; Nishide, H. *Macromolecules* **2013**, *46*, 1361–1367.
- (34) Gracia, R.; Mecerreyes, D. *Polym. Chem.* **2013**, *4*, 2206–2214.
- (35) Wang, S.; Li, F.; Easley, A. D.; Lutkenhaus, J. L. *Nat. Mater.* **2019**, *18*, 69–75.
- (36) Suga, T.; Sakata, M.; Aoki, K.; Nishide, H. *ACS Macro Lett.* **2014**, *3*, 703–707.
- (37) Suguro, M.; Iwasa, S.; Kusachi, Y.; Morioka, Y.; Nakahara, K. *Macromol. Rapid Commun.* **2007**, *28*, 1929–1933.
- (38) Nishide, H.; Iwasa, S.; Pu, Y. J.; Suga, T.; Nakahara, K.; Satoh, M. *Electrochim. Acta* **2004**, *50*, 827–831.
- (39) Jia, Z.; Fu, Q.; Huang, J. *J. Polym. Sci., Part A: Polym. Chem.* **2006**, *44*, 3836–3842.
- (40) Katsumata, T.; Qu, J.; Shiotsuki, M.; Satoh, M.; Wada, J.; Igarashi, J.; Mizoguchi, K.; Masuda, T. *Macromolecules* **2008**, *41*, 1175–1183.
- (41) Nakahara, K.; Iwasa, S.; Satoh, M.; Morioka, Y.; Iriyama, J.; Suguro, M.; Hasegawa, E. *Chem. Phys. Lett.* **2002**, *359*, 351–354.
- (42) Nishide, H.; Suga, T. *Electrochem. Soc. Interface* **2006**, *14*, 32–36.

- (43) Suga, T.; Konishi, H.; Nishide, H. *Chem. Commun.* **2007**, 1730–1732.
- (44) Baradwaj, A. G.; Rostro, L.; Boudouris, B. W. *Macromol. Chem. Phys.* **2016**, *217*, 477–484.
- (45) Suga, T.; Pu, Y.-J.; Kasatori, S.; Nishide, H. *Macromolecules* **2007**, *40*, 3167–3173.
- (46) Zhang, Y.; Park, A.; Cintora, A.; McMillan, S. R.; Harmon, N. J.; Moehle, A.; Flatté, M. E.; Fuchs, G. D.; Ober, C. K. *J. Mater. Chem. C* **2018**, *6*, 111–118.
- (47) Katsumata, T.; Satoh, M.; Wada, J.; Shiotsuki, M.; Sanda, F.; Masuda, T. *Macromol. Rapid Commun.* **2006**, *27*, 1206–1211.
- (48) Koshika, K.; Chikushi, N.; Sano, N.; Oyaizu, K.; Nishide, H. *Green Chem.* **2010**, *12*, 1573–1575.
- (49) Joo, Y.; Agarkar, V.; Sung, S. H.; Savoie, B. M.; Boudouris, B. W. *Science* **2018**, *359*, 1391–1395.
- (50) Kaur, G.; Adhikari, R.; Cass, P.; Bown, M.; Gunatillake, P. *RSC Adv.* **2015**, *5*, 37553–37567.
- (51) Janoschka, T.; Martin, N.; Martin, U.; Friebe, C.; Morgenstern, S.; Hiller, H.; Hager, M. D.; Schubert, U. S. *Nature* **2015**, *527*, 78–81.
- (52) Muench, S.; Wild, A.; Friebe, C.; Haupler, B.; Janoschka, T.; Schubert, U. S. *Chem. Rev.* **2016**, *116*, 9438–9484.
- (53) Suga, T.; Sugita, S.; Ohshiro, H.; Oyaizu, K.; Nishide, H. *Adv. Mater.* **2011**, *23*, 751–754.
- (54) Ezugwu, S.; Paquette, J. A.; Yadav, V.; Gilroy, J. B.; Fanchini, G. *Adv. Electron. Mater.* **2016**, *2*, 1600253.
- (55) Yonekuta, Y.; Susuki, K.; Oyaizu, K.; Honda, K.; Nishide, H. *J. Am. Chem. Soc.* **2007**, *129*, 14128–14129.
- (56) Oyaizu, K.; Sukegawa, T.; Nishide, H. *Chem. Lett.* **2011**, *40*, 184–185.
- (57) Suga, T.; Takeuchi, S.; Nishide, H. *Adv. Mater.* **2011**, *23*, 5545–5549.
- (58) Miura, Y.; Kinoshita, M.; Imoto, M. *Makromol. Chem.* **1971**, *146*, 69–77.
- (59) Price, J. T.; Paquette, J. A.; Harrison, C. S.; Bauld, R.; Fanchini, G.; Gilroy, J. B. *Polym. Chem.* **2014**, *5*, 5223–5226.
- (60) Paquette, J. A.; Ezugwu, S.; Yadav, V.; Fanchini, G.; Gilroy, J. B. *J. Polym. Sci., Part A: Polym. Chem.* **2016**, *54*, 1803–1813.

- (61) Kaneko, T.; Tatsumi, H.; Aoki, T.; Oikawa, E.; Yoshiki, H.; Yoshioka, N.; Tsuchida, E.; Nishide, H. *J. Polym. Sci., Part A: Polym. Chem.* **1999**, *37*, 189–198.
- (62) Suga, T.; Ohshiro, H.; Sugita, S.; Oyaizu, K.; Nishide, H. *Adv. Mater.* **2009**, *21*, 1627–1630.
- (63) Jähnert, T.; Häupler, B.; Janoschka, T.; Hager, M. D.; Schubert, U. S. *Macromol. Chem. Phys.* **2013**, *214*, 2616–2623.
- (64) Sun, W.; Gao, B.; Chi, M.; Xia, Q.; Yang, J. J.; Qian, H.; Wu, H. *Nat. Commun.* **2019**, *10*, 1–13.
- (65) Wang, Z.; Joshi, S.; Savel'ev, S. E.; Jiang, H.; Midya, R.; Lin, P.; Hu, M.; Ge, N.; Strachan, J. P.; Li, Z.; Wu, Q.; Barnell, M.; Li, G.-L.; Xin, H. L.; Williams, R. S.; Xia, Q.; Yang, J. J. *Nat. Mater.* **2017**, *16*, 101–108.
- (66) Ren, L.; Zhang, J.; Bai, X.; Hardy, C. G.; Shimizu, K. D.; Tang, C. *Chem. Sci.* **2012**, *3*, 580–583.
- (67) Love, J. A.; Morgan, J. P.; Trnka, T. M.; Grubbs, R. H. *Angew. Chem. Int. Ed.* **2002**, *41*, 4035–4037.

Chapter 2

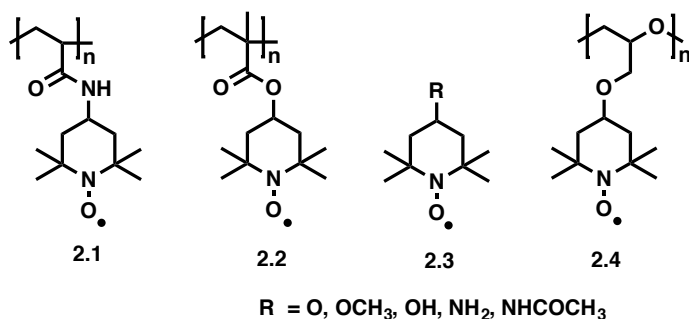
2 Synthesis and Characterization of Nitronyl Nitroxide Polymers *via* ROMP

Adapted from:

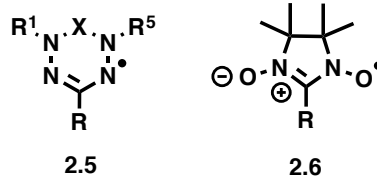
Anghel, M., Magnan, F.; Catingan, S. D.; McCready, M.A.; Aawani, E.; Wong, V.; Singh, D.; Fanchini G.; and Gilroy, J.B. *J. Polym. Sci.* **2020**, *58*, 309–319.

2.1 Introduction

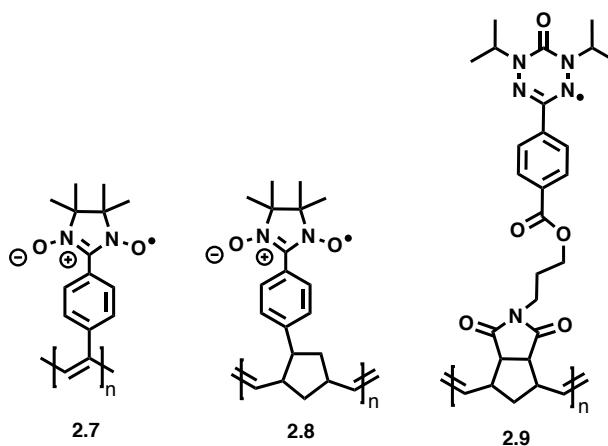
Varying the functional groups present in polymers can drastically change their properties, and, in turn, their applications ranging from stimuli-response to fluorescent materials.^{1,2} One set of unique polymers incorporate stable organic radical functional groups, deemed as stable radical polymers.^{3, 4} These polymers consist of redox-active radical moieties being pendent along either a conjugated or non-conjugated polymer backbone. The redox properties of radical polymers has allowed them to find their widespread use as the electrode active material in organic batteries.⁵⁻⁸ This is due to the rapid charge-discharge rates that radical polymers possess, alongside the flexibility and stability of their non-conjugated backbones. Two examples of stable radical polymers used in organic radical batteries are poly(2,2,6,6-tetramethylpiperidinyloxy methacrylate) **PTMA 2.1**⁹ and poly(2,2,6,6-tetramethylpiperidinyloxy-4-yl acrylamide) (**PTAm 2.2**)¹⁰. These polymers have been the most widely studied in the field largely due to the commercial availability of the TEMPO **2.3** radical precursor. A recent study by Boudouris *et al.* has shown that radical polymers can be fine-tuned to possess high electrical conductivity, where TEMPO-based polymer **2.4** had an electrical conductivity three orders of magnitude higher (0.2 S cm^{-1}) than the highest literature value reported to that date.¹¹ This was a surprising find as typically radical polymers are thought of as insulators rather than semi-conductors. The combination of thermal stability, high optical transparency and good conductivity made this polymer an ideal candidate for use as a solid-state conducting polymer, rivaling the more prevalent polymers in literature which possess highly conjugated backbones.



A common theme amongst the examples discussed above is the lack of diversity in radical species. Organic radicals such as nitronyl nitroxide **2.5** and oxoverdazyl **2.6** have not received as much attention across the literature. Nitronyl nitroxide radical polymers **2.7**¹² and **2.8**¹³ have seen use as anodic and cathodic material in organic radical batteries owing to their ambipolar redox properties. Previous studies in the Gilroy group explored the synthesis and characterization of 6-oxoverdazyl polymer **2.9**.¹⁴ This polymer was synthesized with controllable and narrow molecular weight distributions and was fabricated into thin-films. Polymer **2.9** was incorporated into a single-layer organic flash memristor device which showed bistable flash memory effects.¹⁵ Henceforth, there is a need for further studies on radical polymers to gain a better fundamental understanding to the charge transport properties and redox activity of these unique systems, as there are a multitude of possible applications.



$X = CO, CS, CH_2, CHAr$
 $R = aryl \text{ or } alkyl$



Herein, a novel nitronyl nitroxide polymer is synthesized using ring-opening metathesis polymerization (ROMP) and fully characterized by spectroscopic and electrochemical techniques. Conductivity studies for sandwich-type devices incorporating thin-films of the polymer are also presented.

2.2 Results and Discussion

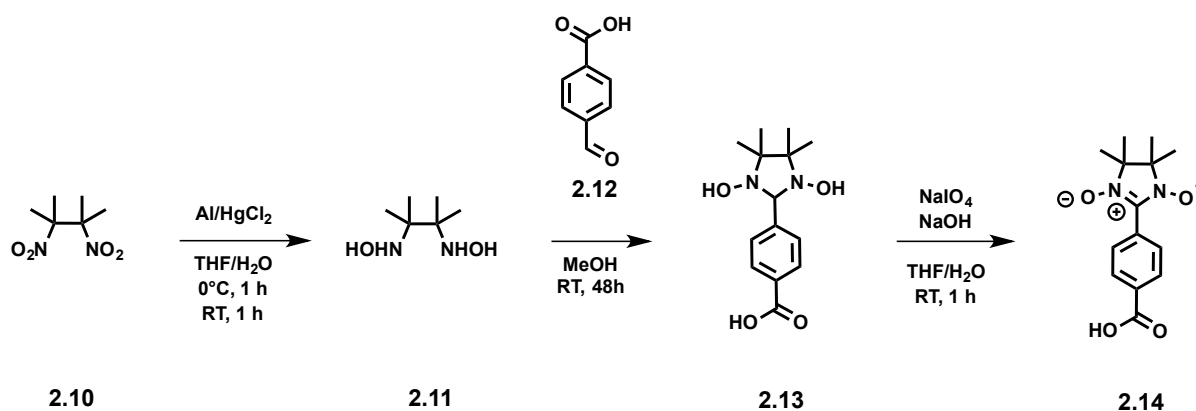
2.2.1 Synthesis of Nitronyl Nitroxide Monomer and Polymer

The precursors to the nitronyl nitroxide monomer as well as the radical itself, were synthesized following published procedures^{16, 17} with slight modifications. The reduction of the dinitrobutane precursor **2.10** to yield bishydroxylamine **2.11** was performed using a mercury/aluminum amalgam in THF/H₂O media providing a yield range of 55–65 % (Scheme 2.1). It was found that leaving the reaction to stir for 2 h total time reduced the amount of the half-reduced intermediate significantly, thus making purification simpler. The reduced product was characterized by ¹H NMR spectroscopy, with chemical shift values of the protons matching those of the literature.¹⁷

The condensation reaction of **2.11** with 4-formylbenzoic acid **2.12** was carried out in MeOH while stirring at RT for 48 h yielding **2.13** in 65–80 % (Scheme 2.1). It is to be noted that, as opposed to the literature report,¹⁶ these reactions were done at RT in smaller scales as well as in the absence of Na₂CO₃, while providing similar, if not, better yields. The product was characterized by ¹H and ¹³C{¹H} NMR spectroscopy, with ¹H NMR chemical shift values matching those of literature.¹⁶

Oxidation of **2.13** to **2.14** was completed using THF/H₂O solvent media, 1 M NaOH, and NaIO₄. The reaction was monitored by thin-layer chromatography, which indicated reaction completion at the 1 h mark. In contrast to the procedure found in the literature,¹⁶ a base (NaOH) was employed with the aim to improve the yield. It was found that the use of NaOH helped increase the yield by 15–20% from ~50% to ~70%. When separating the phases during the work up, the aqueous layer took on a violet colour, attributed to a carboxylate anion intermediate formed upon deprotonation by NaOH,¹⁸ while the organic phase (EtOAc) was clear and colourless. Following the addition of 1 M HCl, phase transfer from the aqueous layer to the organic was observed as the organic phase exhibited a dark blue colour while the aqueous phase took on a dark yellow colour.

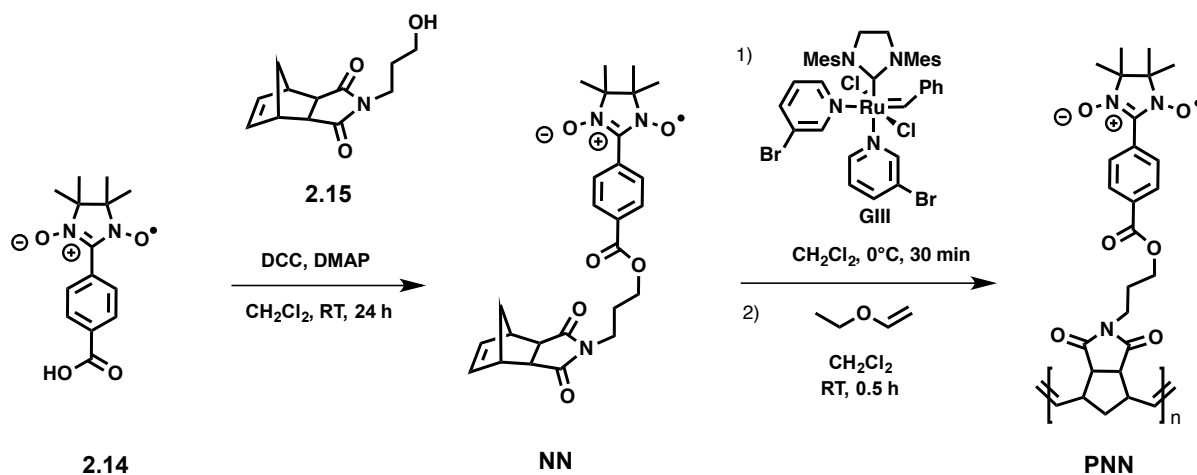
Due to the radical nature of some of the compounds, NMR spectroscopy was unavailable as a characterization technique. The range for $\nu(\text{N-O}\cdot)$ stretches observed using FT-IR spectroscopy of nitronyl nitroxides fall between 1450–1340 cm⁻¹, however, determining a specific N-O• stretching frequency for nitronyl nitroxides can be difficult due to strong coupling between vibrations of the N-O bond with those of the phenyl ring, C-N bonds, and methyl groups.¹⁹ Compound **2.14** possessed a $\nu(\text{N-O}\cdot)$ present at 1340 cm⁻¹ which was in accordance to literature values.¹⁹



Scheme 2.1. Synthetic route for nitronyl nitroxide radical **2.14**.

Monomer synthesis was conducted in a similar fashion as to a previously reported norbornene-functionalized 6-oxoverdazyl radical from the Gilroy group (Scheme 2.2).¹⁴ The nitronyl nitroxide radical **2.14** was coupled to N-(3-hydroxypropyl)-*cis*-5-norbornene-*exo*-2,3-

dicarboximide **2.15**²⁰ through Steglich esterification using dicyclohexylcarbodiimide (DCC), and 4-*N,N*-dimethylaminopyridine (DMAP) in CH₂Cl₂ affording NN in 60–70% yield. NN was polymerized by ring-opening metathesis polymerization (ROMP). The polymerization was initiated by rapid addition of a solution of the 3-bromopyridine derivative of Grubbs' 3rd generation catalyst (**GIII**) to a stirring dry and degassed CH₂Cl₂ solution of NN at 0 °C. The polymerization yielded PNN in 80–90% yield ($M_n = 51,400 \text{ g mol}^{-1}$, $M_w = 60,600 \text{ g mol}^{-1}$, $D = 1.18$).



Scheme 2.2. Synthesis of monomer NN and polymer PNN.

The IR spectra of NN and PNN revealed a broadening of signals in the carbonyl region at 1774 cm⁻¹, and 1697 cm⁻¹. The N-O• stretching frequency at 1360 cm⁻¹ was present in both monomer and polymer spectra, indicating survival of the radical throughout the polymerization process (Figure 2.1).

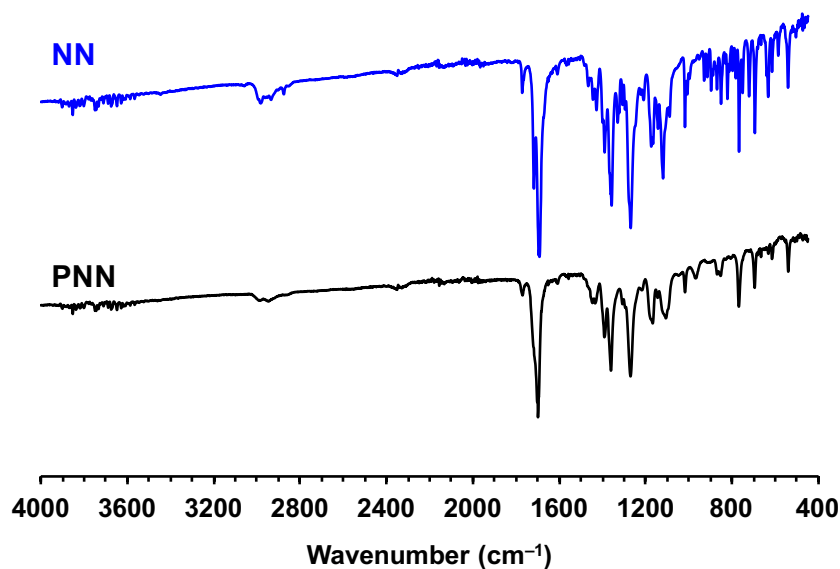


Figure 2.1. FT-IR spectra of NN (blue) and PNN (black).

Comparison of the UV-visible absorption spectra of NN and PNN showed a close resemblance in absorption features (Figure 2.2). The molar absorptivity values for NN were obtained by dividing the absorbance values by the concentration of the monomer solution analyzed. In the case of the polymer, it was assumed that each repeating unit possessed a lone electron, thus when calculating the concentrations, the molecular weight of the polymer was the same as one monomer unit. The nitronyl nitroxide radical presented three different absorption features, at 602 nm ($\epsilon = 300 \text{ M}^{-1} \text{ cm}^{-1}$), 380 nm ($\epsilon = 11,300 \text{ M}^{-1} \text{ cm}^{-1}$), and 365 nm ($\epsilon = 6,000 \text{ M}^{-1} \text{ cm}^{-1}$) while the polymeric backbone absorbed at 295 nm ($\epsilon = 14,000 \text{ M}^{-1} \text{ cm}^{-1}$). When closely examining the region between 450 and 800 nm (Figure 2.2b), the absorption feature at 602 nm appears to possess three distinct absorption features. Each feature is attributed to an electronic transition for the nitronyl nitroxide radical with the three possible transitions being SOMO→LUMO, HOMO→SOMO or HOMO→LUMO. Based on UV-Vis absorption, the polymer incorporates a radical content of approximately 97% per comparison of molar extinction coefficient values between monomer and polymer.

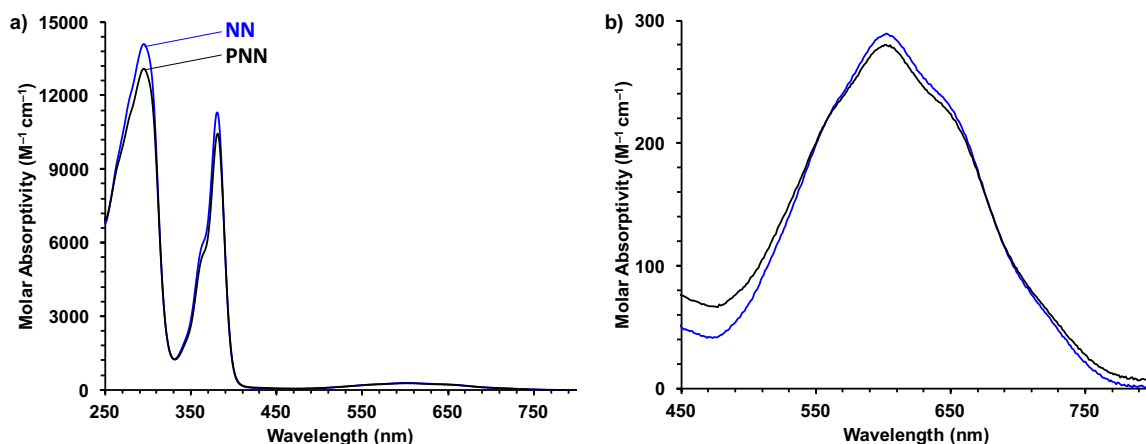


Figure 2.2. UV-vis absorption spectrum of NN (blue) vs. PNN (black) (a). Zoomed inset for absorption region between 450-800 nm (b) shows that the two absorption regions are in very close agreement with 97% radical loading in the polymer as per extinction coefficient ratios.

To further confirm the presence of nitronyl nitroxide radicals in both monomer and polymer, electron paramagnetic resonance (EPR) spectroscopy was performed to quantitatively determine the number of nitronyl nitroxide radical units present in PNN. This was done by comparing the integration of the EPR spectra between a TEMPO polymer containing an assumed one lone electron per monomer unit to PNN. This experiment showed that approximately 97% of the repeating units in the polymer contained an unpaired electron, thus supporting the previous IR and UV-Vis absorption claims. The EPR spectrum of NN showed a typical five-line pattern found for nitronyl nitroxide radicals, with the lone electron coupling to two equivalent nitrogen atoms. Using EasySpin software²¹ that's part of the MATLAB program, a simulation of the EPR of the monomer provided these parameters for NN: $g = 2.0060$, line width = 0.120 mT, $a_{N1} = 0.754$ mT.²¹ These values are closely related to those found for other nitronyl nitroxides.²² A broad isotropic EPR signal was observed for PNN, as is expected for a polymer due to the proximity of the radicals. The three spectra are presented in Figure 2.3.

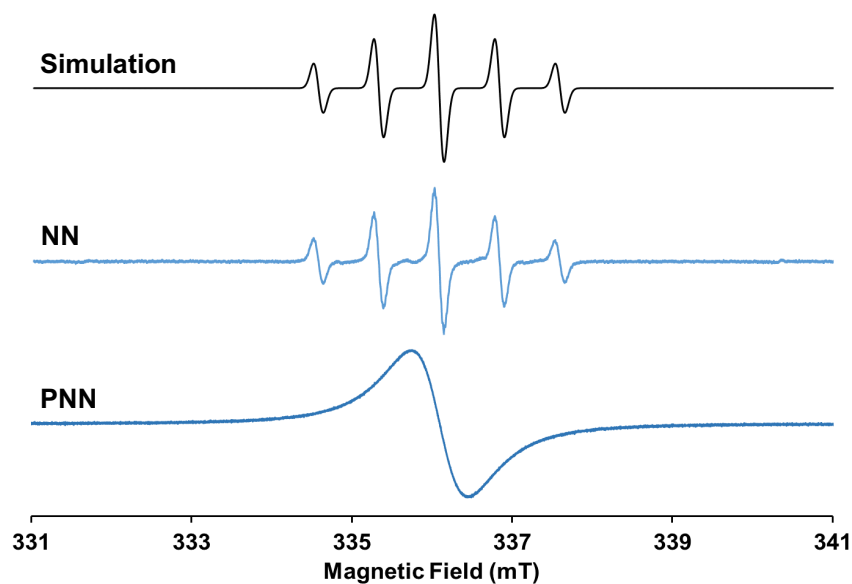


Figure 2.3. Simulated EPR spectrum of **NN** (top), experimental spectrum of **NN** (middle), and experimental spectrum of **PNN** (bottom). Simulation of the spectrum of **NN** yielded these parameters: linewidth = 0.120 mT, $a_{N1} = 0.754$ mT, $g = 2.0060$.

The molecular weight of the polymer was determined by gel permeation chromatography (GPC). Figure 2.4 shows a GPC trace for **PNN** prepared with a feed molar ratio of 100 (monomer:catalyst = 100:1) following the polymer preparation described in experimental section [number average molecular weight (M_n) = 51,400 g mol⁻¹, weight average molecular weight (M_w) = 60,600 g mol⁻¹, dispersity (D) = 1.18.]. A small, high molecular weight shoulder was sometimes observed in the GPC traces, which is assumed to be the result of chain-coupling or similar reactions during the termination step of the polymerization. This is a consistent finding with similar organic radical polymers published by the Gilroy group.¹⁴

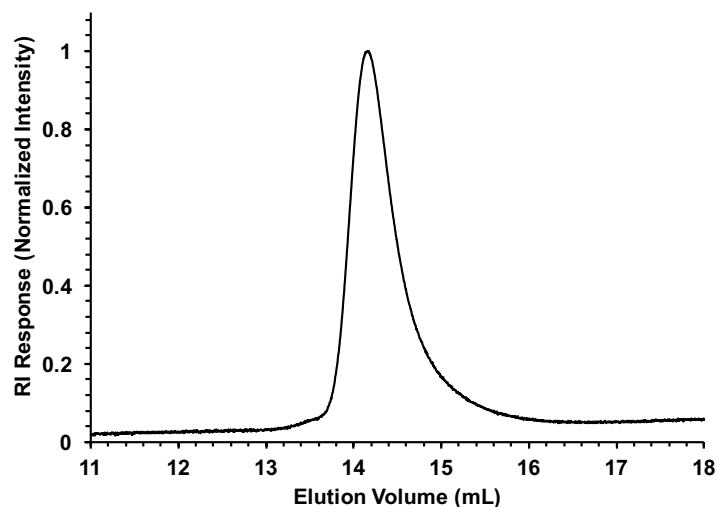


Figure 2.4. GPC trace for a representative sample of PNN ($M_n = 51,400 \text{ g mol}^{-1}$, $M_w = 60,600 \text{ g mol}^{-1}$, $D = 1.18$).

2.2.2 ROMP Studies for NN

Two different experiments were employed to study the polymerization of NN: one to study the reaction progression as a function of time and another to study the reaction as a function of monomer:catalyst ratio. These experiments provide further insight into the ROMP efficiency and compatibility with NN. Traditionally, ^1H NMR spectroscopy is used to help observe the monomer consumption over time as well as the number average degree of polymerization (DP_n), however, due to the radical nature of the polymer this characterization method was unavailable. Thus, GPC analysis was the sole data source for the molecular weights described in these studies.

The timed study examined the behavior of a single ROMP reaction (monomer:catalyst 100:1) where different timed aliquots were analyzed (Figure 2.5a). The aliquots were taken at seven different times. The molecular weight of the polymer samples increased in a non-linear fashion as a function of time, with very small differences in weight between the last three time intervals. This result implies that the rate of elongation decreased over time, consistent with lower concentration of monomer being present as the reaction proceeded. The dispersity (D) of the polymer samples also gradually increased, topping off at a value of 1.18, which indicates relatively monodisperse polymers despite the longer chain lengths. No side reactions were

observed and the ROMP behavior for this system can be described as well-behaved, but not formally living.

The catalyst loading study involved the ROMP of NN at five varying molar feed stock ratios (Figure 2.5b). The GPC traces for the study are presented in Figure 2.5c. The colours of the traces are directly correlated to the colour of the data points in Figure 2.5b. The higher molecular weight polymers eluted faster, and presented broader traces. There were no high molecular weight shoulders found in the GPC traces, indicating no cross-linking or chain-coupling occurred during polymerization. The values of the degree of polymerization (DP_n) increased steadily over time as expected, indicating the formation of longer chains with smaller catalyst amounts. A linear line was plotted on the graph, representing the theoretical relationship between DP_n and feed molar ratio. When comparing the data acquired to the theoretical line, there is a deviation from ideal behavior indicating that the chains were longer than expected. This could be a result of systemic overestimation of the molecular weights by the GPC technique which employs conventional calibration versus polystyrene standards. The rapid chain initiation, constant rate growth and relatively low dispersity are all characteristics of well-behaved ROMP. Thus, this polymerization process provides good precision and control over molecular weight and dispersity of the polymers.

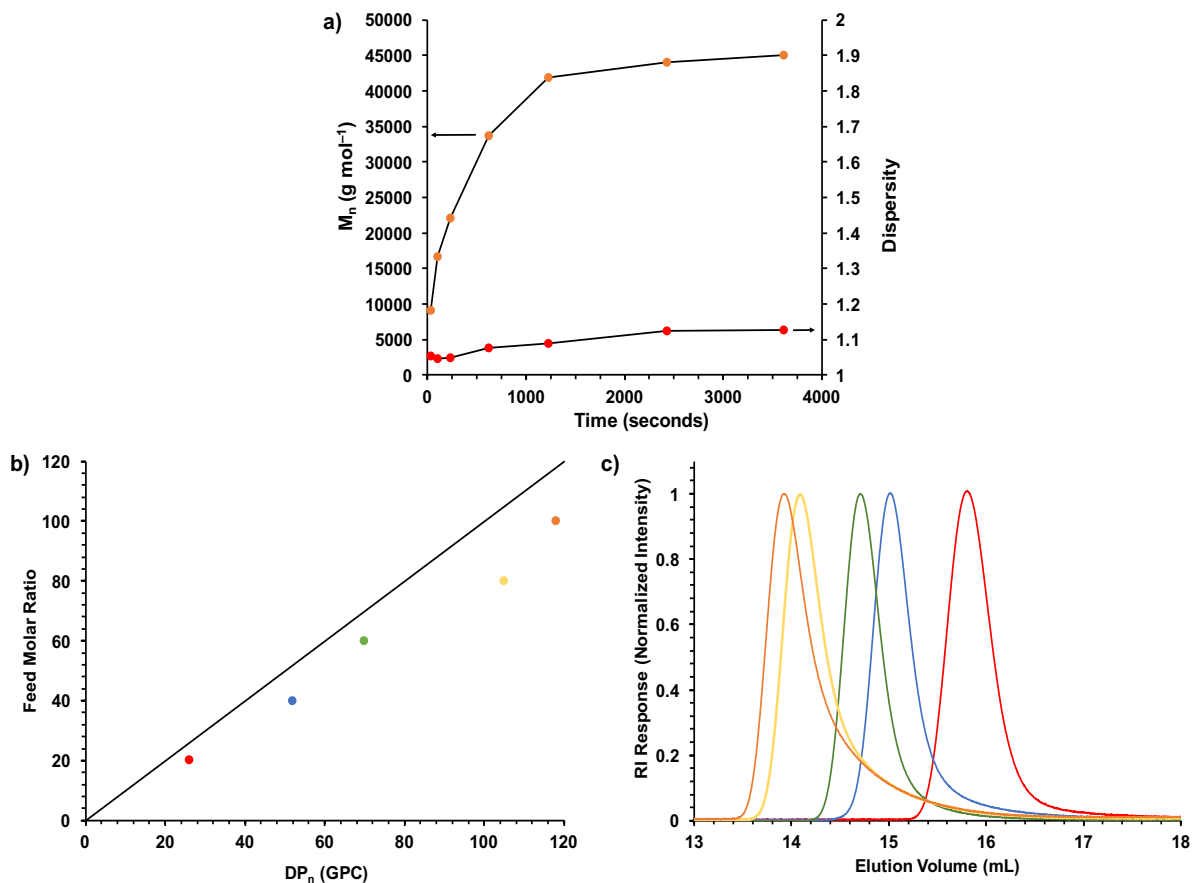


Figure 2.5 (a) Molecular weight (M_n) and dispersity as a function of reaction time. (b) The relationship between feed molar ratio and the DP_n of polymers as determined by GPC. Linear line represents the theoretical relationship between feed molar ratio and DP_n . (c) Representative GPC traces for the catalyst loading study with colour coding for each ratio as presented in (b).

2.2.3 Electrochemical Properties of NN and PNN

The electrochemical properties of NN and PNN were studied using cyclic voltammetry (CV) in a $\text{CH}_2\text{Cl}_2/\text{MeCN}$ (1:1) solvent mixture using $[\text{nBu}_4\text{N}][\text{PF}_6]$ as supporting electrolyte (Figure 2.6, Table 2.1). NN was reversibly oxidized and reduced at half-wave oxidation ($E_{1/2,\text{ox}}$) and reduction ($E_{1/2,\text{red}}$) potentials of 0.42 V and -1.27 V relative to a ferrocene/ferrocenium redox couple. PNN showed reversible oxidation at half-wave oxidation potential of 0.44 V with a diminished current response and peak shape. This could be attributed to the loss of diffusion control at the working electrode surface as a result of poor mobility and/or solubility of PNN. A reversible reduction wave was not observed for PNN despite altering the polymer batches,

solvents and working electrodes. To further probe the issue at hand, cyclic voltammograms were acquired for **PNN** at different scan directions (Figure 2.7) and different scan rates (Figure 2.8) presenting no reversible reduction. Multiple scans without the cleansing of the working electrodes in between runs highlighted a clear diminishing in response signal which is indicative of the polymer plating (Figure 2.9). There are no cyclic voltammograms in solution reported for nitronyl nitroxide polymers in the literature, however, Nishide and co-workers have constructed carbon composite electrodes using nitronyl nitroxide polymers as electrode-active materials which have exhibited reversible oxidation and reduction features.^{12, 13, 23} In all cases the reduction feature provided a weaker signal compared to its oxidation counterpart. It has been postulated that protonation of the radical anionic species can occur as a result of ester hydrolysis generating protic species *in situ*.²³ This would in turn cause the formation of hydroxylamines which would not be observed by cyclic voltammetry. During the experiments, no ester hydrolysis by-products were observed. Therefore working electrode plating and/or protonation of anionic species could both be reasons for the observed phenomenon.

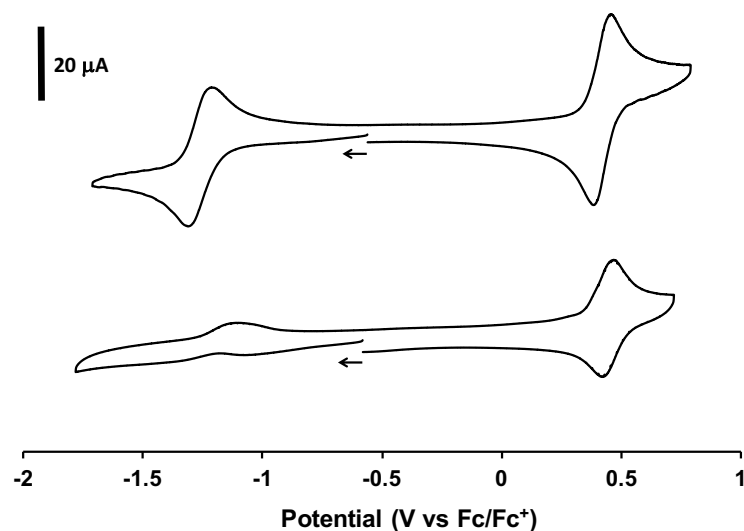


Figure 2.6. Cyclic voltammograms collected for monomer **NN** (top) and **PNN** (bottom) recorded at a scan rate of 250 mV s^{-1} in degassed 50:50 v/v $\text{CH}_2\text{Cl}_2/\text{MeCN}$ solutions containing 1 mM analyte and 0.1 M $[\text{nBu}_4\text{N}][\text{PF}_6]$ as supporting electrolyte.

Table 2.1. Electrochemical properties of **NN** and **PNN**.

Compounds	$E_{1/2,\text{red}}$ (V vs. Fc/Fc^+)	$E_{1/2,\text{ox}}$ (V vs. Fc/Fc^+)
NN	-1.27 V	0.42 V
PNN	N/A	0.44 V

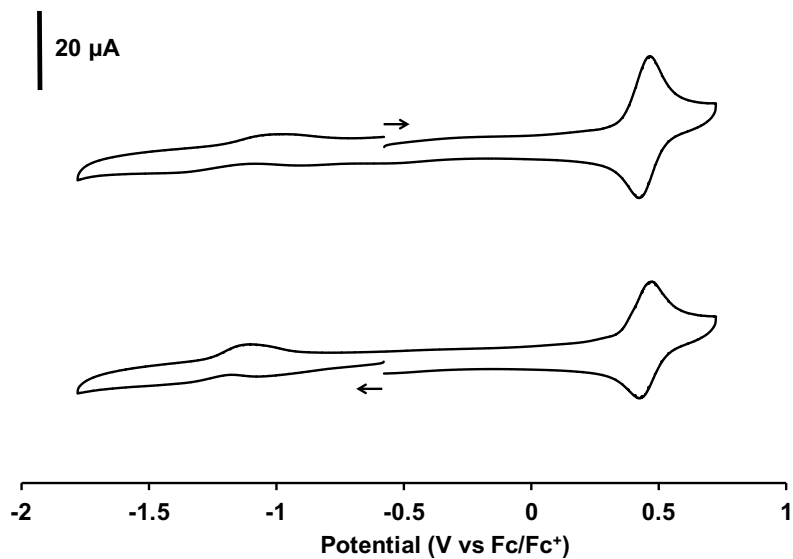


Figure 2.7. Cyclic voltammograms collected for PNN recorded in both directions at a scan rate of 250 mV s⁻¹ in degassed 50:50 v/v CH₂Cl₂/MeCN solutions containing 1 mM analyte and 0.1 M [nBu₄N][PF₆] as supporting electrolyte.

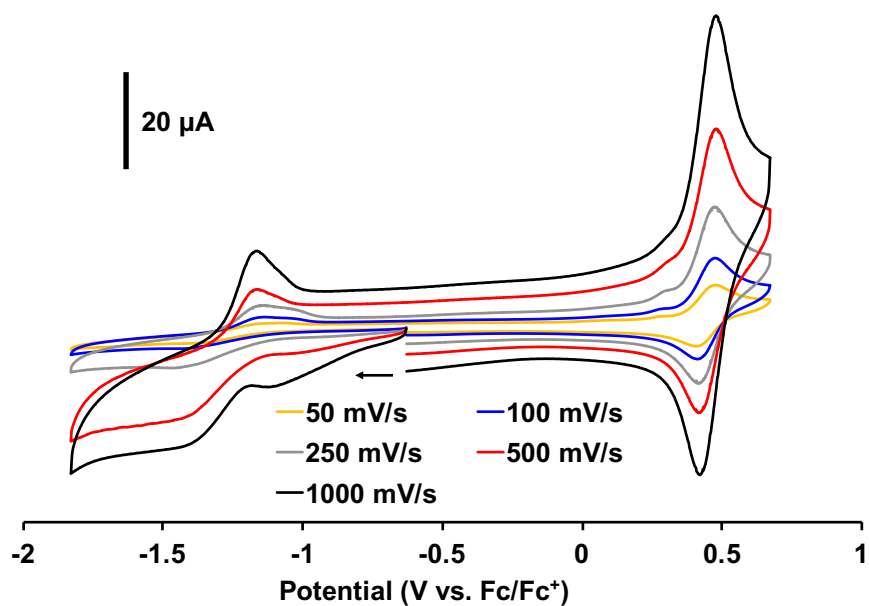


Figure 2.8. Cyclic voltammograms collected for PNN recorded at a scan rates ranging from 50 to 1000 mV s⁻¹ in degassed 50:50 v/v of CH₂Cl₂/MeCN solutions containing 1 mM analyte and 0.1 M [nBu₄N][PF₆] as supporting electrolyte.

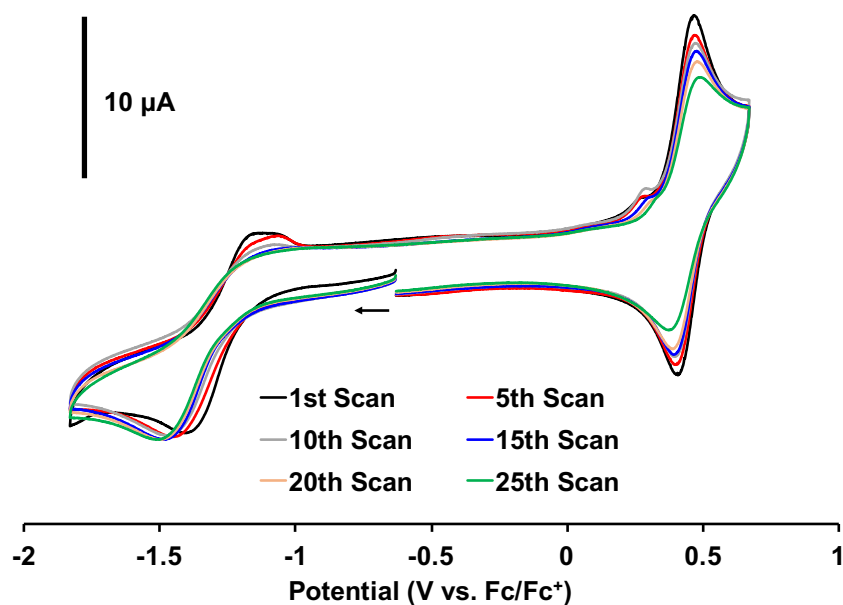


Figure 2.9. Cyclic voltammograms collected for **PNN** recorded at a scan rate of 50 mV s^{-1} over the span of 25 cycles. Experiments were conducted in degassed 50:50 v/v $\text{CH}_2\text{Cl}_2/\text{MeCN}$ solutions containing 1 mM analyte and 0.1 M $[\text{nBu}_4\text{N}][\text{PF}_6]$ as supporting electrolyte. The 1st scan as well as every 5th are depicted for clarity.

2.2.4 Thermal Properties of NN and PNN

Thermal gravimetric analysis (TGA) of **PNN** showed that the polymer was stable up to approximately $165 \text{ }^\circ\text{C}$, with degradation occurring over four steps (Figure 2.10a). The first step of the TGA analysis revealed a rapid degradation feature between $163\text{--}187 \text{ }^\circ\text{C}$, representing a mass loss of 3%. The second step was between $187\text{--}306 \text{ }^\circ\text{C}$ with a mass loss of 8%, the third occurred between $306\text{--}547 \text{ }^\circ\text{C}$ with a mass loss of 54%, and the fourth occurred between $547\text{--}800 \text{ }^\circ\text{C}$, giving an overall char yield of 0%.

The first step of degradation was of interest due to the rapid fashion that it occurred in. The 3% mass loss is remarkably similar to the percentage of total mass (3.3%) that an oxygen atom represents in the polymer. Due to the lack of NMR spectroscopy available, to investigate the potential cause of this degradation, IR spectroscopy was used to analyze both fresh and degraded polymer samples. A small sample of **PNN** was charged into a greaseless Schlenk flask under N_2 and heated in an oil bath to $170 \text{ }^\circ\text{C}$ while stirring in the absence of solvent. Upon reaching $160 \text{ }^\circ\text{C}$, the solid blue polymer began to turn brown and became gooey,

implying degradation had occurred. At 170 °C the polymer undertook a black charred appearance, re-solidifying into rock-like shards. IR spectroscopy of the charred polymer presented significant diminishing in the stretching frequency present at 1360 cm^{-1} ; the frequency corresponding to the N-O• moiety (Figure 2.11). Thus, the displacement of an oxygen atom could be the cause of this mass loss.

Differential scanning calorimetry (DSC) analysis of **PNN** did not reveal a T_g for the polymer despite attempting the study over multiple temperature ranges. Cycling between 20 °C and 150 °C thrice provided the best results, with no observable charring of the polymer. The second heating/cooling cycle is presented in Figure 2.10b. It is to be noted that the 6-oxoverdazyl radical polymer made by the Gilroy group presented a T_g of 152 °C^{14} , however, due to degradation observed in the TGA around similar temperatures for **PNN** it is possible that a T_g was never reached.

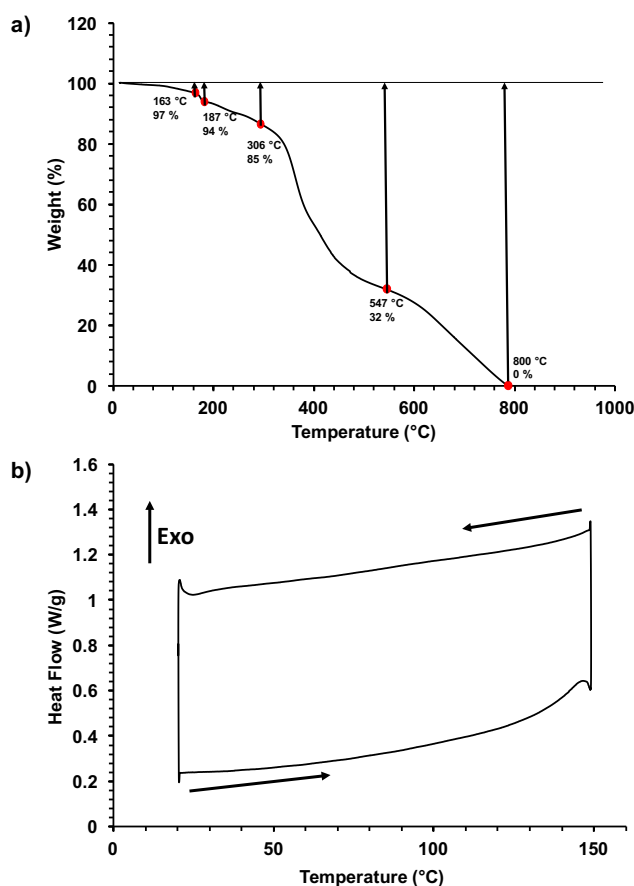


Figure 2.10. (a) TGA trace of **PNN** from 0 to 1000 °C. (b) DSC data for the second heating/cooling cycle for **PNN**. The sample was heated to 150 °C followed by cooling to 20 °C with a heating range of 10 °C min^{-1} .

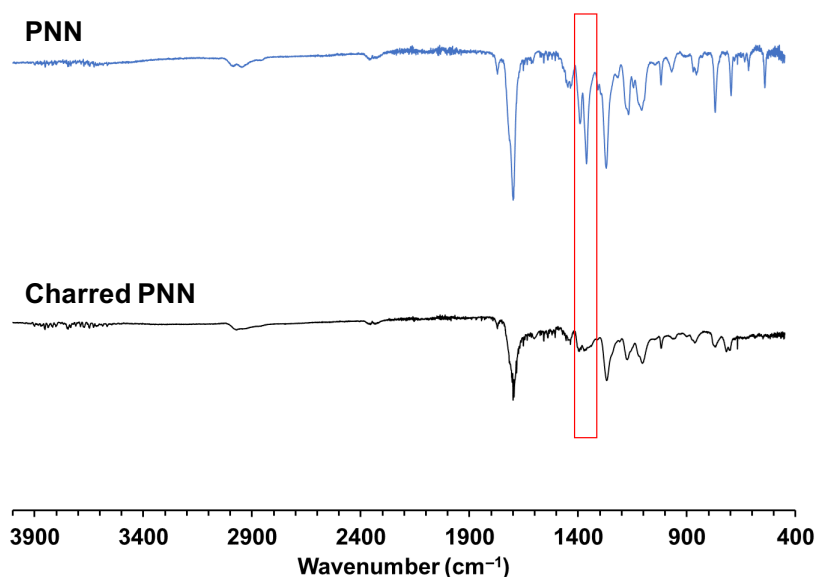


Figure 2.11. IR spectra of fresh **PNN** (top) and charred **PNN** (bottom). Red rectangle indicates the region of importance, where the N-O• stretching frequency is significantly diminished when comparing top spectrum to bottom.

2.2.5 Thin Films of PNN

Due to the spectroscopic, electrochemical and redox properties observed for **PNN**, it was deemed a good candidate as a thin film component in organic electronics. Thin films of **PNN** were spin-coated onto glass substrates which were pre-patterned with indium tin-oxide (ITO) contacts. The resulting thin film presented some roughness on the surface in the forms of grains and particulates as shown in the AFM height image in Figure 2.12. This is attributed to the tendency for polymers to form coils during spinning process.²⁴ However, despite the small defects the polymer presented, the films were deemed suitable for the fabrication of sandwich-type devices with the given composition presented in Figure 2.13.

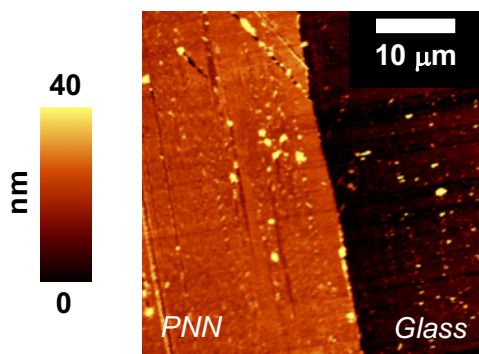


Figure 2.12. AFM image for PNN at $30 \text{ nm} \pm 10\%$ thickness. A small fragment of the film was scraped off to reveal the glass substrate underneath (right side of image). Thin films were spun at 2000 RPM.

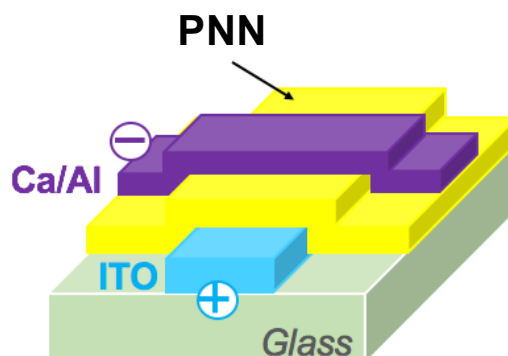


Figure 2.13. Sandwich-type device architecture fabricated for conductivity measurements.

The sandwich-type devices were tested for their memory effect similarly to the previously reported 6-oxoverdazyl polymer from the Gilroy group.¹⁵ Conductivity measurements highlighted that the polymer is in a low conductivity state at rest which persists until a positive voltage bias of +2.0 V is applied, which is shown by the S shape curve in Figure 2.14. This curve was made using the Poole-Frenkel equation as a fit (Eq 2.1), where S is low-field, low-voltage conductance, I is current, V is voltage, and A depends on both the dielectric constant of the medium as well as temperature of the experiment. Upon reaching the positive voltage bias, the device entered a high conductivity state with a conductivity that is four times higher than in the low conductivity state. Interestingly, upon scanning to negative potential bias, the high conductivity state is not dictated by the Poole-Frenkel equation anymore, but instead it presented Ohmic current-voltage behaviour, as represented by the diagonal line in Figure 2.14. This curve was made using the Ohmic behaviour equation as a fit, where R is the resistance

(Eq. 2.2). This behaviour is indicative of extended-state transport as opposed to the localized-state transport exhibited by Poole-Frenkel effects.¹⁵ Upon scanning to a negative potential bias of -1.5 V the device re-entered a low conductivity state. Cycling between high and low conductivity states was reproducible on the same device. These results indicate that **PNN** is a suitable candidate for resistive memory device applications.

$$I = SV \exp(AV^{1/2}) \quad 2.1$$

$$V = IR \quad 2.2$$

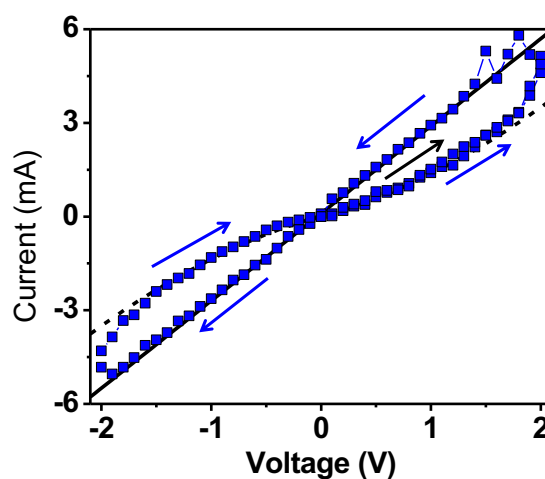


Figure 2.14. Current response as a function of applied voltage for **PNN** device represented by a Poole-Frenkel fit (dashed line, low conductivity) and an Ohmic behaviour fit (solid line, high conductivity).

2.3 Conclusion

In summary, a novel norbornene-based nitronyl nitroxide radical monomer **NN** and its respective polymer **PNN** were synthesized and fully characterized. The FT-IR and UV-Vis absorption spectra of **NN** and **PNN** were in good accordance, indicating the survival of the radical units after ROMP. It was found that the radical polymer possessed a high radical content of approximately 97% based on UV-Vis absorption and EPR studies as well as a reversible oxidation process observed by CV. TGA analysis revealed that the polymer underwent degradation at approximately 165 °C, with an initial mass loss of 3% which is assumed to be due to oxygen cleavage per FT-IR studies. The monitoring of the polymerization progress of

NN by GPC revealed the ring-opening metathesis polymerization to be well behaved, thus allowing for good control of polymer molecular weight. PNN forms thin films which were used as a functional component in a sandwich-type device. Conductivity measurements for the devices revealed memory effects in their electrical transport properties thus rendering PNN as a potential working component of memristors.

2.4 Experimental

2.4.1 General Considerations

All reactions and manipulations were carried out under a N₂ atmosphere using standard Schlenk techniques unless otherwise stated. Reagents were purchased from Sigma-Aldrich, Alfa-Aesar or Oakwood Chemicals and used as received unless otherwise specified. Solvents were purchased from Caledon Laboratories, dried using an Innovative Technologies Inc. solvent purification system, collected under vacuum, and stored under a N₂ atmosphere over 4 Å molecular sieves. Compound *N*-[3-hydroxypropyl]-*cis*-5-norbornene-*exo*-2,3-dicarboximide was prepared according to literature procedures.²⁰

NMR spectra were recorded on 400 MHz (¹H: 400.1 MHz) or 600 MHz (¹³C{¹H}: 150.7 MHz) Varian INOVA instruments at 25 °C. ¹H NMR spectra were referenced to residual CHCl₃ (δ = 7.26) or DMSO-*d*₅ (δ = 2.50) and ¹³C{¹H} NMR spectra were referenced to CDCl₃ (δ = 77.0) and DMSO-*d*₆ (δ = 39.5). Mass spectra were recorded in positive-ion mode using a high-resolution Thermo Scientific DFS (Double Focusing Sensor) mass spectrometer using electron impact ionization. FT-IR spectra were recorded on a PerkinElmer Spectrum Two instrument using an attenuated total reflectance accessory. UV-vis absorption spectra were recorded on a Cary 5000 UV-Vis-NIR spectrophotometer between 200 and 800 nm. Molar extinction coefficients were determined from the slope of a plot of absorbance against concentration based on absorption data of four different concentrations.

2.4.2 Gel Permeation Chromatography (GPC)

GPC experiments were conducted in chromatography-grade THF at concentrations of 5 mg mL⁻¹ using a Viscotek GPCmax VE 2001 GPC instrument equipped with an Agilent PolyPore guard column (PL1113-1500) and two sequential Agilent PolyPore GPC columns

packed with porous poly (styrene-*co*-divinylbenzene) particles (MW range: 200–2,000,000 g mol⁻¹; PL1113-6500) regulated at a temperature of 30 °C. Signal responses were measured using a Viscotek VE 3580 refractive index detector, and molecular weights were determined by comparison of the maximum refractive index response with a calibration curve (10 points, 1,500–786,000 g mol⁻¹) established using monodisperse polystyrene standards purchased from Viscotek.

2.4.3 Electron Paramagnetic Resonance (EPR) Spectroscopy

EPR spectra were recorded for 100 μM CH₂Cl₂ solutions of the **NN** and the **PNN** that had been subjected to three freeze-pump-thaw cycles in 0.4 mm quartz tube using a JEOL JES-FA200 EPR spectrometer. All measurements were made at 25 °C and *g*-factors were referenced relative to a built-in Mn²⁺ marker within the resonant cavity of the instrument.

Quantification of radical content was done by comparing an EPR spectrum of a solid TEMPO sample to a solid sample of **PNN**. Approximately 5 mg of TEMPO and **PNN** were loaded into capillary tubes. It is essential that the density, shape, size, and position of the sample in the resonant cavity of the instrument remain constant. In our case, we filled the capillary tubes to a depth of 1 cm and packed the solid by tapping it gently on a lab bench, before determining an accurate mass. The TEMPO sample was then loaded into the instrument and the resonant cavity tuned before a spectrum was recorded. The polymer samples were analyzed immediately after the TEMPO spectrum was acquired, ensuring that the sample position was identical. The spectra of the polymers were collected without re-tuning the resonant cavity under the same conditions used to collect the spectrum of TEMPO. Working under the assumption that each TEMPO molecule contributes one unpaired electron, the number of unpaired electrons present in the radical polymers can be determined by comparison of the integrations of the spectra collected (after correction for the molecular weight of the radicals involved).

EPR simulations were performed using a least-square fitting method calculated by Easyspin program,²¹ which is part of MATLAB software.

2.4.4 Cyclic Voltammetry

Cyclic voltammetry experiments were performed using a Bioanalytical Systems Inc. (BASi) Epsilon potentiostat and analyzed using BASi Epsilon software. Electrochemical cells consisted of a three-electrode setup including a glassy carbon working electrode, platinum wire counter electrode and silver wire *pseudo* reference electrode. Experiments were run at scan rates of 50, 100, 250, 500 and 1000 mV s⁻¹ in degassed CH₂Cl₂ solutions of the analyte (~1 mM) and supporting electrolyte (0.1 M [nBu₄N][PF₆]). Cyclic voltammograms were referenced against an internal standard (~1 mM ferrocene) and corrected for internal cell resistance using the BASi Epsilon software.

2.4.5 Thermal Analysis

Thermal degradation studies were performed using a TA Instruments Q50 TGA instrument under a N₂ atmosphere. Samples of polymer PNN were placed in a platinum pan and heated at a rate of 10 °C min⁻¹ from 20 °C to 1000 °C under a flow of N₂ (60 mL min⁻¹). Thermal analysis studies were performed under N₂ using differential scanning calorimetry (DSC) on a TA Instruments DSC Q20. Samples of PNN were placed in an aluminum Tzero pan and heated from 0 °C to 150 °C at 10 °C min⁻¹ under a flow of N₂ (50 mL min⁻¹) and cooled to 0 °C at 10 °C min⁻¹, before they underwent two more heating/cooling cycles.

2.4.6 Synthetic Procedures

Preparation of 2,3-bis(hydroxyamino)-2,3-dimethylbutane (2.2).

This procedure was adapted from that reported by Yamauchi and co-workers.¹⁷ Aluminum foil (0.78 g, 28 mmol) was cut into strips and placed into a 2.6% aqueous HgCl₂ (20 mL, 1.9 mmol) solution for 30 s per strip, following washing with EtOH and THF. The strips were subsequently added into THF (80 mL) and stirred at 0 °C. To this reaction mixture H₂O (8 mL) and a THF (80 mL) solution of 2,3-dimethyl-2,3-dinitrobutane **2.1** (1.0 g, 5.7 mmol) was added, and the stirring was continued for 1 h at 0 °C followed by 1 h at r.t. The mixture was filtered over Celite and the ensuing clear filtrate was brought to dryness *in vacuo* yielding a white solid. Et₂O (10 mL) was added to the solid and the reaction flask was stored in the fridge for 2 h. The white precipitate was isolated *via* vacuum filtration and washed with cold Et₂O (3 × 5 mL) to afford **2.2** as a white amorphous solid. Yield: 0.42 g, 56%. M.p.: 149-151 °C. ¹H

NMR (400.1 MHz, DMSO-*d*₆): δ 6.93 (s, 2H, OH), 5.38 (s, 2H, NH), 1.00 (s, 12H, CH₃). The NMR data matched well with those reported previously.¹⁷

Preparation of 2-(4'-Carboxyphenyl)-4,4,5,5-tetramethyl-1,3-dihydroxyimidazoline (2.4).

This procedure was adapted from a procedure published by Miller and co-workers.¹⁶ To a solution of 2,3-bis(hydroxyamino)-2,3-dimethylbutane **2.2** (0.37 g, 2.5 mmol) in MeOH (10 mL) was added 4-formylbenzoic acid **2.3** (0.31 g, 2.1 mmol) in air. The mixture was then stirred at r.t. for 48 h. The resulting white precipitate was isolated *via* vacuum filtration, washed with cold MeOH, and then dried *in vacuo* to give **2.4** as a white amorphous solid. Yield = 0.46 g, 79%. M.p.: >184 °C (decomp.) ¹H NMR (400.1 MHz, DMSO-*d*₆): δ 12.83 (s, 1H, COOH), 7.92 (d, 2H, ³J_{HH} = 8 Hz, aryl CH), 7.84 (s, 2H, OH), 7.60 (d, 2H, ³J_{HH} = 8 Hz, aryl CH), 4.58 (s, 1H, CH), 1.09 (s, 6H, CH₃), 1.05 (s, 6H, CH₃). ¹³C{¹H} NMR (150.7 MHz, DMSO-*d*₆): δ 167.8, 147.5, 130.2, 129.2, 128.9, 90.3, 66.8, 24.8, 17.7. FT-IR (ATR): 3248 (m), 2995 (w), 1611 (w), 1558 (w), 1436 (s), 1366 (m), 1294 (w), 1215 (w), 769 (w), 705 (w). cm⁻¹. Mass Spec. (EI, +ve mode): exact mass calculated for C₁₄H₂₀N₂O₄: 280.1423; found: 280.1418; difference: -1.8 ppm.

Preparation of 2-(4'-Carboxyphenyl)-4,4,5,5-tetramethylimidazolidine-3-oxide-1-oxyl (2.5).

This procedure was adapted from a procedure by Miller and co-workers.¹⁶ To a suspension of 2-(4'-Carboxyphenyl)-4,4,5,5-tetramethyl-1,3-dihydroxyimidazoline **2.4** (0.43 g, 1.5 mmol) in THF (15 mL) and NaOH (1.5 mL, 1.5 mmol, 1 M) was added dropwise a solution of sodium periodate (0.49 g, 2.3 mmol) in H₂O (15 mL) over a 15 min period. Reaction mixture was stirred at r.t. for 1 h. Organic layer was extracted into EtOAc (30 mL) followed by the addition of HCl (3 mL, 1M). The mixture was washed with H₂O (3 × 30 mL) and brine (3 × 40 mL). Organic layer solution was separated, dried with magnesium sulfate and then removed *in vacuo* yielding **2.5** as a dark blue crystalline solid. Yield = 0.272 g, 65%. M.p.: >196 °C (decomp.) FT-IR (ATR): 2922 (br, m), 2498 (br, m), 1700 (s), 1340 (s), 1257 (s), 1108 (w), 1018 (m), 855 (w) cm⁻¹. UV-vis (CH₂Cl₂): λ_{max} = 645 nm (ϵ = 200 M⁻¹ cm⁻¹), 602 nm (ϵ = 240 M⁻¹ cm⁻¹), 563 nm (ϵ = 200 M⁻¹ cm⁻¹), 380 nm (ϵ = 9,300 M⁻¹ cm⁻¹), 365 nm (ϵ = 4,900 M⁻¹ cm⁻¹),

295 nm ($\epsilon = 11,500 \text{ M}^{-1} \text{ cm}^{-1}$). Mass Spec. (EI, +ve mode): exact mass calculated for $\text{C}_{14}\text{H}_{17}\text{N}_2\text{O}_4$: 277.1188; found: 277.1191; difference: +1.0 ppm.

Preparation of Nitronyl Nitroxide Monomer (NN).

To a solution of *N,N'*-dicyclohexylcarbodiimide (0.31 g, 1.5 mmol) and 4-dimethylaminopyridine (0.20 g, 1.6 mmol) in dry CH_2Cl_2 (10 mL) was added 2-(4'-carboxyphenyl)-4,4,5,5-tetramethylimidazolidine-3-oxide-1-oxyl **2.5** (0.38 g, 1.4 mmol) before the mixture was stirred for 10 min at r.t. To this solution was added *N*-[3-hydroxypropyl]-*cis*-5-norbornene-*exo*-2,3-dicarboximide **2.6** (0.33 g, 1.5 mmol) in dry CH_2Cl_2 (3 mL). The reaction mixture was then stirred for 18 h at RT before it was filtered to remove a white precipitate. The dark blue supernatant was then taken to dryness *in vacuo*. The resulting dark blue oil was purified by column chromatography [75 mL neutral alumina, hexanes/EtOAc (2:1), $R_f = 0.49$], and recrystallized from a hot saturated solution of isopropanol to give monomer NN as a blue powder. Yield = 0.41 g, 63%. Mp: 146–148 °C. FT-IR (ATR): 2960 (br, m), 1774 (m), 1719(s), 1697 (w), 1430 (m), 1390 (s), 1360 (s), 1272 (s), 1177, (m), 1122 (m) cm^{-1} . UV-vis (CH_2Cl_2): $\lambda_{\text{max}} = 645 \text{ nm}$ ($\epsilon = 240 \text{ M}^{-1} \text{ cm}^{-1}$), 602 nm ($\epsilon = 290 \text{ M}^{-1} \text{ cm}^{-1}$), 563 nm ($\epsilon = 230 \text{ M}^{-1} \text{ cm}^{-1}$), 380 nm ($\epsilon = 11,300 \text{ M}^{-1} \text{ cm}^{-1}$), 365 nm ($\epsilon = 6,000 \text{ M}^{-1} \text{ cm}^{-1}$), 295 nm ($\epsilon = 14,000 \text{ M}^{-1} \text{ cm}^{-1}$). Mass Spec. (EI, +ve mode): exact mass calculated for $\text{C}_{26}\text{H}_{30}\text{N}_3\text{O}_6$: 480.2135; found: 480.2138; difference: +0.8 ppm. Anal. Calcd. (%) for $\text{C}_{26}\text{H}_{30}\text{N}_3\text{O}_6$: C, 64.99; H, 6.29; N, 8.74. Found: C, 64.92; H, 6.16; N, 8.72.

Preparation of Nitronyl Nitroxide Polymer (PNN).

A greaseless Schlenk flask was charged with monomer NN (0.10 g, 0.21 mmol) and dry CH_2Cl_2 (3.0 mL). The resulting blue solution was degassed by three freeze-pump-thaw cycles. The monomer solution was cooled down to 0 °C in an ice bath for 5 min before a similarly degassed 1 mg mL^{-1} CH_2Cl_2 solution of Grubbs' 3rd generation catalyst (1.84 mL, 2.1×10^{-3} mmol) was quickly added. The polymerization proceeded for 30 min before it was terminated with ethyl vinyl ether (0.40 mL, 4.2 mmol), and the mixture stirred for an additional 30 min at r.t. The crude reaction mixture was filtered through a short pipette neutral alumina plug, and the solvent was removed *in vacuo*. The resulting polymer was dissolved in minimal THF, and precipitated into rapidly stirred cold pentane (40 mL) thrice to afford PNN as a blue powder. Yield = 0.086 g, 86%. FT-IR (ATR): 2950 (m), 1774 (w), 1697 (s), 1447 (m), 1394 (s), 1360 (s), 1268 (s), 1174, (m), 1113 (m) cm^{-1} . UV-vis (CH_2Cl_2): $\lambda_{\text{max}} = 645 \text{ nm}$ ($\epsilon = 230 \text{ M}^{-1} \text{ cm}^{-1}$),

602 nm ($\epsilon = 280 \text{ M}^{-1} \text{ cm}^{-1}$), 563 nm ($\epsilon = 230 \text{ M}^{-1} \text{ cm}^{-1}$), 380 nm ($\epsilon = 10,400 \text{ M}^{-1} \text{ cm}^{-1}$), 365 nm ($\epsilon = 5,600 \text{ M}^{-1} \text{ cm}^{-1}$), 295 nm ($\epsilon = 13,000 \text{ M}^{-1} \text{ cm}^{-1}$). GPC (THF, conventional calibration relative to polystyrene standards): $M_n = 51,400 \text{ g mol}^{-1}$, $M_w = 60,600 \text{ g mol}^{-1}$, $D = 1.18$.

Reaction Characteristics of the ROMP of Nitronyl Nitroxide Monomer

Catalyst Loading Study

Five separate reactions were carried out each using 0.05 g (0.10 mmol) of NN. Polymerization procedure undertaken is done as listed above. Catalyst molar feed stock ratios (monomer:catalyst) varied from 20, 40, 60, 80 and 100. All polymerization times were 30 min. Each polymer sample was run through a short neutral alumina plug, dried *in vacuo*, re-dissolved in GPC-grade THF and then had their degree of polymerization determined by GPC analysis using polystyrene as an internal standard.

Reaction Progress as a Function of Time

A 4.6 mg mL⁻¹ CH₂Cl₂ solution of Grubbs' 3rd generation catalyst (1.0 mL, 5.2×10^{-3} mmol) was added rapidly to a 50 mg mL⁻¹ CH₂Cl₂ stirring solution of NN (5.0 mL, 0.52 mmol). The mixture was stirred on ice for 1 h. Five different timed aliquots (1 mL) were acquired over the span of the reaction time, with each one being placed in a greaseless Schlenk flask containing ethyl vinyl ether (0.15 mL, 1.5 mmol). Following termination, each polymer was run through a short neutral alumina plug, dried *in vacuo*, re-dissolved in GPC-grade THF and then had their M_n analyzed by GPC using polystyrene as an internal standard.

2.5 References

- (1) Wei, M.; Gao, Y.; Li, X.; Serpe, M. J. *Polym. Chem.* **2017**, *8*, 127–143.
- (2) Alvarez, A.; Costa-Fernández, J. M.; Pereiro, R.; Sanz-Medel, A.; Salinas-Castillo, A. *Trends Anal. Chem.* **2011**, *30*, 1513–1525.
- (3) Zhang, K.; Monteiro, M. J.; Jia, Z. *Polym. Chem.* **2016**, *7*, 5589–5614.
- (4) Tomlinson, E. P.; Hay, M. E.; Boudouris, B. W. *Macromolecules* **2014**, *47*, 6145–6158.
- (5) Nakahara, K.; Oyaizu, K.; Nishide, H. *Chem. Lett.* **2011**, *40*, 222–227.

- (6) Nishide, H.; Iwasa, S.; Pu, Y. J.; Suga, T.; Nakahara, K.; Satoh, M. *Electrochim. Acta* **2004**, *50*, 827–831.
- (7) Muench, S.; Wild, A.; Friebe, C.; Haupler, B.; Janoschka, T.; Schubert, U. S. *Chem. Rev.* **2016**, *116*, 9438–9484.
- (8) Janoschka, T.; Hager, M. D.; Schubert, U. S. *Adv. Mater.* **2012**, *24*, 6397–6409.
- (9) Suga, T.; Konishi, H.; Nishide, H. *Chem. Commun.* **2007**, 1730–1732.
- (10) Koshika, K.; Chikushi, N.; Sano, N.; Oyaizu, K.; Nishide, H. *Green Chem.* **2010**, *12*, 1573–1575.
- (11) Joo, Y.; Agarkar, V.; Sung, S. H.; Savoie, B. M.; Boudouris, B. W. *Science* **2018**, *359*, 1391–1395.
- (12) Oyaizu, K.; Sukegawa, T.; Nishide, H. *Chem. Lett.* **2011**, *40*, 184–185.
- (13) Sukegawa, T.; Kai, A.; Oyaizu, K.; Nishide, H. *Macromolecules* **2013**, *46*, 1361–1367.
- (14) Paquette, J. A.; Ezugwu, S.; Yadav, V.; Fanchini, G.; Gilroy, J. B. *J. Polym. Sci., Part A: Polym. Chem.* **2016**, *54*, 1803–1813.
- (15) Ezugwu, S.; Paquette, J. A.; Yadav, V.; Gilroy, J. B.; Fanchini, G. *Adv. Electron. Mater.* **2016**, *2*, 1600253.
- (16) Del Sesto, R. E.; Arif, A. M.; Miller, J. S. *Inorg. Chem.* **2000**, *39*, 4894–4902.
- (17) Shimono, S.; Tamura, R.; Ikuma, N.; Takimoto, T.; Kawame, N.; Tamada, O.; Sakai, N.; Matsuura, H.; Yamauchi, J. *J. Org. Chem.* **2004**, *69*, 475–481.
- (18) Schiodt, N. C.; de Biani, F. F.; Caneschi, A.; Gatteschi, D. *Inorg. Chim. Acta.* **1996**, *248*, 139–146.
- (19) Rintoul, L.; Micallef, A. S.; Bottle, S. E. *Spectrochim. Acta. A.* **2008**, *70*, 713–717.
- (20) Ren, L.; Zhang, J.; Bai, X.; Hardy, C. G.; Shimizu, K. D.; Tang, C. *Chem. Sci.* **2012**, *3*, 580–583.
- (21) Stoll, S.; Schweiger, A. *J. Magn. Reson.* **2006**, *178*, 42–55.
- (22) Ullman, E. F.; Osiecki, J. H.; Boocock, D. G. B.; Darcy, R. *J. Am. Chem. Soc.* **1972**, *94*, 1078–1079.
- (23) Suga, T.; Sugita, S.; Ohshiro, H.; Oyaizu, K.; Nishide, H. *Adv. Mater.* **2011**, *23*, 751–754.
- (24) Norrman, K.; Ghanbari-Siahkali, A.; Larsen, N. B. *Annu. Rep. Prog. Chem., Sect. C: Phys. Chem.* **2005**, *101*, 174–201.

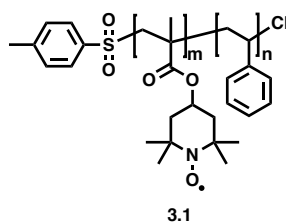
Chapter 3

3 6-Oxoverdazyl and Nitronyl Nitroxide Radical Co-Polymers

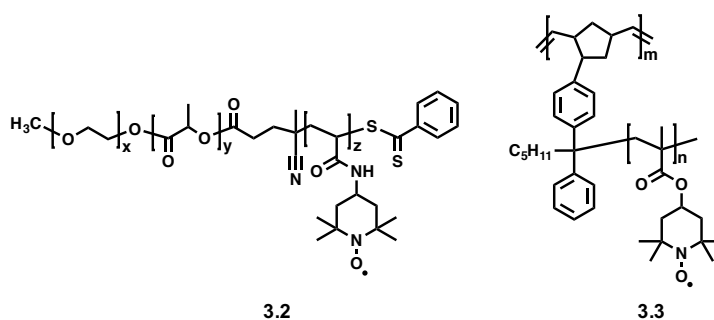
3.1 Introduction

Polymers composed of two or more monomers, also deemed as co-polymers, are used in many materials today, such as acrylonitrile butadiene styrene (ABS) used to make LEGO pieces.¹ When co-polymerization occurs, the monomers (repeating units) may adopt various structural arrangements when assembling, leading to formations of linear or branched co-polymers. Linear co-polymers include alternating,² random and block³ co-polymers while branched co-polymers include grafted⁴ and brush⁵ co-polymers. The arrangement of the repeating units in the co-polymers dictates their morphology and chemical properties.

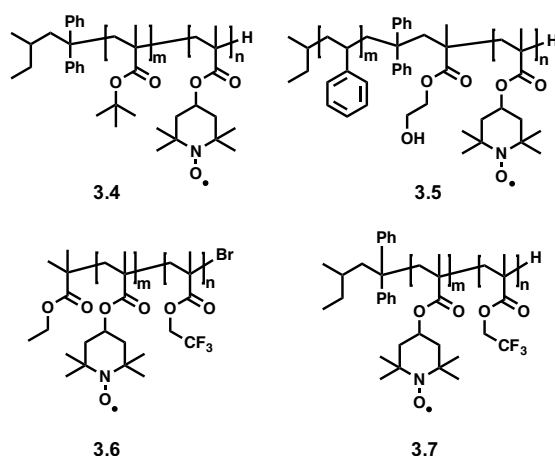
Stable radical polymers have garnered significant attention as electrochemically active materials due to the combination of processability, flexibility and tunable redox properties. They have found use as cathode materials in organic radical batteries,⁶⁻¹¹ EPR probes,^{12,13} and as the functional component of solid-state electronics.^{14,15} In all cases, the performance of the devices is affected by the density, location and stability of organic radicals within the polymer. This is due to charge transport occurring by movement of electrons through pendent radical groups, and not through π -electron conjugation. Thus, researchers have expanded the scope of stable radical polymers by exploring co-polymer architectures and, in turn, combining the redox activity of radicals with the functionality of other organic subunits. As mentioned earlier, the choice of co-monomer when synthesizing radical co-polymers is crucial towards dictating both morphology and functionality. For example, the Gohy group synthesized block co-polymer **3.1** composed of 2,2,6,6-tetramethylpiperidinyloxy-4-yl methacrylate, a nitroxide radical monomer, and styrene. This was done to circumvent the solubility of the radical subunit in electrolytes with the introduction of styrene reducing the solubility.¹⁶ The reduced solubility allowed for the fabrication of a half-cell battery using **3.1** as the cathode active material, which showed reversible oxidation of nitroxide radicals to oxoammonium cations while ensuring minimal leaching into the electrolyte.



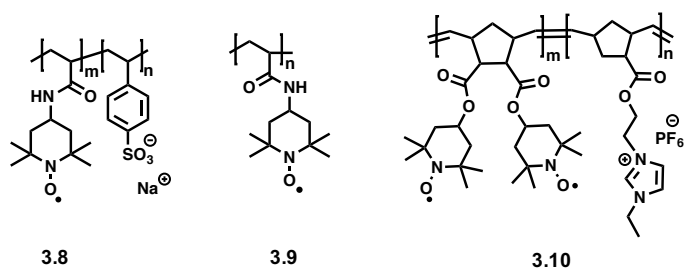
Nishide and co-workers synthesized the amphiphilic triblock co-polymer **3.2** that self-assembles into micelles containing nitroxide radicals within the hydrophobic core when placed in aqueous solutions.¹⁷ Due to the micelles possessing many unpaired electrons, they could be used as electron paramagnetic resonance probes for applications such as *in vivo* imaging. Moreover, Nishide and co-workers also synthesized bottlebrush co-polymer **3.3**.¹⁸ Thin-layer electrodes composed of the bottlebrush co-polymers exhibited rapid charging/discharging rates.



Ober *et al.* explored the co-polymerization of 2,2,6,6-tetramethylpiperidinyloxy-4-yl methacrylate, with organic subunits such as *tert*-butyl methacrylate and polystyrene groups, respectively (**3.4** and **3.5**).¹⁹ The polystyrene group was introduced for its ability to crosslink, while the methacrylate groups can be hydrolyzed to poly(acrylic acid). These polymers were fabricated into thin films by spin-coating and thermal or solvent annealing. The pendent nitroxide radical groups formed nanoscale patterns such as lamellae, cylinders or spheres on various surfaces; the first such examples for block co-polymers involving pendent radicals. Furthermore, the Ober group has also shown the formation of long-range ordered morphologies involving co-polymers with radical and fluorinated blocks (**3.6** and **3.7**).^{20, 21} The addition of a fluorinated methacrylate block alters the co-polymers properties by increasing thermal stability and optical properties.

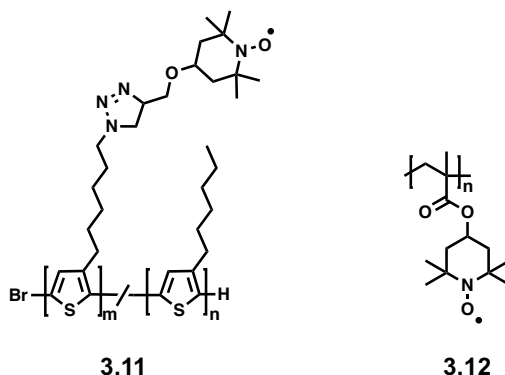


The Zhang group synthesized the co-polymer (**3.8**) which incorporates a styrene sulfonate ion moiety alongside a TEMPO radical moiety.²² They found that the charge-discharge capabilities of the co-polymer were improved when implemented as positive electrodes in coin-type batteries when compared to the control homopolymer poly(2,2,6,6-tetramethylpiperidin-4-yl acrylamide) **3.9**. **3.9** was chosen as the control due to its rapid charging-discharging rates reported in literature.²³ Furthermore, the charge specific capacity of the co-polymer batteries was also increased, thus indicating the benefits of the synergistic effect between the electrochemical properties of both sulfonate ions and radicals. In a similar fashion, the Nishide group investigated the effect on the electrochemical properties of radical co-polymers by introducing an imidazolium ion block (**3.10**).²⁴ The co-polymer highlighted changes in conductivity under a bias voltage, making them suitable candidates as materials for solid-state devices such as memristors.



A rare example of a radical co-polymer involving a conjugated backbone was synthesized by the Ober group.²⁵ This random co-polymer (**3.11**) possesses a thiophene backbone with varying pendent hexyl chains or TEMPO moieties. This is a rare example of a radical co-polymer

involving a conjugated backbone. The co-polymer displayed exponential decreases in conductivity upon lowering of TEMPO loading. This was due to the TEMPO units bringing disorder in the crystallinity which is typically observed in regioregular poly(3-hexylthiophene) polymers.



Despite the numerous examples of radical co-polymers in the literature, radical co-polymers involving stable radicals other than TEMPO have been few. This is largely due to the commercial availability of TEMPO derivatives as well as the exceptional rapid charge-discharge and long cycle life performances of organic battery devices based on the polymers PTAm (3.9) and PTMA (3.12).

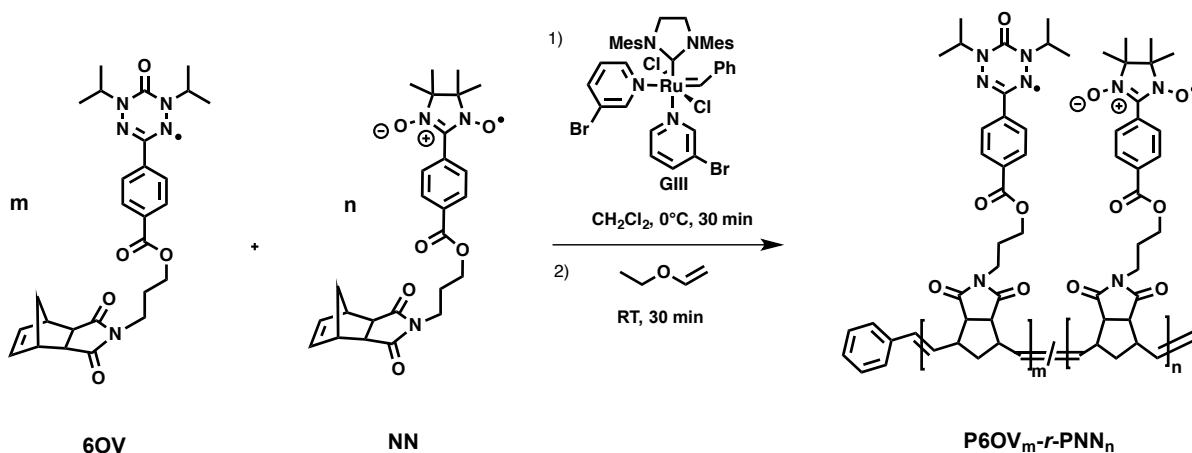
This chapter will describe the synthesis and characterization of various random and block co-polymers containing 6-oxoverdazyl (6OV) and nitronyl nitroxide (NN) subunits. These co-polymers were all synthesized using ROMP, and had their spectroscopic, thermal and electrochemical properties investigated.

3.2 Results and Discussion

3.2.1 Synthesis of Random Co-Polymers Containing 6OV and NN

Synthesis of random co-polymers $\text{P6OV}_m\text{-}r\text{-PNN}_n$ was done in a similar fashion to the NN homopolymer presented in Chapter 2.²⁶ Monomers NN and 6OV were dissolved in dry, degassed CH_2Cl_2 . A 1 mol% CH_2Cl_2 solution of the 3-bromopyridine derivative of Grubbs' third generation catalyst (GIII) was then added to the mixture, and the solution was stirred for 30 min at 0 °C. Polymerization was halted with the addition of a large excess of ethyl vinyl

ether (Scheme 3.1). Reaction mixtures were passed through a neutral alumina plug ensuring the removal of residual **GIII**. The polymers were precipitated out of cold pentanes using THF as a solvent. This methodology was applied for the synthesis of three random co-polymers with ratios of $\text{P6OV}_m\text{:PNN}_n$ where targeted $m:n$ ratios are 25:75, 50:50 and 75:25. Overall, the yields were in the range of 85–90%, with complete conversion of monomers.



Scheme 3.1 Synthesis of random co-polymers $\text{P6OV}_m\text{-}r\text{-PNN}_n$.

Molecular weights for each of the co-polymers were determined by gel permeation chromatography (GPC). When comparing the GPC traces for the co-polymers, each exhibited high molecular weight tailing (Figure 3.1). GPC analysis revealed that the $\text{P6OV}_{75}\text{-}r\text{-PNN}_{25}$ polymer had the highest M_n value, while the other two co-polymers possessed similar M_n values. The high M_n value for $\text{P6OV}_{75}\text{-}r\text{-PNN}_{25}$ is partly due to the higher molecular weight of **6OV** in comparison to **NN**. It is to be noted that, as for homopolymer **PNN**, the GPC analysis was done comparing to a polystyrene standard making the obtained M_n and M_w values estimates. D values for the random co-polymers ranged between 1.22–1.23, indicating low dispersity polymers as expected for similar polymers synthesized by ROMP (Table 3.1).

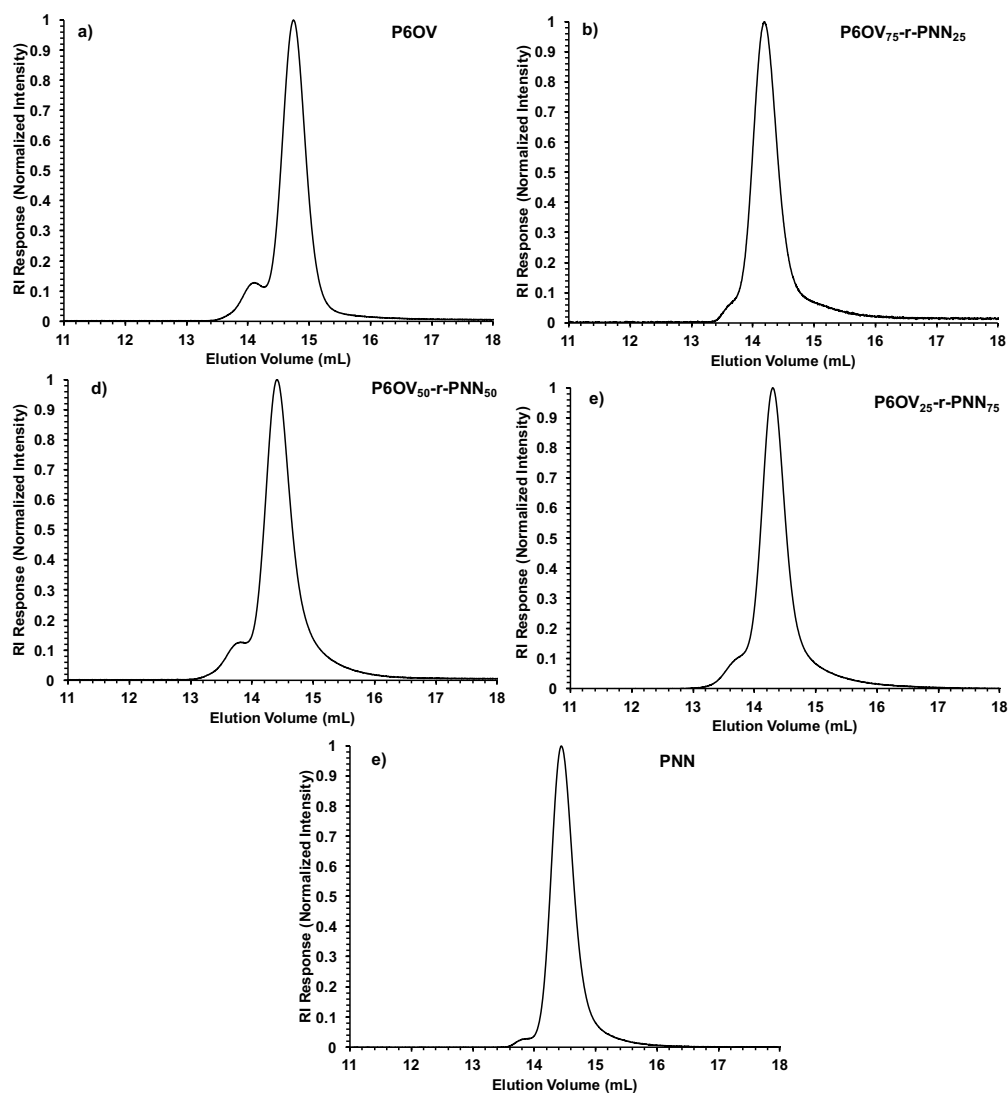


Figure 3.1 GPC traces (in THF) for polymers (a) **P6OV**, (b) **P6OV_{75-r}-PNN₂₅**, (c) **P6OV_{50-r}-PNN₅₀**, (d) **P6OV_{25-r}-PNN₇₅**, and (e) **PNN**.

Table 3.1. M_n , M_w and D values for **P6OV_{m-r}-PNN_n** random co-polymers.

Polymer	M_n (g/mol)	M_w (g/mol)	Theoretical M_n (g/mol)	D
P6OV_{75-r}-PNN₂₅	63,400	76,100	50,000	1.23
P6OV_{50-r}-PNN₅₀	48,500	59,200	49,400	1.23
P6OV_{25-r}-PNN₇₅	44,700	54,600	48,700	1.22

FT-IR spectroscopy confirmed the presence of **6OV** and **NN** radicals in the random co-polymers (Figure 3.2). When comparing the carbonyl region between 1600–1800 cm^{-1} for the monomers **6OV** and **NN** and their respective homopolymers, there is a noticeable broadening

in the peak shapes. This is attributed to the closer proximity of the C=O moieties present on the radical monomers when polymerized and therefore indicates that the radicals are present after the ROMP reactions. This trend is observable for the random co-polymers as well as they all presented broadening in the same region. Furthermore, the N-O• stretching frequency at 1360 cm^{-1} is most intense in NN and PNN, while gradually decreasing in intensity upon incorporation of 6OV in the co-polymers.

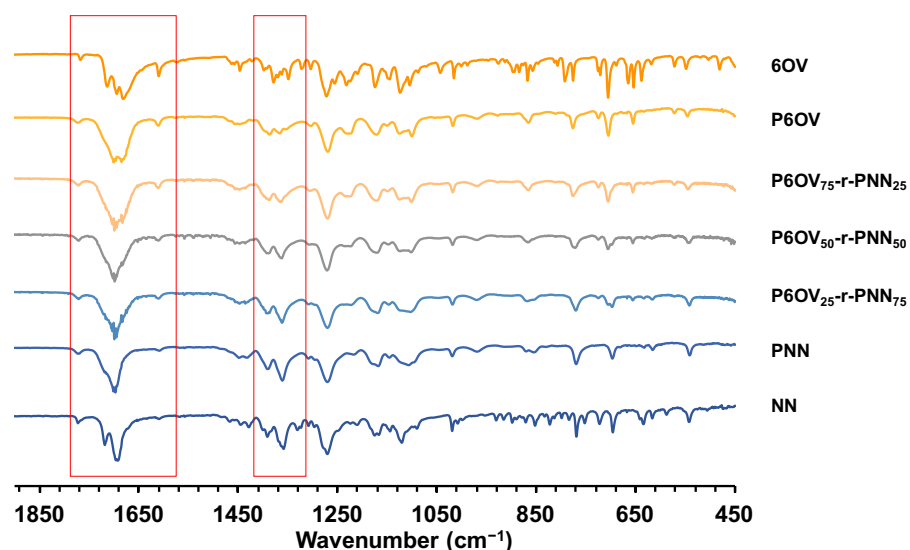


Figure 3.2. FT-IR spectra for 6OV, P6OV, P6OV_{75-r}-PNN₂₅, P6OV_{50-r}-PNN₅₀, P6OV_{25-r}-PNN₇₅, PNN and NN with red boxes highlighting regions between $1400\text{--}1300\text{ cm}^{-1}$ and $1800\text{--}1600\text{ cm}^{-1}$.

Due to the unavailability of ^1H NMR spectroscopy for paramagnetic compounds, the determination of the true ratio between the two subunits was done by using UV-absorption spectroscopy. The UV-Vis absorption spectra for each co-polymer was modeled using a fit to obtain a more accurate representation of the ratios (Figure 3.3). The model fits were calculated using Eq. 3.1, where a factor, x , was used to adjust for variable concentrations. Variables Abs_{PNN} and Abs_{P6OV} refer to the absorbance values of respective homopolymers, while χ_{PNN} and χ_{P6OV} refer to the mole fraction values used for each co-polymer.

$$x((\text{Abs}_{\text{PNN}} \times \chi_{\text{PNN}}) + (\text{Abs}_{\text{P6OV}} \times \chi_{\text{P6OV}})) \quad 3.1$$

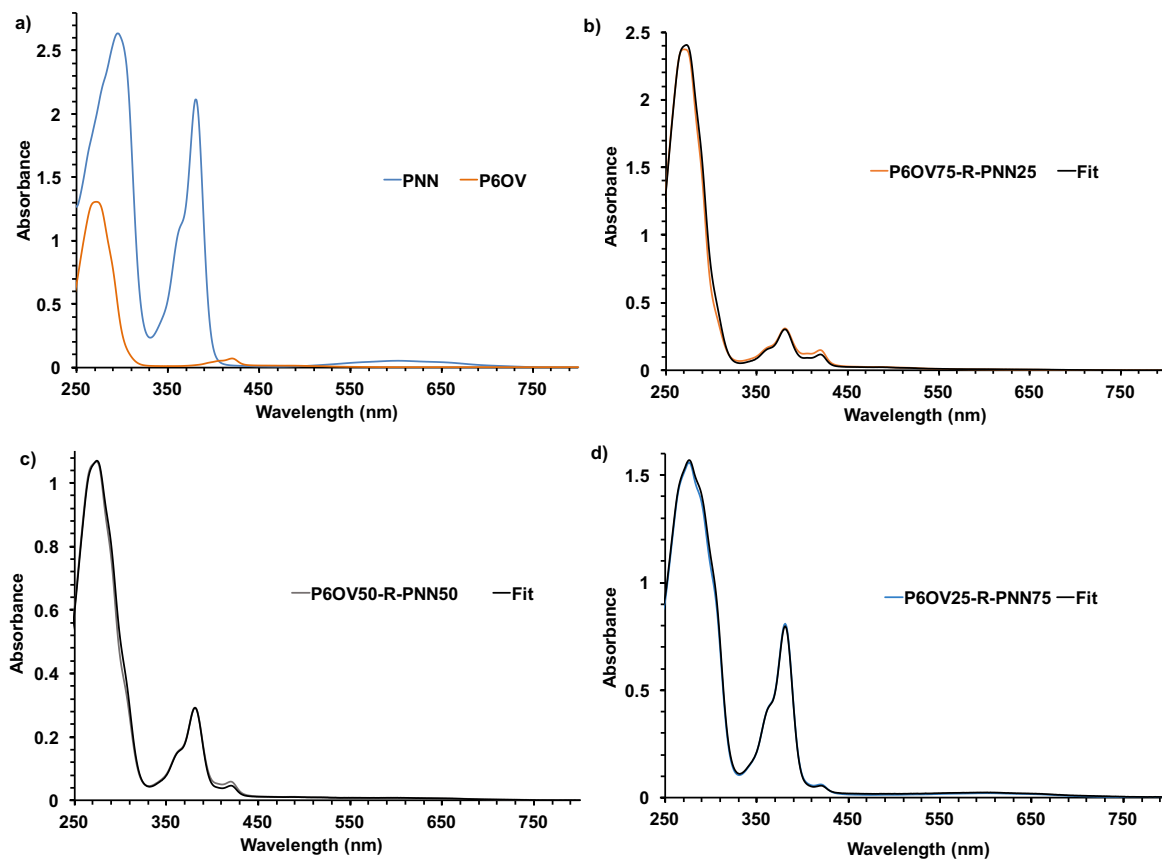


Figure 3.3. UV-Vis absorption spectra for homopolymers **PNN** and **P6OV** (a), as well as absorption spectra and model fits for random co-polymers (b) **P6OV_{75-r}-PNN₂₅**, (c) **P6OV_{50-r}-PNN₅₀**, and (d) **P6OV_{25-r}-PNN₇₅**.

The model fits were optimized using a R-factor, also known as a discrepancy index, as it helped determine the goodness of fit (Eq. 3.2). This was done by sweeping between different integer values of χ_{PNN} and χ_{P6OV} until the R-factor was minimized (Table 3.2). In the equation, Abs_{obs} refers to the experimental co-polymer absorbance values while Abs_{calc} refers to the model fit absorbance values. Based on these model fits, the calculated ratios for the co-polymers highlighted a systematically high incorporation of NN (Table 3.2). This could be attributed to the fact that the polymerization rate for the homopolymer **NN** is faster than homopolymer **6OV**,^{26, 27} thus suggesting that the NN units react more quickly, hindering the ability for 6OV monomers to add to the living chain.

$$\text{R-factor} = \frac{\sum |\text{Abs}_{\text{obs}} - \text{Abs}_{\text{calc}}|}{\sum |\text{Abs}_{\text{obs}}|} \quad 3.2$$

Table 3.2. Calculated ratios for random co-polymers $\text{P6OV}_m\text{-}r\text{-PNN}_n$ with their respective R-factor.

Theoretical m:n Ratios	Calculated m:n Ratios	R-factor
$\text{P6OV}_{75}\text{-}r\text{-PNN}_{25}$	$\text{P6OV}_{64}\text{-}r\text{-PNN}_{36}$	0.063
$\text{P6OV}_{50}\text{-}r\text{-PNN}_{50}$	$\text{P6OV}_{39}\text{-}r\text{-PNN}_{61}$	0.039
$\text{P6OV}_{25}\text{-}r\text{-PNN}_{75}$	$\text{P6OV}_{18}\text{-}r\text{-PNN}_{82}$	0.030

3.2.2 Synthesis of Block Co-Polymers Containing 6OV and NN

Initial attempts at synthesizing block co-polymers $\text{PNN}_m\text{-}b\text{-P6OV}_n$ where monomer NN was the starting block yielded broad bi-modal GPC traces, indicating little chain growth from the initial growing PNN chains (Figure 3.4). During the reaction procedure, it was also noted that there was unreacted 6OV monomer in the supernatant, indicating that not all monomer was used up in the reaction. Further changes in reaction time both for primary block growth and secondary block growth yielded no improved results. Henceforth, monomer 6OV was chosen as the starting block.

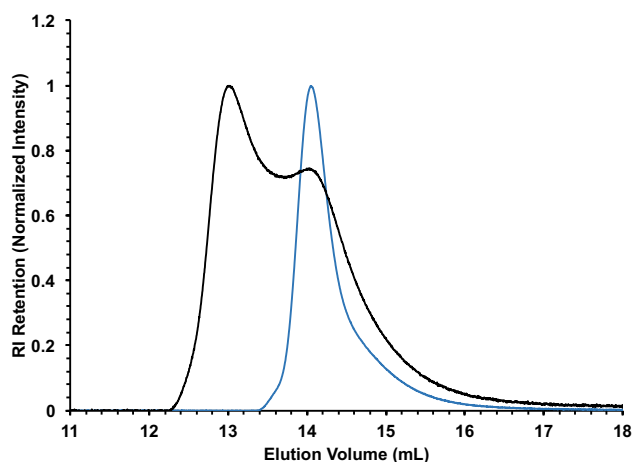
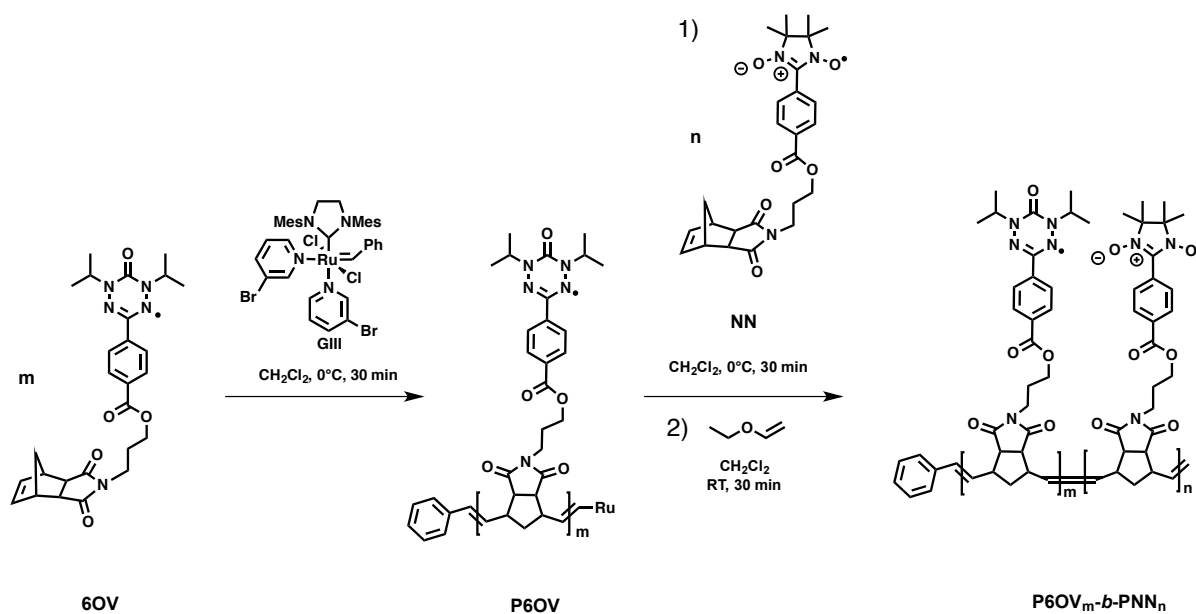


Figure 3.4. GPC traces for PNN aliquot (blue) and block co-polymer $\text{PNN}_{50}\text{-}b\text{-P6OV}_{50}$ (black) where NN was used as the starting block.

Attempts to synthesize block co-polymers $\text{P6OV}_m\text{-}b\text{-PNN}_n$ where 6OV is the starting block began by the dissolution of monomer 6OV in dry, degassed CH_2Cl_2 . A 1 mol % CH_2Cl_2 solution of **GIII** was then added to the solution mixture, and stirred at 0 °C for 30 min. An aliquot of the reaction mixture containing the growing P6OV block was extracted and added

to a flask containing ethyl vinyl ether. This was done to monitor the polymerization progress by GPC, as it provides an M_n value prior to secondary block addition. This method was applied for the synthesis of three block co-polymers with variation between the ratios of $\text{P6OV}_m\text{:PNN}_n$ where target $m:n$ ratios were 25:75, 50:50 and 75:25.



Scheme 3.2. Synthesis of block co-polymers $\text{P6OV}_m\text{-}b\text{-PNN}_n$.

GPC traces for block co-polymers $\text{P6OV}_m\text{-}b\text{-PNN}_n$ can be seen in Figure 3.5. Each trace illustrated some level of high molecular weight tailing, as observed for the random copolymers. When comparing the GPC traces for aliquots (orange traces) of the first block to their respective co-polymers, there is an increase in M_n and M_w as expected for a growing block copolymer highlighted by the shift to lower elution volume upon block addition (Figure 3.5). The D for the co-polymers ranged between 1.12-1.32 as expected for a controlled polymerization such as ROMP (Table 3.3).

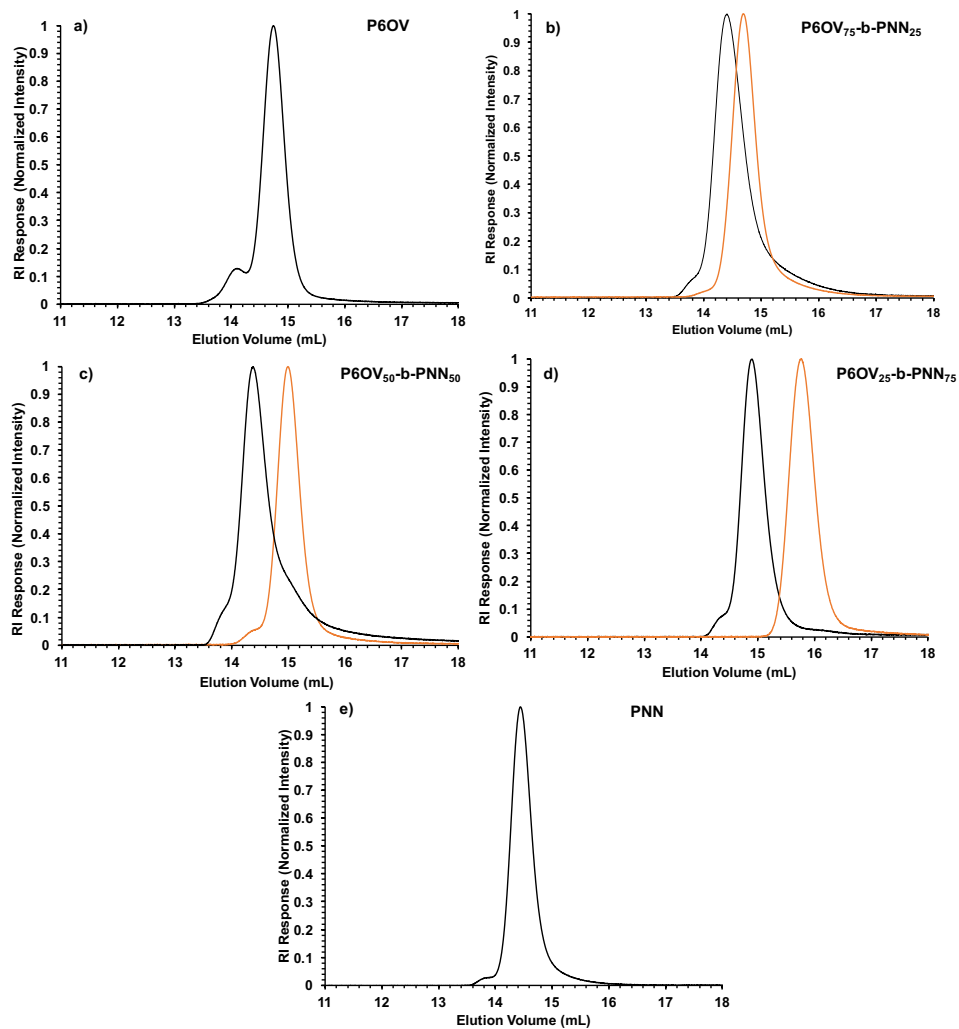


Figure 3.5. GPC traces of (in THF) for polymers (a) **P6OV**, (b) **P6OV₇₅-b-PNN₂₅**, (c) **P6OV₅₀-b-PNN₅₀**, (d) **P6OV₂₅-b-PNN₇₅**, and (e) **PNN**. The orange GPC traces present in (b), (c) and (d) belong to the aliquot of the first **P6OV** block prior to secondary block addition.

Table 3.3. M_n , M_w , and \mathcal{D} values for aliquots of the first **P6OV** block and **P6OV_m-b-PNN_n** block co-polymers.

Polymer	M_n aliquot (g/mol)	M_w aliquot (g/mol)	\mathcal{D} aliquots	M_n co- polymer (g/mol)	M_w co- polymer (g/mol)	\mathcal{D} co- polymer
P6OV₇₅-b-PNN₂₅	32,000	37,100	1.16	35,400	46,100	1.30
P6OV₅₀-b-PNN₅₀	31,900	35,600	1.12	44,800	59,200	1.32
P6OV₂₅-b-PNN₇₅	14,700	16,200	1.10	34,500	38,600	1.12

FT-IR spectroscopy for the block co-polymers highlighted similar trends in the carbonyl region when compared to the random co-polymers with broadening present in the C=O peaks when compared to respective monomers. The peak indicative of the nitroxyl radical in NN also followed a similar trend as in the random co-polymers with increase of intensity for the higher NN content block co-polymers (Figure 3.6).

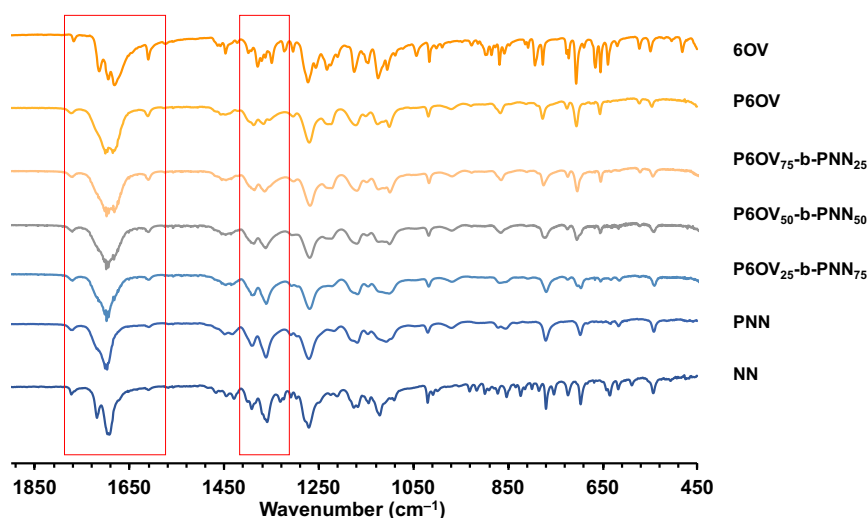


Figure 3.6. FT-IR spectra for **6OV**, **P6OV**, **P6OV₇₅-b-PNN₂₅**, **P6OV₅₀-b-PNN₅₀**, **P6OV₂₅-b-PNN₇₅**, **PNN** and **NN** with red boxes highlighting regions between $1400\text{--}1350\text{ cm}^{-1}$ and $1600\text{--}1800\text{ cm}^{-1}$.

As for the random co-polymers, UV-Vis absorption spectroscopy was used to help accurately determine the ratio of subunits. Using Eq. 3.1, model fits were made to the absorbance data (Figure 3.7). It was found that the ratios for the block co-polymers all incorporated slightly

more **NN** than **6OV**, as was the case for the random co-polymers. Using Eq. 3.2., the block co-polymers showed good agreement as R-factor values were close to 0 (Table 3.4).

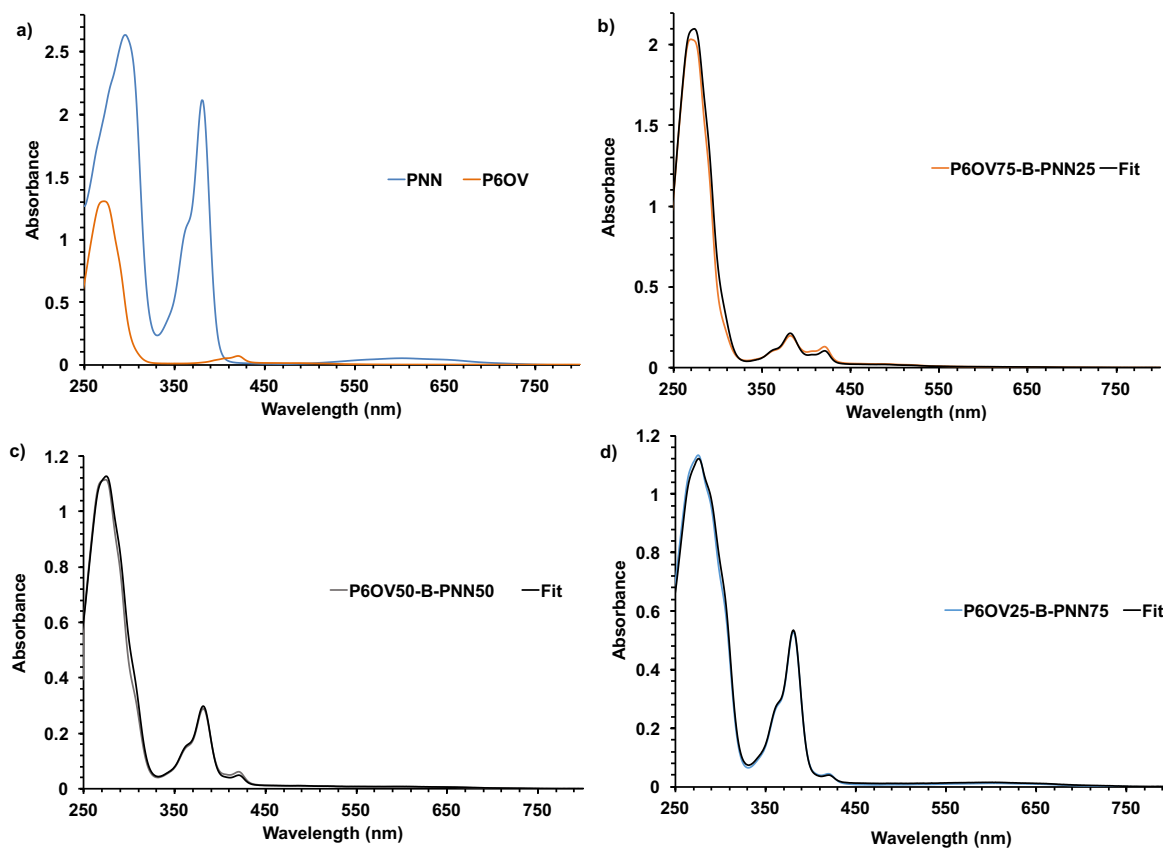


Figure 3.7. UV-Vis absorption spectra for homopolymers **PNN** and **P6OV** (a), as well as absorption spectra and model fits for block co-polymers (b) **P6OV₇₅-*b*-PNN₂₅**, (c) **P6OV₅₀-*b*-PNN₅₀**, and (d) **P6OV₂₅-*b*-PNN₇₅**.

Table 3.4. Calculated block ratios for block co-polymers **P6OV_m-*b*-PNN_n** with R-factor.

Theoretical m:n Ratios	Calculated m:n Ratios	R-factor
P6OV₇₅-<i>b</i>-PNN₂₅	P6OV₇₀-<i>b</i>-PNN₃₀	0.080
P6OV₅₀-<i>b</i>-PNN₅₀	P6OV₄₀-<i>b</i>-PNN₆₀	0.054
P6OV₂₅-<i>b</i>-PNN₇₅	P6OV₂₀-<i>b</i>-PNN₈₀	0.040

3.2.3 Thermal Properties of Co-Polymers

Using thermal gravimetric analysis (TGA), the thermal stability of the co-polymers was explored in duplicate for different polymer batches. All samples were heated from 25–1000 °C at a rate of 10 °C/min. For the random co-polymers, **P6OV_{75-r}-PNN₂₅** had the highest onset of decomposition at 147 °C, only slightly higher than **P6OV_{50-r}-PNN₅₀** at 145 °C. **P6OV_{25-r}-PNN₇₅** had the lowest thermal stability with an onset of decomposition at 115 °C. Overall, no char yield was observed for any of the co-polymers (Figure 3.8 and Table 3.5).

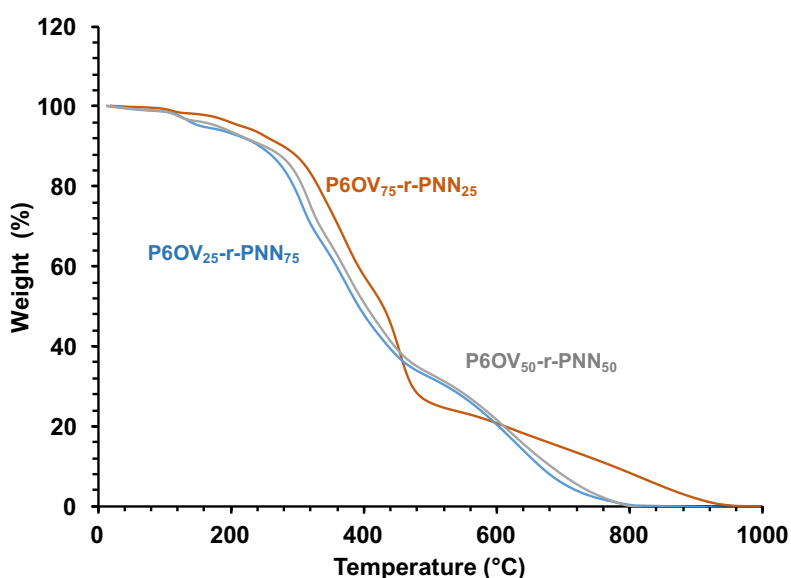


Figure 3.8 TGA graphs for **P6OV_{m-r}-PNN_n** random co-polymers.

Table 3.5. Onset of decomposition temperatures for **P6OV_{m-r}-PNN_n** random co-polymers.

Polymer	Onset of Decomposition (°C)
P6OV_{75-r}-PNN₂₅	147
P6OV_{50-r}-PNN₅₀	145
P6OV_{25-r}-PNN₇₅	115

A similar set of TGA experiments was conducted for the block co-polymers, which highlighted that there wasn't a great difference in the onset of decompositions for the block co-polymers (Figure 3.9 and Table 3.6). As for the random co-polymers, the polymer which contained

majority P6OV, **PNN₂₅-*b*-P6OV₇₅**, had the highest onset of decomposition at 136 °C. **PNN₇₅-*b*-P6OV₂₅** presented a char yield of 3%.

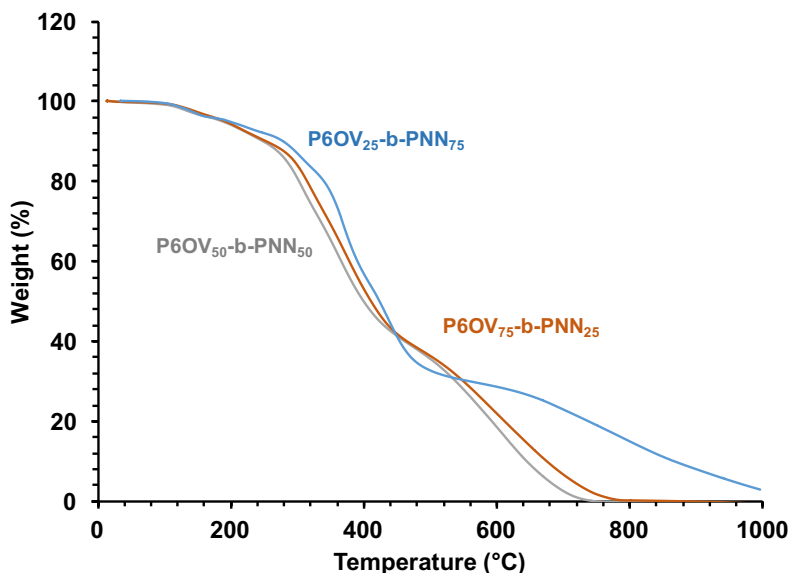


Figure 3.9. TGA graphs for **P6OV_m-*b*-PNN_n** block co-polymers.

Table 3.6. Onset of decomposition temperatures for **P6OV_m-*b*-PNN_n** block co-polymers.

Polymer	Onset of Decomposition (°C)
P6OV₇₅-<i>b</i>-PNN₂₅	136
P6OV₅₀-<i>b</i>-PNN₅₀	132
P6OV₂₅-<i>b</i>-PNN₇₅	127

Based on the onset of decomposition temperatures acquired in the TGA studies, differential scanning calorimetry (DSC) studies were employed for all co-polymers (Figure 3.10 and Figure 3.11). All but one DSC study employed a temperature range of 20–110 °C, with the exception being **P6OV₂₅-*r*-PNN₇₅** which was run between 20–90 °C. No glass transition temperatures (T_g) were observed within the stability windows determined by TGA due to the degradation of the polymer occurring first. Previous studies highlighted that **P6OV** possessed a T_g at 152 °C,²⁷ which is out of the temperature range of the studies, while **PNN** possessed no T_g in its stability window.²⁶

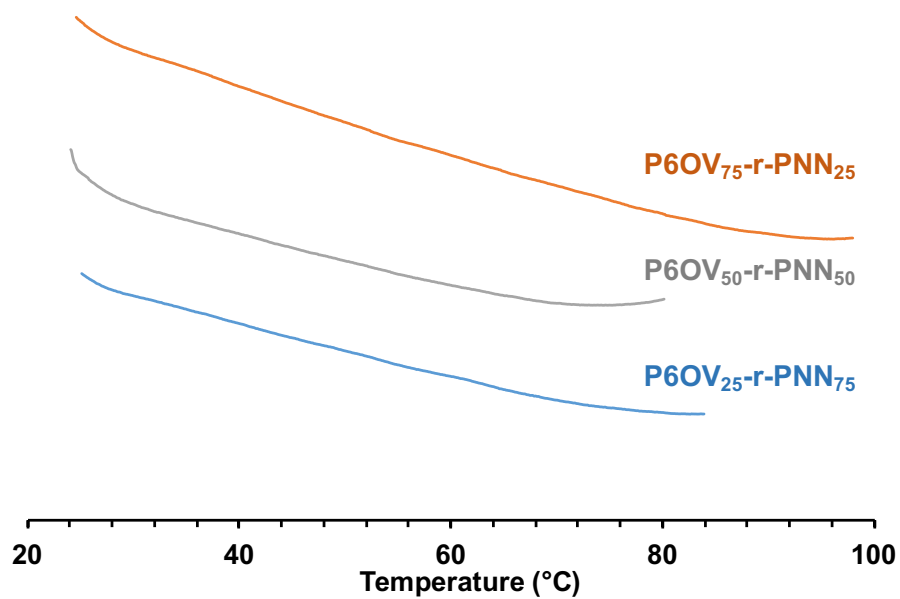


Figure 3.10 DSC traces for **P6OV_m-r-PNN_n** random co-polymers.

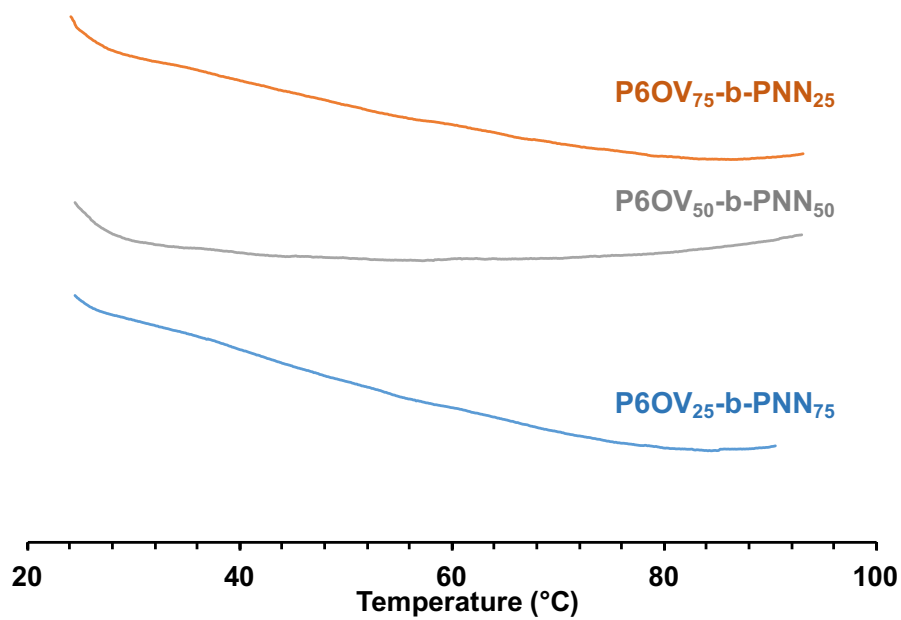


Figure 3.11 DSC traces for **P6OV_m-b-PNN_n** block co-polymers.

3.2.4 Electrochemical Properties of Co-Polymers

Investigation of the electrochemical properties of the co-polymers was done using cyclic voltammetry (CV) and the results were compared to similar data for homopolymers **PNN** and **P6OV** (Figure 3.12 and Figure 3.13). The measurements were done in a 1:1 $\text{CH}_2\text{Cl}_2/\text{MeCN}$ solution while using the Fc/Fc^+ redox couple as an internal redox reference system.

Homopolymer **PNN** was reversibly oxidized at half-wave oxidation potential $E_{1/2\text{ox}} = 0.43\text{V}$, while possessing no reversible reduction (Figure 3.12, vertical blue line). Homopolymer **P6OV** was reversibly oxidized and reduced at half-wave oxidation and reduction potentials $E_{1/2\text{ox}} = 0.26\text{ V}$ and $E_{1/2\text{red}} = -1.36\text{ V}$ respectively (Figure 3.12, vertical orange lines). For all random co-polymers, the reversibility of oxidation/reduction was affected upon mixing of the radicals. All random-copolymers exhibited at least one reversible oxidation wave, while **P6OV_{50-r-PNN₅₀}** exhibited two reversible oxidation waves attributed to **P6OV** and **PNN** oxidations ($E_{1/2\text{ox}} = 0.27\text{ V}, 0.44\text{ V}$). The only co-polymer to exhibit a reversible reduction wave was **P6OV_{75-b-PNN₂₅}** ($E_{1/2\text{red}} = -1.36\text{ V}$). The block co-polymers possessed similar oxidation and reduction features as the random co-polymers (Figure 3.13).

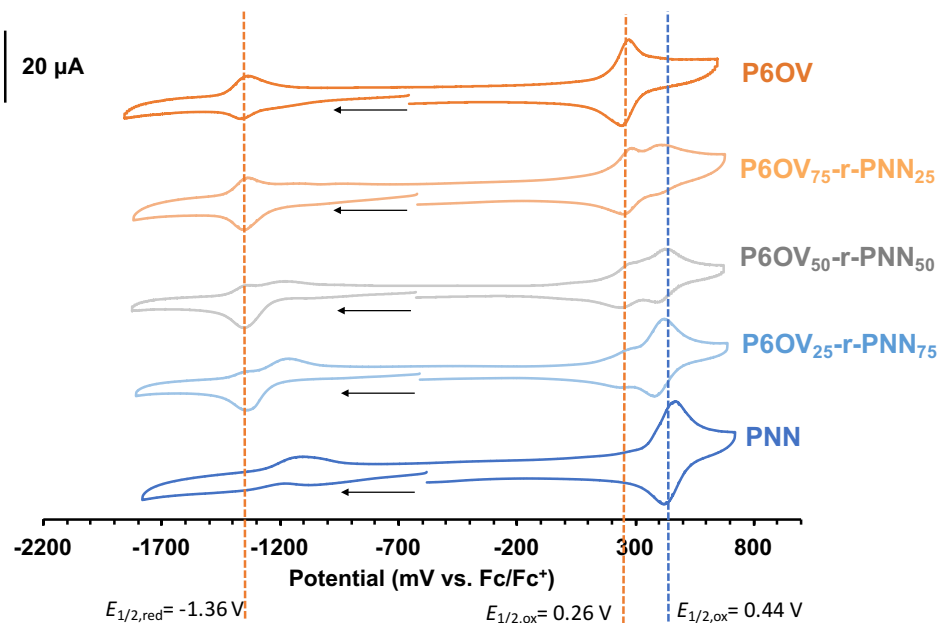


Figure 3.12. Cyclic voltammograms collected for $\text{P6OV}_m\text{-}r\text{-PNN}_n$ random co-polymers. Experiments were conducted in degassed mixtures of 50:50 v/v $\text{CH}_2\text{Cl}_2/\text{CH}_3\text{CN}$ containing approximately 1 mM of analyte and 0.1 M $[\text{nBu}_4\text{N}][\text{PF}_6]$ at scan rates of 250 mV s^{-1} . Blue vertical line indicates **PNN** oxidation potential, while the two orange vertical lines indicate **P6OV** oxidation and reduction potentials.

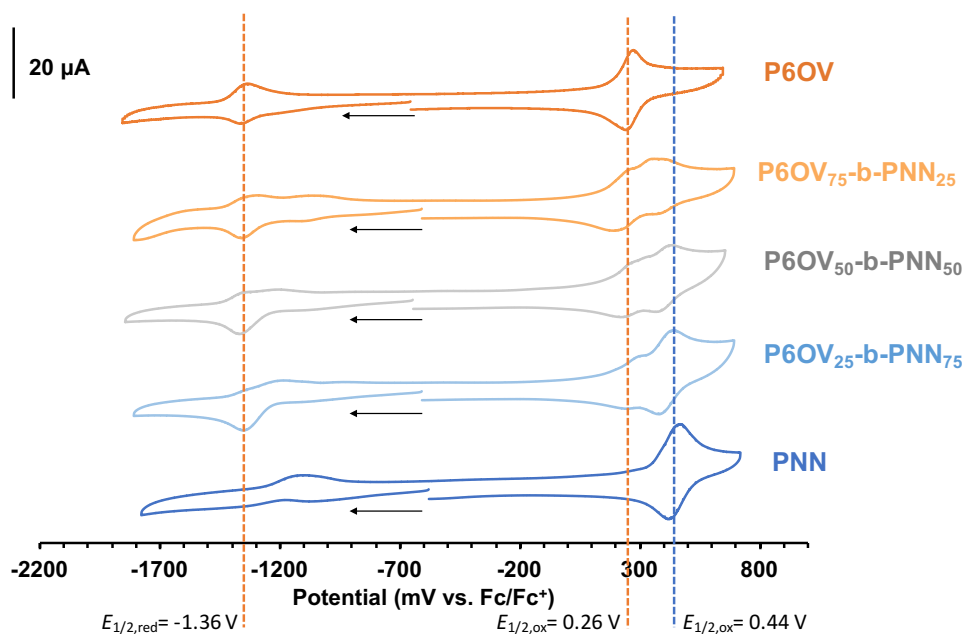


Figure 3.13. Cyclic voltammograms collected for $\text{P6OV}_m\text{-}b\text{-PNN}_n$ block co-polymers. Scan is in the negative direction at 250 mV s^{-1} scan rate. Experiments were conducted in degassed mixtures of 50:50 v/v $\text{CH}_2\text{Cl}_2/\text{CH}_3\text{CN}$ containing approximately 1 mM of analyte and 0.1 M $[\text{nBu}_4\text{N}][\text{PF}_6]$ at scan rates of 250 mV s^{-1} . Blue vertical line indicates **PNN** oxidation potential, while the two orange vertical lines indicate **P6OV** oxidation and reduction potentials.

3.3 Conclusion

This chapter highlighted that three random and three block co-polymers containing **NN** and **6OV** radical monomers were successfully synthesized using ROMP in varying monomer ratios. During the synthesis, it was found that the order of addition of monomers is crucial for block co-polymer formation, as co-polymers using **NN** as the starting block yielded polymers that showed bi-modal GPC traces. All co-polymers were characterized using spectroscopic techniques such as FT-IR and UV-vis spectroscopy, which revealed that the radicals survived the polymerization processes. To determine an accurate representation of the true monomer ratios, model fits were created for the co-polymer UV-vis absorption data, using an R-factor to determine goodness of fit. Based on the model fits, all co-polymers unexpectedly incorporated more **NN** than **6OV**. This was attributed to the faster polymerization rate of **NN** as opposed to **6OV**. DSC studies revealed no T_g for any co-polymer, while TGA studies implied that degradation occurs prior to reaching that temperature. All co-polymers revealed at least one reversible oxidation wave which was characteristic to their homopolymer counterparts, while no reversible reduction waves were observed. With the co-polymers fully characterized, future work will involve the processing of thin-films made of these polymers, as well as their incorporation into solid-state devices.

3.4 Experimental

3.4.1 General Considerations

Reactions and manipulations were carried out under a N_2 atmosphere using standard Schlenk techniques unless otherwise stated. Reagents were purchased from Sigma-Aldrich, Alfa-Aesar or Oakwood Chemicals and used as received unless otherwise specified. Solvents were purchased from Caledon Laboratories, dried using an Innovative Technologies Inc. solvent purification system, collected under vacuum, and stored under a N_2 atmosphere over 4 Å molecular sieves. FT-IR spectra were recorded on a PerkinElmer Spectrum Two instrument using an attenuated total reflectance accessory. UV-vis absorption spectra were recorded on a Cary 5000 UV-Vis-NIR spectrophotometer between 200 and 800 nm.

3.4.2 Gel Permeation Chromatography (GPC)

GPC experiments were conducted in chromatography-grade THF at concentrations of 5 mg mL^{-1} using a Viscotek GPCmax VE 2001 GPC instrument equipped with an Agilent PolyPore guard column (PL1113-1500) and two sequential Agilent PolyPore GPC columns packed with porous poly (styrene-*co*-divinylbenzene) particles (MW range: 200–2,000,000 g mol^{-1} ; PL1113-6500) regulated at a temperature of $30 \text{ }^\circ\text{C}$. Signal responses were measured using a Viscotek VE 3580 refractive index detector, and molecular weights were determined by comparison of the maximum refractive index response with a calibration curve (10 points, 1,500–786,000 g mol^{-1}) established using monodisperse polystyrene standards purchased from Viscotek. All co-polymer samples were stirred for 45 min and then passed through a $0.2 \text{ }\mu\text{m}$ syringe filter prior to GPC analysis to ensure full dissolution.

3.4.3 Cyclic Voltammetry

Cyclic voltammetry experiments were performed using a Bioanalytical Systems Inc. (BASi) Epsilon potentiostat and analyzed using BASi Epsilon software. Electrochemical cells consisted of a three-electrode setup including a glassy carbon working electrode, platinum wire counter electrode and silver wire *pseudo* reference electrode. Experiments were run at scan rates of 250 mV s^{-1} in degassed CH_2Cl_2 solutions of the analyte ($\sim 1 \text{ mM}$) and supporting electrolyte ($0.1 \text{ M } [n\text{Bu}_4\text{N}][\text{PF}_6]$). Cyclic voltammograms were referenced against an internal standard ($\sim 1 \text{ mM}$ ferrocene) and corrected for internal cell resistance using the BASi Epsilon software.

3.4.4 Thermal Analysis

Thermal degradation studies were performed using a TA Instruments Q50 TGA instrument under a N_2 atmosphere. Samples of all co-polymers were placed in a platinum pan and heated at a rate of $10 \text{ }^\circ\text{C min}^{-1}$ from $20 \text{ }^\circ\text{C}$ to $1000 \text{ }^\circ\text{C}$ under a flow of N_2 (60 mL min^{-1}). Differential scanning calorimetry studies were performed using a TA Instruments DSC Q20. Polymer samples were placed in an aluminum Tzero pan and subjected to three heating cooling cycles at a rate of $10 \text{ }^\circ\text{C min}^{-1}$ under a flow of N_2 (50 mL min^{-1}). The first heating/cooling cycles are reported.

3.4.5 Synthetic Procedures

Representative procedure for the preparation of random copolymers P6OV_m-*r*-PNN_n

P6OV₅₀-*r*-PNN₅₀

Monomer **6OV** (0.053 g, 0.10 mmol) and monomer **NN** (0.050 g, 0.10 mmol) were dissolved in degassed CH₂Cl₂ (6.0 mL, 3 freeze-pump-thaw cycles). The solution was cooled to 0 °C and stirred in an ice bath for 5 min before a 1 mg mL⁻¹ CH₂Cl₂ solution of the 3-bromopyridine derivative of Grubbs' 3rd generation catalyst (1.84 mL, 2.10 × 10⁻³ mmol) was quickly added. The polymerization proceeded for 30 min before termination with ethyl vinyl ether (0.40 mL, 4.2 mmol) and stirring for an additional 30 min at RT. The crude reaction mixture was filtered through a short neutral alumina plug using THF as the eluent before the solvent was removed *in vacuo*. The resulting solid was dissolved in a minimal amount of THF and precipitated into rapidly stirred cold pentane (40 mL) thrice to afford (PNN)₅₀-*r*-(P6OV)₅₀ as a gray powder. Yield = 0.090 g, 87%. FT-IR (ranked intensity, assignment): 1774 (8), 1697 (1), 1612 (9), 1447 (7), 1392 (4), 1362 (3), 1272 (2), 1174 (5), 1113 (6) cm⁻¹. UV-vis (CH₂Cl₂): λ_{max} = 645 nm, 602 nm, 563 nm, 420 nm, 380 nm, 363 nm, 274 nm. GPC (THF, conventional calibration relative to polystyrene standards): M_n = 44,700 g mol⁻¹, M_w = 54,600 g mol⁻¹, Đ = 1.22

P6OV₇₅-*r*-PNN₂₅

From monomer **6OV** (0.100 g, 0.198 mmol) and **NN** (0.032 g, 0.066 mmol). Yield = 0.12 g, 90%. FT-IR (ranked intensity, assignment): 1774 (9), 1697 (1), 1612 (8), 1447 (7), 1392 (6), 1362 (5), 1272 (2), 1174 (4), 1113 (3) cm⁻¹. UV-vis (CH₂Cl₂): λ_{max} = 645 nm, 602 nm, 420 nm, 380 nm, 363 nm, 274 nm. GPC (THF, conventional calibration relative to polystyrene standards): M_n = 63,400 g mol⁻¹, M_w = 76,100 g mol⁻¹, Đ = 1.23.

P6OV₂₅-*r*-PNN₇₅

From monomer **6OV** (0.036 g, 0.069 mmol) and **NN** (0.100 g, 0.207 mmol). Yield = 0.11 g, 87%. FT-IR (ranked intensity, assignment): 1774 (8), 1697 (1), 1612 (9), 1447 (7), 1392 (4), 1362 (3), 1272 (2), 1174 (5), 1113 (6) cm⁻¹. UV-vis (CH₂Cl₂): λ_{max} = 645 nm, 602 nm, 563 nm, 420 nm, 380 nm, 363 nm, 274 nm. GPC (THF, conventional calibration relative to polystyrene standards): M_n = 48,500 g mol⁻¹, M_w = 59,200 g mol⁻¹, Đ = 1.23.

Representative procedure for preparation of block copolymers **P6OV_m-b-PNN_n**

P6OV₅₀-b-PNN₅₀

Monomer **6OV** (0.063g, 0.124 mmol) and monomer **NN** (0.047g, 0.099 mmol) were each dissolved in degassed CH₂Cl₂ (3.0 mL, in separate flasks with 3 freeze-pump-thaw cycles) and cooled down to 0 °C. A 1 mg mL⁻¹ CH₂Cl₂ solution of the 3-bromopyridine derivative of Grubbs' 3rd generation catalyst (2.18 mL, 2.48 x 10⁻³ mmol) was quickly added to the solution of monomer **6OV**, and the polymerization proceeded for 30 min. After 30 min, a small aliquot (1.30 mL, 0.025 mmol) was removed and added to a flask containing ethyl vinyl ether (0.40 mL, 4.2 mmol) and stirred at RT for 30 min, while subsequently the **NN** solution was quickly syringed into the initial reaction mixture and stirred at 0 °C for 30 min. Termination was completed by adding ethyl vinyl ether (0.40 mL, 4.2 mmol) and stirring for an additional 30 min at RT. The crude reaction mixture was filtered through a short pipette neutral alumina plug, using THF, and the solvent was removed *in vacuo*. The resulting polymer was dissolved in THF and precipitated into rapidly stirred cold pentane (40 mL) thrice to afford **(PNN)₅₀-b-(P6OV)₅₀** as a gray powder. Yield = 0.085 g, 87%. FT-IR (ranked intensity, assignment): 1774 (8), 1697 (1), 1612 (9), 1447 (7), 1392 (4), 1362 (3), 1272 (2), 1174 (5), 1113 (6) cm⁻¹. UV-vis (CH₂Cl₂): λ_{max} = 645 nm, 602 nm, 563 nm, 420 nm, 380 nm, 363 nm, 274 nm. GPC (THF, conventional calibration relative to polystyrene standards): M_n = 44,800 g mol⁻¹, M_w = 59,200 g mol⁻¹, *D* = 1.32

P6OV₇₅-b-PNN₂₅

From monomer **6OV** (0.125 g, 0.247 mmol; 0.049 mmol removed as aliquot for MW analysis) and **NN** (0.032 g, 0.066 mmol). Yield = 0.12 g, 90%. FT-IR (ranked intensity, assignment): 1774 (9), 1697 (1), 1612 (8), 1447 (7), 1392 (6), 1362 (5), 1272 (2), 1174 (4), 1113 (3) cm⁻¹. UV-vis (CH₂Cl₂): λ_{max} = 645 nm, 602 nm, 420 nm, 380 nm, 363 nm, 274 nm. GPC (THF, conventional calibration relative to polystyrene standards): M_n = 35,400 g mol⁻¹, M_w = 46,100 g mol⁻¹, *D* = 1.30.

P6OV₂₅-b-PNN₇₅

From monomer **6OV** (0.038 g, 0.074 mmol; 0.015 mmol removed as aliquot for MW analysis) and **NN** (0.085 g, 0.177 mmol). Yield = 0.10 g, 87%. FT-IR (ranked intensity, assignment): 1774 (8), 1697 (1), 1612 (9), 1447 (7), 1392 (4), 1362 (3), 1272 (2), 1174 (5), 1113 (6) cm⁻¹. UV-vis (CH₂Cl₂): λ_{max} = 645 nm, 602 nm, 563 nm, 420 nm, 380 nm, 363 nm, 274 nm. GPC

(THF, conventional calibration relative to polystyrene standards): $M_n = 34,500 \text{ g mol}^{-1}$, $M_w = 38,600 \text{ g mol}^{-1}$, $D = 1.12$.

3.5 References

- (1) Fan, L.; Wei, L.; Zhu, Y.; Wang, Y.; Fei, J.; Li, Y. *Materials* **2020**, *13*, 1–9.
- (2) Nishimori, K.; Ouchi, M. *Chem. Commun.* **2020**, *56*, 3473–3483.
- (3) Feng, H.; Lu, X.; Wang, W.; Kang, N.-G.; Mays, J. W. *Polymers* **2017**, *9*, 1–31.
- (4) Hadjichristidis, N.; Iatrou, H.; Pitsikalis, M.; Mays, J. *Prog. Polym. Sci.* **2006**, *31*, 1068–1132.
- (5) Verduzco, R.; Li, X.; Pesek, S. L.; Stein, G. E. *Chem. Soc. Rev.* **2015**, *44*, 2405–2420.
- (6) Suga, T.; Konishi, H.; Nishide, H. *Chem. Commun.* **2007**, 1730–1732.
- (7) Nishide, H.; Iwasa, S.; Pu, Y. J.; Suga, T.; Nakahara, K.; Satoh, M. *Electrochim. Acta* **2004**, *50*, 827–831.
- (8) Nishide, H.; Suga, T. *Electrochem. Soc. Interface* **2006**, *14*, 32–36.
- (9) Janoschka, T.; Hager, M. D.; Schubert, U. S. *Adv. Mater.* **2012**, *24*, 6397–6409.
- (10) Bugnon, L.; Morton, C. J. H.; Novak, P.; Vetter, J.; Nesvadba, P. *Chem. Mater.* **2007**, *19*, 2910–2914.
- (11) Oyaizu, K.; Nishide, H. *Adv. Mater.* **2009**, *21*, 2339–2344.
- (12) Hayashi, H.; Karasawa, S.; Tanaka, A.; Odoi, K.; Chikama, K.; Kuribayashi, H.; Koga, N. *Magn. Reson. Chem.* **2009**, *47*, 201–204.
- (13) Li, L.; Chu, C.-C. *J. Biomater. Sci. Polym. Ed.* **2009**, *20*, 341–361.
- (14) Yonekuta, Y.; Susuki, K.; Oyaizu, K.; Honda, K.; Nishide, H. *J. Am. Chem. Soc.* **2007**, *129*, 14128–14129.
- (15) Rostro, L.; Galicia, L.; Boudouris, B. W. *J. Polym. Sci., Part B: Polym. Phys.* **2015**, *53*, 311–316.
- (16) Hauffman, G.; Rolland, J.; Bourgeois, J. P.; Vlad, A.; Gohy, J. F. *J. Polym. Sci., Part A: Polym. Chem.* **2013**, *51*, 1–8.
- (17) Zhuang, X.; Xiao, C.; Oyaizu, K.; Chikushi, N.; Chen, X.; Nishide, H. *J. Polym. Sci., Part A: Polym. Chem.* **2010**, *48*, 5404–5410.
- (18) Sukegawa, T.; Masuko, I.; Oyaizu, K.; Nishide, H. *Macromolecules* **2014**, *47*, 8611–8617.
- (19) Liedel, C.; Ober, C. K. *Macromolecules* **2016**, *49*, 5884–5892.

- (20) Liedel, C.; Moehle, A.; Fuchs, G. D.; Ober, C. K. *MRS Commun.* **2015**, *5*, 441–446.
- (21) Cintora, A.; Takano, H.; Khurana, M.; Chandra, A.; Hayakawa, T.; Ober, C. K. *Polym. Chem.* **2019**, *10*, 5094–5102.
- (22) Zhu, J.; Zhu, T.; Tuo, H.; Zhang, W. *Polymers* **2019**, *11*, 1–13.
- (23) Koshika, K.; Chikushi, N.; Sano, N.; Oyaizu, K.; Nishide, H. *Green Chem.* **2010**, *12*, 1573–1575.
- (24) Suga, T.; Sakata, M.; Aoki, K.; Nishide, H. *ACS Macro Lett.* **2014**, *3*, 703–707.
- (25) Zhang, Y.; Park, A. M.; McMillan, S. R.; Harmon, N. J.; Flatté, M. E.; Fuchs, G. D.; Ober, C. K. *Chem. Mater.* **2018**, *30*, 4799–4807.
- (26) Anghel, M.; Magnan, F.; Catingan, S. D.; McCready, M. A.; Aawani, E.; Wong, V.; Singh, D.; Fanchini, G.; Gilroy, J. B. *J. Polym. Sci.* **2020**, *58*, 309–319.
- (27) Paquette, J. A.; Ezugwu, S.; Yadav, V.; Fanchini, G.; Gilroy, J. B. *J. Polym. Sci., Part A: Polym. Chem.* **2016**, *54*, 1803–1813.

Chapter 4

4 Conclusions and Future Work

The original research in this thesis begins in Chapter 2 (Figure 4.1) where the synthetic procedure for the production of a stable organic radical monomer and its respective polymer as well as the characterization of their physical and chemical properties were presented. The radical monomer was composed of a nitronyl nitroxide radical appended to the polymerizable group *cis*-5-norbornene-*exo*-2,3-dicarboximide. This allowed for the use of ring-opening metathesis polymerization (ROMP) using the 3-bromopyridine derivative Grubb's 3rd generation catalyst, yielding narrow dispersity polymers with controllable molecular weights. Two different studies on the ROMP behavior of the polymerization were undertaken. The first study involved the monitoring of molecular weights after various catalyst loadings. The second study involved the removal of timed aliquots from the reaction, where the molecular weight growth was observed over a period of time. Both studies revealed the ROMP to be well-behaved, but not formally living. Using EPR and UV-Vis spectroscopy, radical content was determined to be high (~97%). CV studies of the monomer revealed two reversible redox events, while the polymer possessed one reversible oxidation event. Thin-films of the polymer were processed by Fanchini and co-workers with smoothness that allowed them to be processed into sandwich-type solid-state devices. These devices demonstrated memory effects upon the application of bias voltages, making the polymer a good candidate for memory device applications.

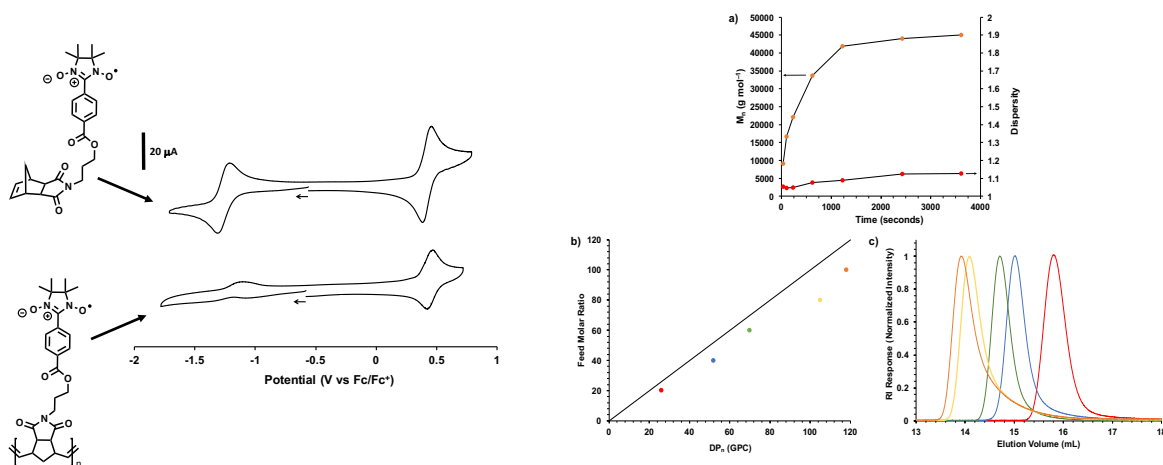
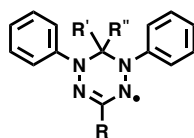


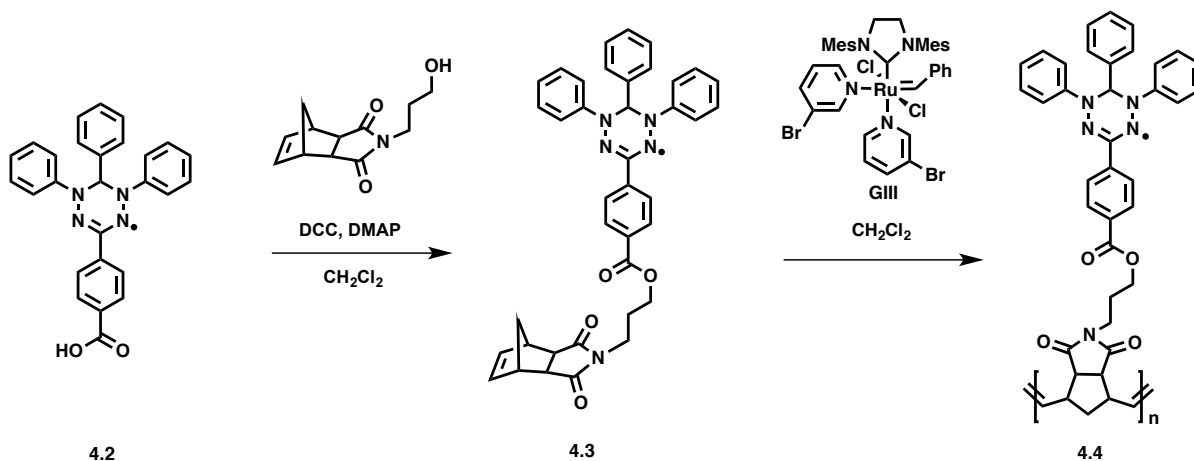
Figure 4.1 Graphical summary of Chapter 2.

There is still work to be done towards understanding the unique redox properties of radical polymers and their functionality in solid-state devices. Expanding upon the findings related to my nitronyl nitroxide polymer, studying a different radical system with varying redox properties, would provide new insight into the behavior of these species in solid-state devices. Kuhn verdazyls **4.1** have been incorporated into polymers before, however, they often yielded insoluble solids, or low molecular weight polymers with low radical content.¹⁻³ A proposed synthesis (Scheme 4.1) involves appending a phenyl Kuhn verdazyl radical **4.2** to a *cis*-5-norbornene-*exo*-2,3-dicarboximide backbone, giving the verdazyl monomer **4.3**. Then using ROMP, a phenylverdazyl polymer **4.4** yielding narrow dispersity with high and controlled molecular weight, while also providing high radical content could be achieved. These polymers would eventually be tested as active materials in memristors.



4.1

R', R'' = aryl, alkyl or H
R = aryl or alkyl



Scheme 4.1 Proposed synthesis of a Kuhn verdazyl polymer using ROMP.

Work in Chapter 3 expanded upon the findings in Chapter 2, where the nitronyl nitroxide monomer previously synthesized was co-polymerized with a 6-oxoverdazyl monomer yielding random and block co-polymers. During the synthesis process of the block co-polymers it was found that successful polymerization was only achieved when using the 6-oxoverdazyl monomer as the starting unit, while using nitronyl nitroxide first yielded polymers with bimodal GPC traces. Three different ratios of monomers were employed for both co-polymers: 25:75, 50:50, and 75:25. Using UV-Vis spectroscopy, model fits for the absorbance of the co-polymers were processed. Comparison between the model fits and the acquired absorbance data gave R-factors close to 0, indicating good agreement. Overall, all co-polymers incorporated slightly more nitronyl nitroxide which corresponded with its faster polymerization rate when compared to 6-oxoverdazyl. CV studies of the co-polymers showed oxidation and reduction events for the 6-oxoverdazyl moieties, while nitronyl nitroxide only showed oxidation events. These redox events are also observed in their homopolymer counterparts.

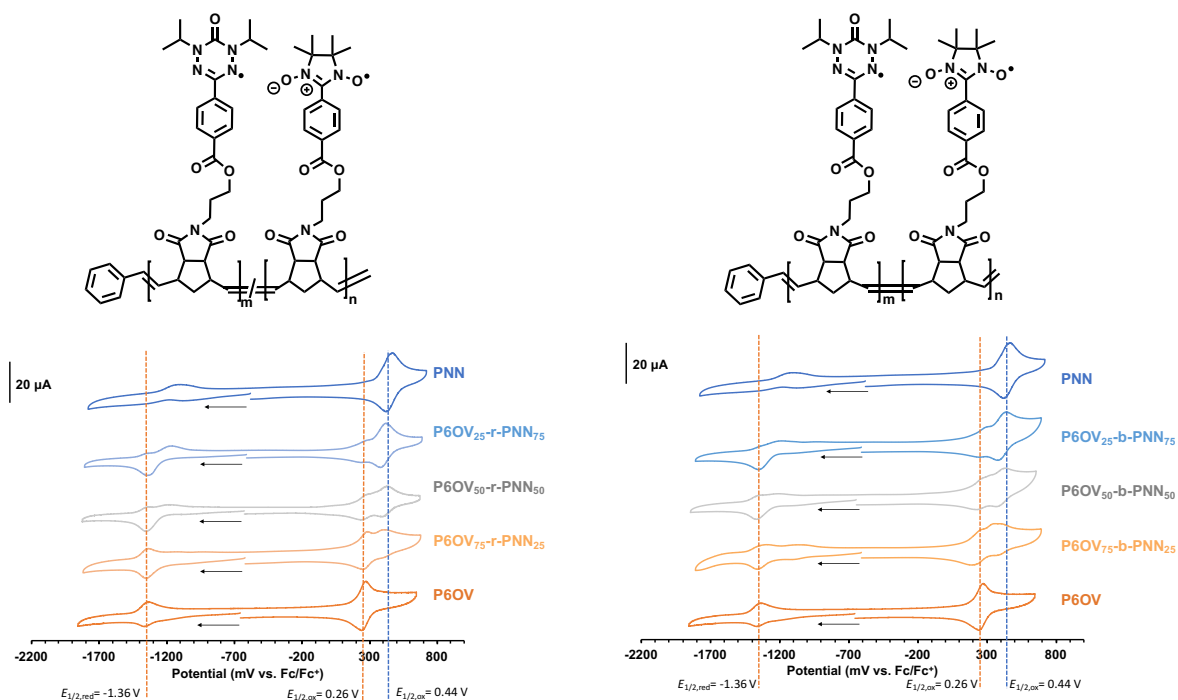


Figure 4.2 Graphical summary of Chapter 3.

Future work based on these co-polymers will involve the development of thin-films and their incorporation into solid-state devices. Collaborating with the Fanchini group, these devices would be tested for their conductive properties to further probe the memory effects that radical polymers possess as seen in Chapter 2, as well as the effect of the co-polymer architecture on these devices. As seen beforehand, there was distinguishability in redox events between the two radicals in the co-polymers, which could lead to interesting memory effects in devices as electronic communication between radicals is present. The different ratios of monomers could also lead to different effects, offering a wide-variety of tunability for these devices. To our knowledge, memristor devices based on radical co-polymers of two different radicals have not yet been discussed in the literature, implying there is a significant need for further work to be done in this field.

This thesis has resulted in the development of new radical polymers, shown that they can exhibit exceptional stability and properties, and paved the way for their use in organic electronics such as memristors.

4.1 References

- (1) Miura, Y.; Kinoshita, M.; Imoto, M. *Makromol. Chem.* **1971**, *146*, 69–77.
- (2) Miura, Y.; Kinoshita, M.; Imoto, M. *Makromol. Chem.* **1972**, *157*, 51–61.
- (3) Kamachi, M.; Enomoto, H.; Shibasaka, M.; Mori, W.; Kishita, M. *Polym. J.* **1986**, *18*, 439–441.

Appendices

Appendix 1 - Permission to Reuse Copyrighted Material

8/27/2020 Rightslink® by Copyright Clearance Center



RightsLink®

Home
Help
Email Support
Michael Anghel ▾



Cathode- and Anode-Active Poly(nitroxylstyrene)s for Rechargeable Batteries: p- and n-Type Redox Switching via Substituent Effects

Author: Takeo Suga, Yong-Jin Pu, Shinji Kasatori, et al
Publication: Macromolecules
Publisher: American Chemical Society
Date: May 1, 2007

Copyright © 2007, American Chemical Society

PERMISSION/LICENSE IS GRANTED FOR YOUR ORDER AT NO CHARGE

This type of permission/license, instead of the standard Terms & Conditions, is sent to you because no fee is being charged for your order. Please note the following:

- Permission is granted for your request in both print and electronic formats, and translations.
- If figures and/or tables were requested, they may be adapted or used in part.
- Please print this page for your records and send a copy of it to your publisher/graduate school.
- Appropriate credit for the requested material should be given as follows: "Reprinted (adapted) with permission from (COMPLETE REFERENCE CITATION). Copyright (YEAR) American Chemical Society." Insert appropriate information in place of the capitalized words.
- One-time permission is granted only for the use specified in your request. No additional uses are granted (such as derivative works or other editions). For any other uses, please submit a new request.

If credit is given to another source for the material you requested, permission must be obtained from that source.

BACK
CLOSE WINDOW

© 2020 Copyright - All Rights Reserved | [Copyright Clearance Center, Inc.](#) | [Privacy statement](#) | [Terms and Conditions](#)
Comments? We would like to hear from you. E-mail us at customercare@copyright.com

<https://s100.copyright.com/AppDispatchServlet>

1/1

8/28/2020

Rightslink® by Copyright Clearance Center



RightsLink®



Home



Help



Email Support



Michael Anghel ▾

An aqueous, polymer-based redox-flow battery using non-corrosive, safe, and low-cost materials

Author: Tobias Janoschka et al

Publication: Nature

Publisher: Springer Nature

Date: Oct 21, 2015

Copyright © 2015, Springer Nature

Order Completed

Thank you for your order.

This Agreement between University of Western Ontario -- Michael Anghel ("You") and Springer Nature ("Springer Nature") consists of your license details and the terms and conditions provided by Springer Nature and Copyright Clearance Center.

Your confirmation email will contain your order number for future reference.

License Number 4897660698061

[Printable Details](#)

License date Aug 28, 2020

☑ Licensed Content

Licensed Content Publisher	Springer Nature
Licensed Content Publication	Nature
Licensed Content Title	An aqueous, polymer-based redox-flow battery using non-corrosive, safe, and low-cost materials
Licensed Content Author	Tobias Janoschka et al
Licensed Content Date	Oct 21, 2015

📄 Order Details

Type of Use	Thesis/Dissertation academic/university or research institute
Requestor type	print and electronic
Format	figures/tables/illustrations
Portion	
Number of figures/tables/illustrations	1
High-res required	no
Will you be translating?	no
Circulation/distribution	1 - 29
Author of this Springer Nature content	no

📄 About Your Work

Title	Synthesis of Stable Organic Radical Homo and Co-Polymers and Their Applications as Functional Materials in Solid-State Devices
Institution name	University of Western Ontario
Expected presentation date	Oct 2020

📄 Additional Data

Portions	Figure 1.6
----------	------------

8/28/2020

Rightslink® by Copyright Clearance Center



RightsLink®



Home



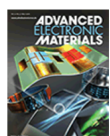
Help



Email Support



Michael Anghel ▾



Design Criteria for Ultrathin Single-Layer Flash Memristors from an Organic Polyradical

Author: Sabastine Ezugwu, Joseph A. Paquette, Vishal Yadav, et al

Publication: Advanced Electronic Materials

Publisher: John Wiley and Sons

Date: Oct 10, 2016

© 2016 WILEY-VCH Verlag GmbH & Co. KGaA, Weinheim

Order Completed

Thank you for your order.

This Agreement between University of Western Ontario -- Michael Anghel ("You") and John Wiley and Sons ("John Wiley and Sons") consists of your license details and the terms and conditions provided by John Wiley and Sons and Copyright Clearance Center.

Your confirmation email will contain your order number for future reference.

License Number 4897660492275

[Printable Details](#)

License date Aug 28, 2020

☑ Licensed Content

Licensed Content Publisher	John Wiley and Sons
Licensed Content Publication	Advanced Electronic Materials
Licensed Content Title	Design Criteria for Ultrathin Single-Layer Flash Memristors from an Organic Polyradical
Licensed Content Author	Sabastine Ezugwu, Joseph A. Paquette, Vishal Yadav, et al
Licensed Content Date	Oct 10, 2016
Licensed Content Volume	2
Licensed Content Issue	11
Licensed Content Pages	10

📄 Order Details

Type of use	Dissertation/Thesis
Requestor type	University/Academic
Format	Print and electronic
Portion	Figure/table
Number of figures/tables	2
Will you be translating?	No

📄 About Your Work

Title	Synthesis of Stable Organic Radical Homo and Co-Polymers and Their Applications as Functional Materials in Solid-State Devices
Institution name	University of Western Ontario
Expected presentation date	Oct 2020

📄 Additional Data

Portions	Figure 1.8 on page 16
----------	-----------------------

Curriculum Vitae

Name:	Michael Anghel		
Post-secondary Education and Degrees:	Mount Allison University Sackville, New Brunswick, Canada 2014–2018		B.Sc Hons.
	The University of Western Ontario London, Ontario, Canada 2018–2020		M.Sc.
Related Work Experience	Teaching Assistant Lab Coordinator – CH3371, CH3320 The University of Western Ontario 2019–2020		
	Teaching Assistant – CH3371, CH3320 The University of Western Ontario 2018–2019		
	Teaching Assistant – CHEM1001, CHEM1021, CHEM3321 Mount Allison University 2016–2018		

Publications:

1. **Anghel, M.**, Magnan, F.; Catingan, S. D.; McCready, M.A.; Aawani, E.; Wong, V.; Singh, D.; Fanchini G.; and Gilroy, J.B. *Journal of Polymer Science.*, **2020**, 58, 309–319.

Conference Presentations:

2. Poster Presentation (regional): **Anghel, M.**, Magnan, F.; Catingan, S. D.; McCready, M.A.; Aawani, E.; Wong, V.; Singh, D.; Fanchini G.; and Gilroy, J.B. “Synthesis and Characterization of a Nitronyl Nitroxide Polymer”. 47th Physical Organic Minisymposium (POMS) 2019 – Toronto, ON.
1. Poster Presentation (national): **Anghel, M.**, Magnan, F.; Catingan, S. D.; McCready, M.A.; Aawani, E.; Wong, V.; Singh, D.; Fanchini G.; and Gilroy, J.B. “Synthesis and Characterization of a Nitronyl Nitroxide Polymer”. 102nd Canadian Chemistry Conference and Exhibition (CCCE) 2019 – Quebec City, Qc.